Mathematical Modeling and Experimental Approaches Reveal Novel Roles of Cortical Dynein in Spindle Dynamics and Centrosome Clustering

by
Dayna L. Mercadante

A Thesis

Submitted to the Faculty
of the
WORCESTER POLYTECHNIC INSTITUTE
In Partial Fulfillment of the Requirements for the
Degree of
DOCTOR OF PHILOSOPHY
in
Bioinformatics and Computational Biology

May 5, 2022

Approved By:

Amity L. Manning, PhD
Associate Professor
Biology and Biotechnology
Worcester Polytechnic Institute

Sarah D. Olson, PhD
Professor & Department Head
Mathematical Sciences
Worcester Polytechnic Institute

Luis Vidali, PhD
Professor
Biology and Biotechnology
Worcester Polytechnic Institute

Min Wu, PhD
Assistant Professor
Mathematical Sciences
Worcester Polytechnic Institute

Patricia Wadsworth, PhD
Professor
Biology
University of Massachusetts Amherst

Abstract

Faithful cell division requires the mitotic spindle, a tightly regulated biophysical machine composed of rigid microtubule filaments along with motor and non-motor proteins. A balance of forces on and within the spindle structure is required for efficient and error-free cell division. A key player in this balance of forces is dynein, a motor protein whose localization and function at the cell cortex regulates spindle positioning and orientation. By creating a mathematical and computational model to capture spindle formation and maintenance, I have found novel dynein-dependent force contributions to bipolar spindle dynamics. I use biological experimentation to both inform and validate the model, and confirm that dynein-derived forces impact spindle dynamics in cells. Furthermore, I use a combined experimental-modeling approach to explore the role of dynein in cells with multipolar spindles, an alteration to spindle morphology that is common in cancer cells. Through this work I find that dynein-derived forces may be important for the continued proliferation of cancer cells with multipolar spindles. Studying the physical forces driving division in cells with altered spindle structure provides insight into potential drug targets to prevent cancer progression.

Acknowledgements

There's a nearly endless list of people who have guided me to where I am now, and I am incredibly thankful to each of them. First to my advisors, Dr. Sarah Olson and Dr. Amity Manning. With your patience, guidance, and encouragement, I have developed into a confident and independent researcher. I would also like to thank all of the scientists, past and present, in both of these labs. My research has grown and developed through your questions and our conversations. In particular, I would like to thank all of the members of the Manning Lab. Even though I wasn't in the same program, there was never a time when I felt like I didn't belong. The supportive, collaborative, and friendly environment created within this lab made grad school bearable.

I would not be in graduate school if Dr. Carl Brezovec hadn't asked me to be the calculus tutor at Franklin Pierce University after my freshman year, and encourage me to make the crazy decision to declare a double major in mathematics in addition to biology. If anyone is ever questioning whether they like math, they need to take a class with Carl. After having some 10 classes with him in college, I embraced my love for math and decided to apply for graduate school.

After not getting in the first time around and applying frantically to jobs, I got only one interview and one offer for a research position. The Cystic Fibrosis Foundation Therapeutics Lab, and all of its members, became and have remained valuable mentors and incredibly close friends. In particular, Dr. Hermann Bihler has never been anything other than encouraging and supportive. To this day, Hermann makes sure that I know my worth and that I never forget it. I am so grateful to have your continued guidance.

Finally, to my friends and family who have been there through this entire journey. While parts of graduate school and the life that ran parallel to it were incredibly tough at times, you all were the best support system I could have asked for. Kendyl, there aren't words to describe how much our fourteen years of friendship have meant to me. With you by my side it makes it easier to see everything as the "least mist". Finally, to my incredible and patient partner Jake. Thank you for not running away when I told you I might not have a lot of time to put into a relationship because of graduate school. Thank you for standing by my side as I've navigated this journey and transition to the next. Thank you for being you.

Contents

List of Figures

List of Tables

List of Abbreviations

CA	Centrosome Amplification
DCB	Dihydrocytochalasin B
ERM	Ezrin-Radixin-Moesin
MTs	Microtubules
RPE	Retinal Pigment Epithelial
SAC	Spindle Assembly Checkpoint

1 Introduction

1.1 Mitosis Overview

Nearly two trillion cells divide in the human body every day. These divisions occur through mitosis, the part of the cell cycle where previously duplicated genetic material is separated to form two, genetically identical daughter cells [165]. Throughout mitotic progression, important molecular and physical changes occur that are essential for error-free cell division.

As mitosis begins in prophase, the nuclear membrane, which houses the cell's genetic material (DNA) during non-mitotic stages of the cell cycle, breaks down. The long, string-like filaments of DNA, called chromatin, then condense to form tightly compacted chromosome structures [165] (Fig. 1). As mitosis progresses into prometaphase, a molecular machine known as the mitotic spindle, which is composed of dynamic cytoskeletal filaments called microtubules (MTs), is formed [194]. Other prominent components of the spindle are motor and non-motor proteins, whose localization and function throughout the mitotic spindle regulate its shape, structure, and movement. MT attachments to the chromosomes regulate chromosome movement and eventual alignment at the cell center in metaphase [77] (Fig. 1). Specifically, MTs bind dynamically to chromokinesin motor proteins localized along the length of the chromosome and more stably to the kinetochore, a protein complex localized to the centromeric region of each chromosome [40, 256].

Once chromosomes are aligned, a series of physical and molecular cues initiate the onset of a mitotic stage known as anaphase, leading to chromosome segregation and eventual daughter cell formation following telophase and cytokinesis [234] (Fig.1). Progression into anaphase is dependent on the satisfaction of the Spindle Assembly Checkpoint (SAC), which monitors MT attachments to the kinetochore [182]. It is crucial that the replicated chromosomes are separated properly during anaphase, as errors in segregation result in loss or gain of chromosomes, a characteristic of nearly all cancers that is termed aneu-

ploidy [90].

1.2 Building Blocks of the Mitotic Spindle.

The mitotic spindle is a complex biophysical machine composed of MT filaments, non-motor, and motor proteins. These structures work together to ensure that mitosis progresses faithfully and successfully.

1.2.1 Microtubules

MTs are hollow filaments composed of thirteen linear protofilaments [46]. MTs are polar, with dynamic plus ends and more stable minus ends. The minus ends remain anchored and

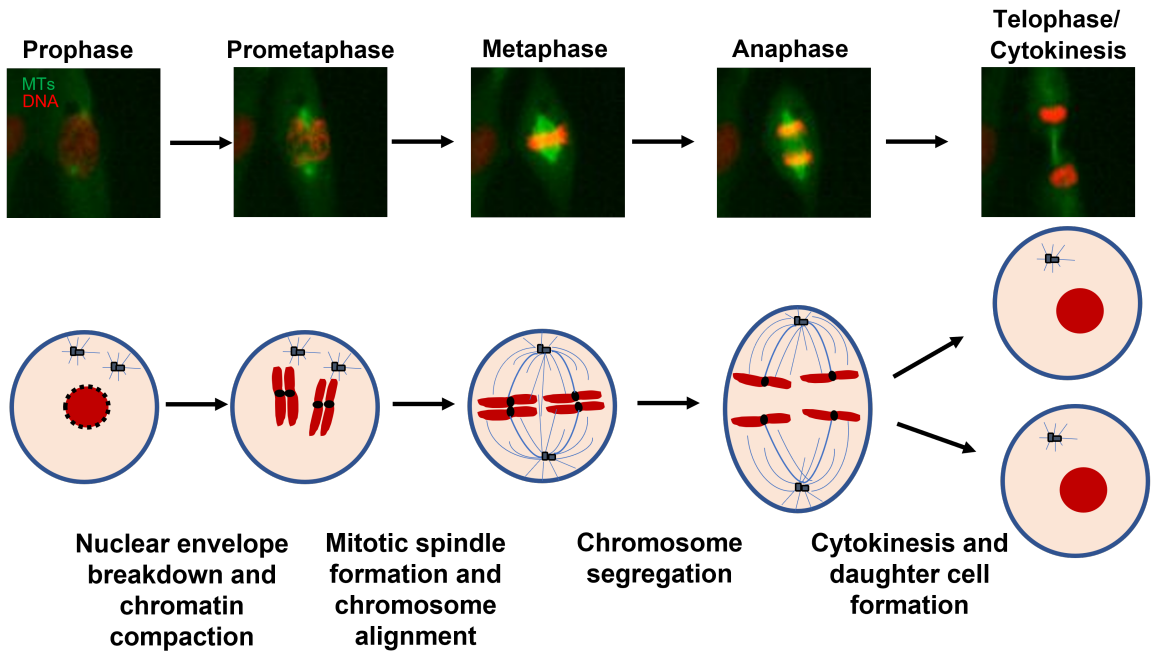

Figure 1: **Mitotic progression.** (Top) Still frames from a cell progressing through mitosis at 5 min increments. MTs are shown in green and DNA is shown in red. (Bottom) Schematic of a cell progressing through mitosis. For simplicity, only two mitotic chromosomes are depicted. The nuclear envelope breaks down upon mitotic entry at the start of prophase. The chromatin compacts to form distinct chromosome structures. Two mitotic centrosomes nucleate MTs during prometaphase, forming the mitotic spindle. MTs bind to and move mitotic chromosomes towards the cell center until chromosome alignment at metaphase and eventual chromosome segregation in anaphase. The cell progresses through telophase and cytokinesis and results in two, genetically identical daughter cells.

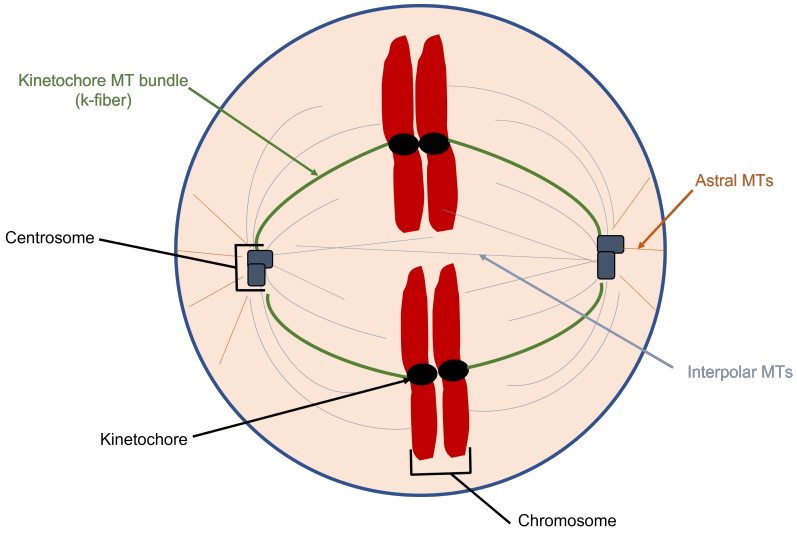

Figure 2: **The mitotic spindle.** Centrosomes nucleate astral, interpolar, and kinetochore MTs which form the mitotic spindle. K-fibers are bundles of 20 MTs that bind to the kinetochore region of the chromosome. Astral and interpolar MTs are dynamic and interact with the cell cortex and other MTs, respectively.

crosslinked near the MT nucleation (origination) site while the plus ends emanate outward; this organization creates a radial, star-like array (Fig. 2).

During interphase, the time during the cell cycle when division is not taking place, MTs are responsible for intracellular transport and nuclear positioning [46]. During mitosis, MT structure and function changes drastically, with the disassembly of stable interphase MTs and subsequent formation of dynamic MTs that comprise the mitotic spindle [211]. Spindle MTs can be further characterized into three distinct populations; astral, interpolar, and kinetochore MTs (Fig. 2) [169]. Astral and interpolar MTs make up the majority of the MTs in the mitotic spindle. Astral MTs interact with the cell boundary while interpolar MTs project towards the spindle midzone and interact primarily with other MTs emanating from the opposing spindle pole. MTs interact with each other or the cell boundary via MT-protein interactions, which generate force and drive spindle formation and maintenance [71]. Kinetochore MTs form stabilized parallel MT bundles (k-fibers) and bind to the kinetochore. K-fibers and associated forces are largely responsible for chromosome alignment and proper chromosome segregation during anaphase [40].

While kinetochore MTs are largely stable during mitotic progression, astral and interpolar MTs undergo a process known as dynamic instability, where they switch constantly between states of growth and shrinkage [172]. MTs switch from growing to shrinking

through catastrophe, and from shrinking to growing through rescue [84, 85, 121, 172, 176]. Both proper MT organization and dynamics are essential for faithful cell division (Fig. 2).

1.2.2 Centrosomes

Centrosomes play a critical role in cell signaling, motility, and division [254]. The centrosome is composed of two centrioles surrounded by a dense matrix known as the pericentriolar material. Centrosomes are the major MT organizing center of the cell, which is largely a consequence of the pericentriolar material [106]. The pericentriolar material contains molecules that nucleate (create), anchor, and release MTs, making the centrosome structure critical for MT-driven processes [9]. The centrosome duplicates once per cell cycle, where each centrosome acts as the initiation and focal point of the two spindle poles of a bipolar mitotic spindle [106] (Fig.2). During mitosis, the centrosomes and associated spindle poles move in response to MT-derived forces generated by interactions with the cell boundary, chromosomes, and/or other MTs. The two daughter cells following mitosis each have one centrosome, ensuring they can repeat the cycle of duplication, mitosis, and division in the next cell cycle.

1.2.3 Non-motor and motor proteins

Non-motor proteins

Non-motor microtubule associated proteins (MAPs) participate in MT nucleation, organization, and dynamics [158]. These proteins localize throughout the cell during prometa/metaphase, with prominence at the spindle poles, kinetochores, and/or cell cortex. The proteins in each of these regions have distinct roles in the regulation of mitotic spindle formation and maintenance, in addition to chromosome movement, alignment, and segregation [158]. One essential function of non-motor MAPs during mitosis is MT crosslinking activity, which provides structural support for the spindle. In this section, I will highlight key non-motor crosslinking proteins in mitosis.

Non-motor proteins enriched at or near the spindle poles contribute to the maintenance of pole focusing. Nuclear and mitotic apparatus (NuMA) and TPX2 are two of the many proteins with increased localization and activity at spindle poles. These proteins bind directly to MTs to form and maintain the crosslinked MT network that comprises the spindle poles [168]. Loss of either of these proteins disrupts spindle structure and results in fragmentation or unfocusing of spindle poles [86, 91, 248, 265]. This loss of NuMA-dependent crosslinking of microtubule minus ends disrupts the mechanical linkage between spindle poles and chromosomes, leading to defects in chromosome alignment and segregation [223].

In addition to crosslinking MT minus ends at spindle poles, non-motor protiens are essential for crosslinking adjacent parallel MTs to form large MT bundles that become k-fibers. The protein TACC3, in a complex with ch-TOG and clathrin, form an intermicrotubule bridge between parallel MTs [55]. This complex additionally regulates k-fiber dynamics by stabilizing MTs through a reduction in MT catastrophe [15].

Motor proteins

Cellular trafficking, ciliary movement, and cell division are driven by motor protein movement along MTs. Motor proteins are characterized by a motor domain that hydrolyzes ATP, allowing it to undergo conformational changes that regulate its movement [238]. There are three distinct classes of motor proteins: mysoin, kinesin, and dynein. Conventional myosin motors bind to actin, cytoskeletal filaments that help the cell maintain its structural integrity, while kinesin and dynein bind to MTs. While all of these proteins have important roles throughout the cell cycle, I will specifically be focusing on their known roles in mitosis.

Myosin

Non-muscle myosin II has traditionally been associated with cytokinesis, the final stage of cell division where an actin-dense contractile ring forms to create the two daughter

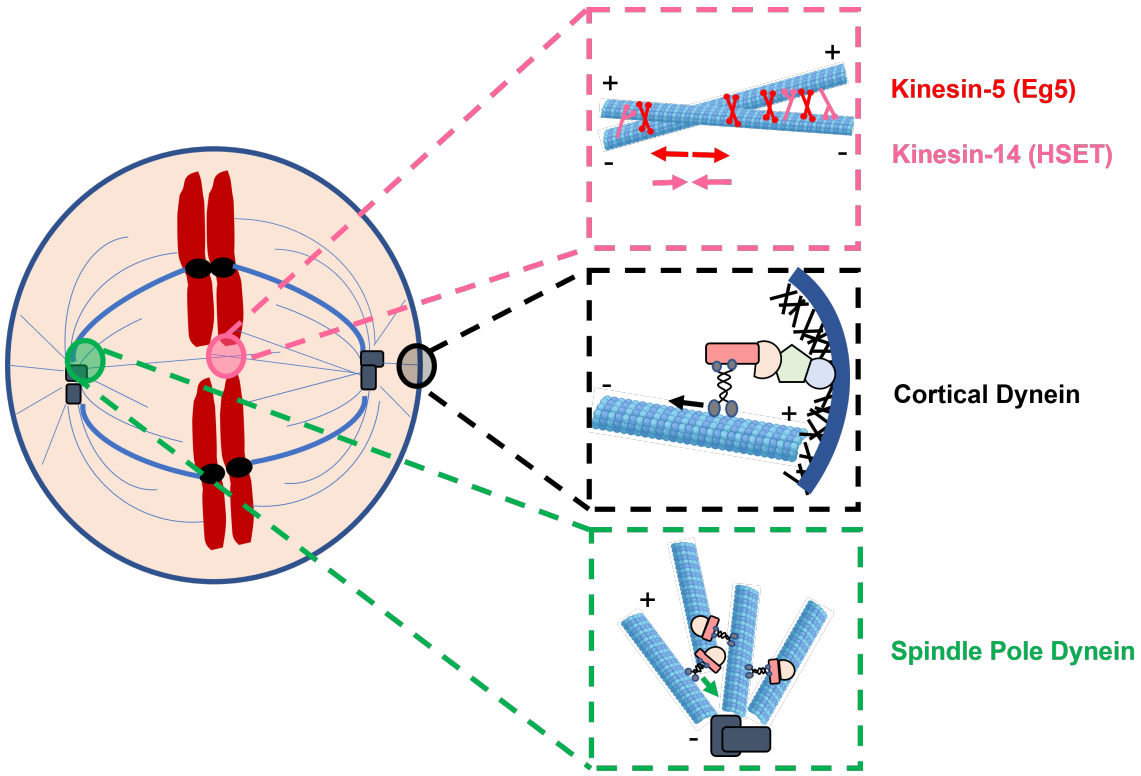

Figure 3: **Prominent motor proteins in mitosis.** Schematic of three major force-generating motor proteins involved in mitotic spindle formation and function. Kinesin-5 (Eg5) and Kinesin-14 (HSET) localize on interpolar MTs and generate opposing forces. Dynein localized to the cell cortex, where it regulates spindle positioning and orientation, and at the spindle poles where it is integral to the maintenance of focused poles. The arrows indicate the direction in which the motor moves along the MT.

cells [258]. Myosin II, however, is also essential during mitosis where it crosslinks short actin filaments to form a stiff cortex [45]. Proper cell cortex function and integrity is essential for cell rounding during mitosis. This characteristic of mitotic cells is important for MT interactions with the cell boundary and kinetochores, where a smaller confinement within the cell allows MTs to interact with both structures rapidly and efficiently [136]. These interactions are critical for spindle formation and positioning through cortical pushing and pulling forces, and chromosome alignment through kinetochore MT stabilization by the Ndc80 complex, a four protein complex consisting of Nuf2, Hec1, Spc24, and Spc25 that is responsible for MT binding to the kinetochore [249,263,264]. Furthermore, a contractile actin-myosin II network on the nuclear envelope has recently been implicated in chromo-

some alignment, where remnants of this network following nuclear envelope breakdown interact directly with chromosomes to aid in chromosome movement towards the spindle midzone, independent if MT interactions [14]. However, the mechanism by which the nuclear acto-myosin network drives chromosome movement remains to be explored.

The non-conventional myosin motor, myosin X, which can bind to both actin and MTs, has been found to be required for both mitotic spindle pole integrity and regulation of spindle length [270]. Myosin X likely aids the maintenance of spindle pole integrity through its interaction and co-localization with the crosslinking protein TPX2 at spindle poles, which is essential for MT minus-end focusing [265,270]. Myosin X-dependent regulation of spindle length has been shown to be a consequence of direct binding between astral MTs and an amorphous rotating actin cloud during metaphase. Myosin X also modulates astral MT dynamics, which have direct implications on bipolar spindle length through their interactions with the cell cortex [132, 174, 261].

Kinesin

Kinesin can be characterized as a superfamily containing 14 subfamilies, nearly all of which play a role in mitotic progression. Their grouping is dependent on genetic sequence, structure, and function. Broadly, kinesins are classified by how they move along and impact MTs. Kinesins-1 through -7 and kinesin-12 move along MTs towards the plus-end while kinesin-14 moves toward the minus end. Other kinesins (kinesin-8 and -13) promote MT catastrophe [271]. Kinesins that line the arms of mitotic chromosomes, appropriately named chromokinesins, such as kinesin-4 (Kif4a) and kinesin-10 (Kid), walk toward the plus-end of polymerizing MTs that they are bound to [6, 19]. Forces generated by these motors, in combination with plus-end directed movement of the kinetochore-localized kinesin-7 (CENP-E) drive chromosome movement toward the cell center during mitosis [6, 26, 114]. There remains, however, kinesin motors whose motility and function are largely unknown (kinesins-9 through -11). While kinesin motors have diverse functions in mitosis from spindle assembly and elongation [13, 26, 32, 73, 115, 147] to the mainte-

nance of spindle integrity [63], chromosome congression [2,76,83,114,140,163,233,255], and k-fiber dynamics and stability [233, 272], I will primarily highlight the function of kinesin-5 and kinesin-14, two of the primary force generators in spindle formation and maintenance [181].

Kinesin-5, called Eg5 in mammalian cells, is a homotetrameric motor protein with two motor domains on either side of an elongated stalk [117]. Eg5 interacts on antiparallel MTs emanating from opposing centrosomes [113, 156]. Each of the motor domains binds to a MT and walks towards the plus-end [12]. When the MTs are antiparallel, as they are in the interpolar region of the spindle, this movement causes MT sliding in opposite directions and drives centrosome separation and early spindle formation [115, 162]. Eg5 is not required for interphase MT organization so its inhibition specifically impacts mitotic cells, where spindles fail to form and result in a monopolar configuration. This has made Eg5 a promising target for rapidly dividing cancer cells [35, 155].

Kinesin-14, HSET in mammalian cells, is a minus-end directed dimeric motor protein with two motor heads on one end of the molecule and non-motor MT binding domains on the other [17, 70]. HSET binds to both parallel and antiparallel astral and interpolar MTs in the mitotic spindle [181,220]. On parallel MTs, minus-end accumulation and static crosslinking activity of HSET contributes to MT bundling near the spindle poles, which aids the maintenance of minus-end focusing [70, 138, 188]. At the interpolar region of the spindle, HSET facilitates antiparallel MT-MT sliding to help maintain mitotic spindle length [70]. HSET movement opposes that of Eg5, resulting in an inward force between spindle poles [181, 219]. Consequently, HSET-derived forces contribute to centrosome collapse in the absence of Eg5 [115, 162].

Dynein

Cytoplasmic dynein-1 (dynein) is the major minus-end directed motor protein in mammalian cells. Dynein is a 1.2 MDa complex composed of two heavy chains which regulate the motor activity of the protein [200]. These heavy chains, in combination with a

number of intermediate, light intermediate, and light chains are required for both linking dynein to adaptor proteins and cargo, and maintaining the structural integrity of the complex [200,246]. During prophase dynein helps to tether centrosomes to the nuclear envelope and separate the centrosomes [202, 252]. As mitosis progresses, dynein localizes in three distinct regions: (1) at the kinetochore where it has been implicated in MT-attachment, chromosome movement, and the initiation of anaphase onset [4]; (2) at the spindle poles where it is essential for maintaining MT minus-end focusing [168]; and (3) at the cell cortex where it is largely responsible for spindle positioning and orientation (described further in Section 1.3) [25, 53, 190, 191].

For nearly all of dynein's activities throughout the cell cycle, it requires adaptor proteins that regulate its localization and function [116]. Dynein's primary binding partner, dynactin, recruits dynein to the nuclear envelope, MT plus-ends, the cell cortex, and kinetochores [60, 201, 229, 230]. More recently, NuMA has been identified as an additional direct dynein-activating adaptor that modulates its mitotic functions [191, 206]. Additional adaptors, such as LIS1, BICD2, NDEL1, and the RZZ complex facilitate dynein's localization and function at the kinetochore and cell cortex and regulate dynein-dependent forces within the spindle [116, 179, 200, 201, 230].

Dynein localized to the kinetochore participates in two distinct roles during mitosis: chromosome alignment and SAC silencing. By moving toward the minus-end of MTs, dynein bound to kinetochores transports chromosomes toward the spindle poles [6, 144, 218]. This is particularly relevant early in mitosis, where chromosomes are dispersed throughout the cell and MT attachments to kinetochores are initiated. When chromosomes are mono-oriented, having only one of their two kinetochores bound to MTs, the dynein-dependent poleward movement of chromosomes is counteracted by chromokinesin- and CENP-E-driven movement toward the cell equator [6]. Once stable bi-oriented kinetochore attachments are established, physical and molecular cues signal satisfaction of the SAC, allowing chromosome segregation. Dynein has been implicated in this signaling by removing

essential components of the SAC, such as Mad1, Mad2, Bub1, and BubR1, through direct binding and subsequent trafficking along MTs toward the minus-end [200, 226]. These roles of dynein at the kinetochore are essential for error-free cell division.

Dynein has additional roles in spindle organization during mitosis. Specifically, dynein activity in the interpolar region of the spindle, where interpolar MTs overlap, counteracts that of Eg5, with one of dynein's two motor heads walking along each MT. This movement pulls spindle poles together, antagonizing centrosome separation and bipolar spindle formation [68, 200, 201]. Additionally, dynein motor activity on parallel MTs is critical for maintaining MT minus-end focusing at spindle poles, where loss of dynein results in splayed poles and barrel-like spindles [60, 91]. While this is an important aspect of mammalian spindle formation and maintenance, it is essential in systems where the spindle forms in the absence of centrosomes, such as *Drosophila, Xenopus*, and *Caenorhabditis elegans* oocytes, and mammalian meiotic spindles. In these systems, dynein is integral to spindle formation by focusing MT minus-ends together at spindle poles [58, 100, 101, 119].

1.3 Regulation of Spindle Positioning and Orientation

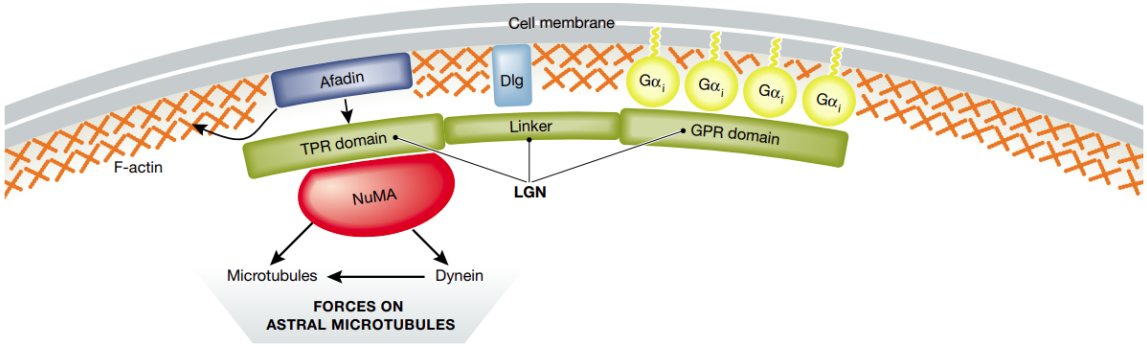

Figure 4: **Proteins involved in anchoring dynein to the cell cortex.** Schematic representation of proteins involved in cortical dynein localization at the cell cortex. Anchoring of cortical dynein to the actin cell cortex can occur through independent mechanisms involving either Gαi or Afadin binding LGN. LGN then binds directly to NuMA which regulates dynein and dynactin localization and activity, which generates pulling forces on astral MTs. Image from di Pietro, et al. (2016), Figure 1A [53].

1.3.1 Cortical dynein localization is dependent on the Gαi-LGN-NuMA complex

Spindle positioning and orientation is essential for proper daughter cell formation, epithelial tissue maintenance, and morphogenesis. Positioning and orientation of the mitotic spindle is reliant on an evolutionarily conserved protein complex bound to the cell cortex, a network of crosslinked actin filaments located inside of the plasma membrane of the cell. This complex consists of the heterotrimeric Gα protein Gαi, LGN, and NuMA. While Gαi lines the entire inner surface of the cell during mitosis, LGN and NuMA are localized in crescents facing the spindle pole(s) (Fig. 4) [53, 56, 122]. Localization of LGN throughout mitotic progression is dependent on chromosome positioning, such that the RAN^{GTP} chromosomal gradient restricts cortical LGN (Fig. 5) [122]. Independent of the Gαi-LGN-NuMA complex, the proteins Afadin and Discs large (Dlg) binds simultaneously to the actin cell cortex and LGN to regulate NuMA localization (Fig. 4) [28, 53].

NuMA binds to LGN, MTs, and dynein to directly modulate active force generation on centrosomes and spindle poles [127, 128, 191]. Dynein's ability to bind to cortical NuMA and generate force is dependent on NuMA's phosphorylation state. Three distinct kinases have been shown to regulate cortical NuMA localization and/or activity: CDK1, PLK1, and Aurora A [80, 127, 214, 216]. Phosphorylation of NuMA by CDK1 or PLK1 regulate its cortical localization, such that inhibition of either kinase results in cortical NuMA enrichment during mitosis [127, 214, 216]. However, inhibition or loss of Aurora A results instead in the accumulation of NuMA at spindle poles and a reduction in cortical NuMA localization [80]. These studies additionally reveal that dynein localization and activity mimics that of NuMA, such that high or low cortical NuMA corresponds to high or low cortical dynein, respectively.

1.3.2 Astral MTs regulate cortical dynein localization

Force generation by cortical dynein on the mitotic spindle is dependent on astral MTs, as they link the motor protein to the centrosome and associated spindle pole. Disruption to

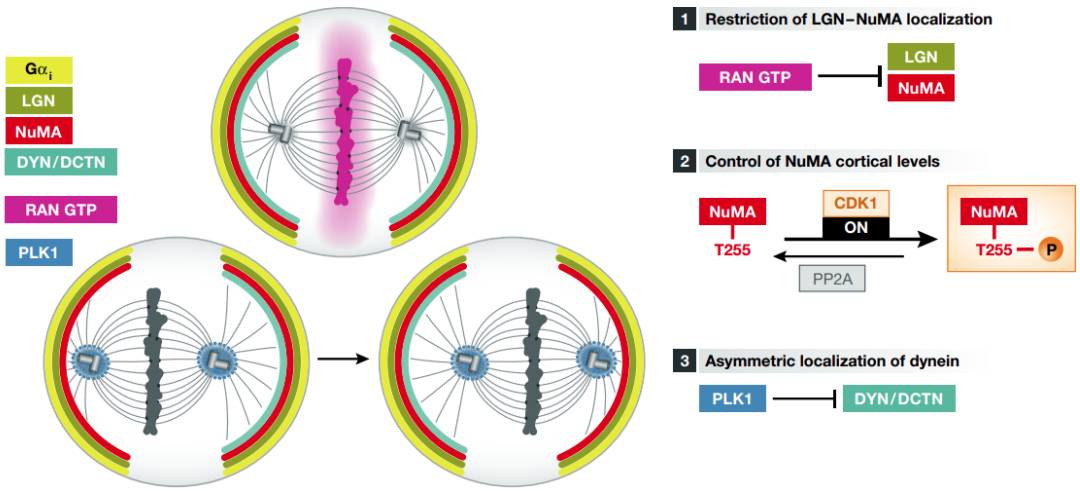

Figure 5: **Regulation of cortical dynein localization**. Schematic representation of the spatial and temporal regulation of cortical dynein localization and activity in metaphase. Image from di Pietro, et al. (2016), Figure 2 [53].

astral MT nucleation and dynamics can impact the localization and/or activity of dynein at the cell cortex.

MT Nucleation

Proteins at the centrosome that are involved in MT nucleation, such as the centrosomal protein pericentrin, impact the density of MTs at each spindle pole [42]. The number of astral MTs reaching the cell boundary are a direct consequence of MT nucleation, such that loss or reduction in MT nucleating proteins reduces the number of MTs interacting with the cell boundary and leads to defects in spindle orientation [240]. Importantly, this defect seems to be independent of cortical dynein transport and localization, since no reduction in cortical dynein was observed following loss of the MT nucleation protein pericentrin [240]. These results suggest that spindle orientation and positioning are dependent on a sufficient number of astral MTs interacting with the cell cortex.

MT Dynamics

MT dynamics are regulated in part by non-motor microtubule associated proteins [158]. EB1, a protein localized to the plus-end of MTs, has been implicated in spindle orientation

through its role in MT stabilization, such that loss of EB1 reduces MT length and causes a decrease in spindle length and spindle mis-orientation [245]. These results suggest that EB1-dependent MT stabilization reduces frequent and rapid MT depolymerization through MT stabilization, allowing a sufficient number of astral MTs to interact with the cell cortex to orient the spindle.

Antagonistic to the previously described role of EB1 in astral MT dynamics, γ-tubulin ring complexes, a protein primarily known for its role in MT nucleation at centrosomes, regulate MT polymerization [16]. Loss of γ-tubulin ring complexes increases MT length and results in defects in spindle orientation [16]. Loss of both EB1 and γ-tubulin ring complexes rescues spindle orientation, suggesting that their roles in MT stabilization are antagonistic. How increased astral MT length impairs spindle orientation remains elusive, although orientation defects could be associated with abnormal or ineffective interactions with the cell cortex.

1.3.3 Actin plays two independent roles in spindle orientation

The complex actin network within the cell has emerged as an important regulator of spindle orientation. LGN localization is dependent on the presence of the actin cell cortex [279], and Afadin directly links the force-generating machinery to the actin cytoskeleton (Fig. 4) [28]. Furthermore, the stiffness of the actin cortex prevents deformations and balances the force on the cell surface induced by MT binding to the NuMA/dynein/dynactin complex [204]. Independent of the the actin cell cortex, an amorphous cloud of actin filaments undergoes rotational movement during metaphase and directly links actin to the spindle MTs via myosin X [174]. It has been shown that myosin X impacts spindle orientation by directly regulating astral MT dynamics and interactions with the cell cortex while generating force and pulling MTs toward the subcortical actin cloud on which it acts [132]. Importantly, cells lacking both myosin X and LGN together have a synergistic impact on spindle orientation, such that loss of both proteins results in more dramatic de-

fects in spindle orientation than loss of either individually [132]. This suggests that myosin X/actin network and the LGN/NuMA/dynein/dynactin complex act independently to orient the mitotic spindle.

1.3.4 Ezin-radixin-moesin proteins impact spindle orientation

Ezin-radixin-moesin (ERM) proteins are the proteins that bind the phospholipids of the plasma membrane to the actin filaments of the cell cortex [66]. The impact of ERM proteins in spindle orientation was first demonstrated in *Drosophila*, where loss of moesin resulted in cortical blebbing and defects in spindle positioning [29, 130]. ERM proteins have since been implicated in spindle orientation and positioning in vertebrate cells, such that loss or inactivation of ERM results in spindle misorientation [102, 153]. There have been two described mechanisms by which ERM can influence spindle orientation: (1) through direct regulation of LGN and NuMA cortical localization [153], and (2) regulation of MT dynamics [228]. Loss of ERM disrupts localization of LGN and NuMA to the cell cortex while maintaining cortical localization of Gαi, suggesting that ERM likely acts at the level of LGN [153]. Furthermore, ERM binds directly to (although at low binding affinity) and stabilizes astral MTs in mitosis. This activity influences spindle movement either directly (through binding to MTs) or indirectly (through modulating dynein activity or other proteins regulating MT dynamics), although the exact mechanism remains unclear [228].

1.4 Centrosome Amplification is a Hallmark of Cancer

1.4.1 Causes of centrosome amplification

The centrosome duplication cycle is tightly controlled, and its proper regulation is required to maintain centrosome numerical stability throughout the cell cycle [20]. Defects in the centrosome duplication cycle, in addition to cytokinesis failure or cell-cell fusion, can result in more than the normal complement of two centrosomes in a mitotic cell, termed

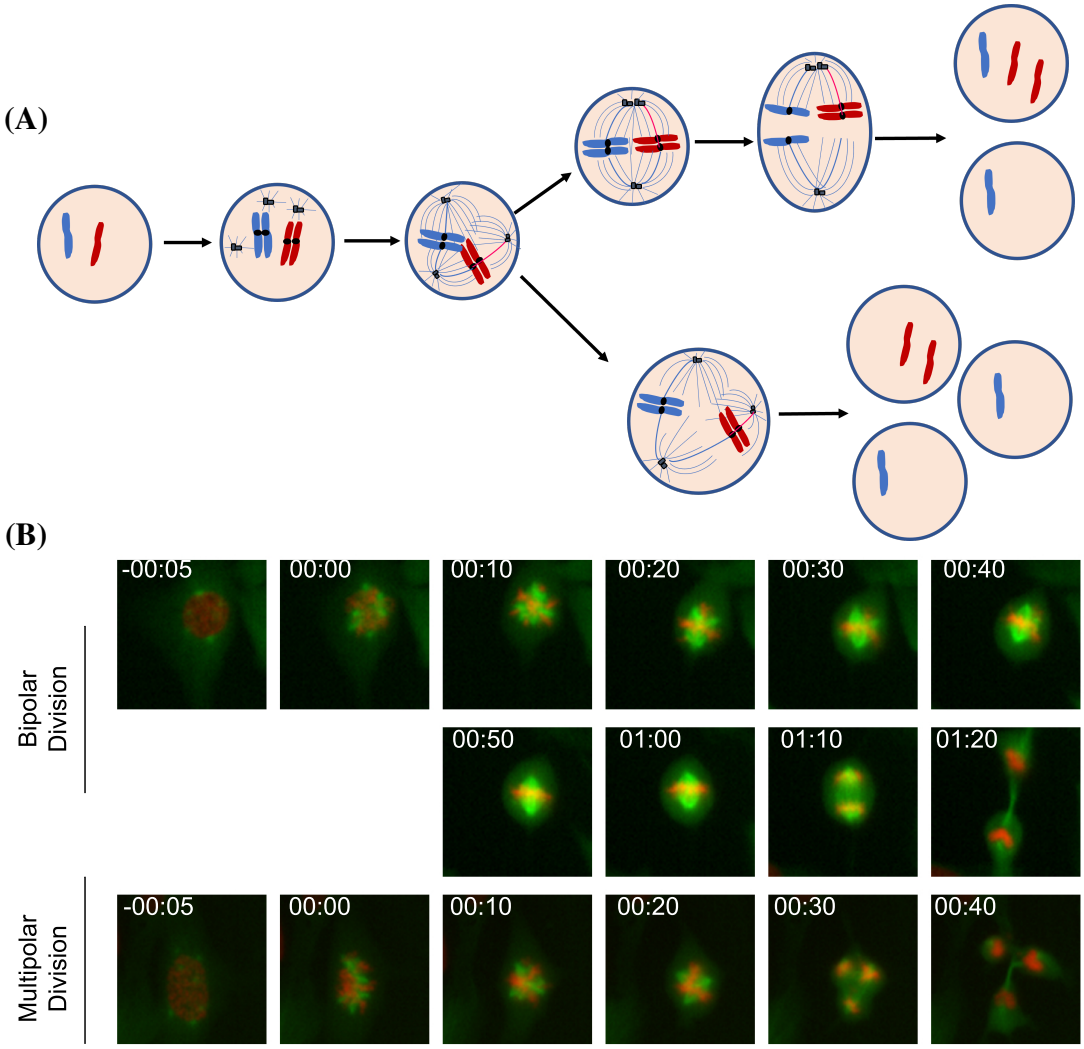

Figure 6: **Centrosome clustering in cells with CA.** (A) Schematic of a cell with extra centrosomes progressing through mitosis. Each centrosome forms a spindle pole, creating a multipolar spindle with defects in MT attachments to kinetochores (mal-attachment indicated by pink k-fiber). The multipolar spindle can either: (top) be transient with centrosomes clustering to form a functional, bipolar spindle and undergo a bipolar division, or (bottom) remain with the cell progressing through a multipolar division, resulting in unviable daughter cells. (B) Still frames of single cells expressing RFP-H2B to visualize chromatin and α-tubulin-GFP to monitor centrosome and spindle pole organization. The top panel of images depicts a cell with extra centrosomes forming a bipolar spindle and undergoing a bipolar division. The bottom panel of images depicts a cell with extra centrosomes forming a multipolar spindle and undergoing a multipolar division, resulting in three daughter cells. Figure modified from Mercadante, et al. (2019) [166].

centrosome amplification (CA) [20, 82, 88, 89]. An important regulator of centrosome duplication is the Polo-like kinase 4 (Plk4), such that overexpression of Plk4 leads to centriole amplification [98, 108, 124]. Many of the proteins involved in centriole duplication and the centrosome cycle, including Plk4, are dependent on ubiquitin regulators, and alterations to this regulation can impact protein stability and expression, leading to CA [47, 209, 266]. Alterations to the components of the pericentriolar material, centriole length, and cell cycle regulation can additionally impact the centrosome duplication cycle and result in CA [148, 160, 231].

1.4.2 Consequences of centrosome amplification

CA and is a hallmark of cancer, and the presence of CA is associated with poor patient prognosis [1, 34]. Cancer cells with CA often cluster their centrosomes to form a functional bipolar spindle during mitosis (Fig. 6 A(top), B(top)) [131, 183, 199, 207]. Centrosome clustering in cells with CA is required for continued cancer cell proliferation since cells with CA that do not cluster their centrosomes, and instead form and maintain a multipolar spindle structure, undergo a multipolar division (Fig. 6 A(bottom), B(bottom)). These divisions result in more than two daughter cells all with gross aneuploidy, which are unviable and likely to undergo programmed cell death within their next cell cycle [81].

When cancer cells cluster their centrosomes, there are resulting defects in MT attachments to kinetochores [81, 225]. SAC signaling and chromosome segregation are highly dependent on proper attachments to kinetochores, where there must be a one-to-one interaction between each k-fiber and kinetochore. If a kinetochore is bound to more than one k-fiber, either from the same spindle pole or a different one, chromosomes will not segregate properly [93]. These types of attachments are common in cells with CA, where improper attachments are made during a transient multipolar state prior to centrosome clustering [81]. If unresolved, these defects can contribute to the initiation or propagation of aneuploidy, tumor heterogeneity, and drug resistance, making it important to prevent pro-

liferation of cancer cells with CA [81, 89, 160].

1.4.3 Targeting centrosome clustering as a cancer-specific therapy

Due to the requirement of cancer cells with CA to cluster their centrosomes to remain proliferative, researchers have focused on preventing centrosome clustering in cancer cells with this phenotype [89, 131, 137, 212]. In identifying druggable targets to prevent centrosome clustering, it is important to identify the impact on normal cells, with the goal of selectively targeting cells with CA while allowing healthy cells to remain proliferative. The first identified protein to contribute to centrosome clustering in cells with CA was dynein, specifically dynein localized at or near spindle poles [199]. Quintyne, et al. found that overexpression of NuMA reduces dynein localization at spindle poles and increases the frequency of multipolar spindles, suggesting that dynein contributes to the centrosome clustering process. Shortly thereafter, additional MAPs and force-dependent mechanisms were identified in contributing to centrosome clustering in *Drosophila* S2 cells [131].

One key motor protein, HSET, has been found to be required for centrosome clustering [131]. HSET-dependent forces at regions of interpolar MT overlap between adjacent centrosomes were found to be required for clustering, as this force acts to pull centrosome together [131, 207]. Actin-dependent cortical contractility was also shown to contribute to centrosome clustering by restricting centrosome movement, allowing centrosomes to get close enough for HSET-dependent pulling forces to actively cluster centrosomes [207]. Additional proteins associated with the actin cell cortex, such as ERM, have been shown to contribute to centrosome clustering [102]. Based on known roles of ERM in spindle orientation, the impact on centrosome clustering may be a result of altered MT dynamics or cortical dynein activity, although the mechanism by which ERM proteins aid centrosome clustering remains elusive [102].

Additional proteins, including Aurora A kinase, those involved in the SAC, kinetochore-MT attachment and tension, and the ubiquitin/proteasome system have also been identified

as potential targets for cells with CA, however no target has yet been appropriate for clinical intervention [18, 131, 137, 183, 212]. While targeting centrosome clustering remains a cancer-specific mechanism to prevent proliferation of cells with CA, other mechanisms including centrosome inactivation, degradation, or extrusion from the cell have also been proposed [212].

1.5 Mathematical Modeling of the Mitotic Spindle

Mathematical biology involves the application of mathematical equations to study and explore dynamic biological systems. While biological experimentation can be costly and time consuming, modeling can bypass these limitations to rapidly make predictions about biological processes. As a dynamic, biophysical machine, mathematical biologists are drawn to the mitotic spindle [177, 244]. Biology has informed many of the necessary parameters and motor-dependent force-velocity relationships within the spindle, and Newton's laws of motion allow modelers to apply and study these forces within the confinement of the cell. While mathematicians rely on experimentalists to inform their model, biologists similarly rely on mathematicians to make novel predictions about the experimental system. Herein lies the continuous, iterative loop that allows interdisciplinary research to progress. This loop involves generating experimental data, analyzing the experimental results, creating a theoretical model informed and motivated by biological hypotheses, using the model to make predictions about the biological system, testing the predictions experimentally, then updating the model as necessary based on new experimental results. In this section, I will describe how this process has been used and implemented to study the mitotic spindle (summarized in Tables 5, 6, 7, 8, 9, 10, 11 in the Appendix).

1.5.1 Modeling MTs and motor proteins

To understand the mitotic spindle, one must understand the individual components within the spindle, namely MTs and motor proteins. While considering each of these individ-

ual components when modeling the entire spindle is mathematically and computationally intensive, studying and simulating their basic function helps modelers understand how to best simplify their dynamics to reduce computational complexity. This benefits modelers while providing valuable insight into the basic properties and functions of MTs and motor proteins.

The fascinating property of MT dynamic instability was first characterized in 1984 by Mitchison and Kirschner [172]. Shortly thereafter, Hill introduced a theoretical model to describe the kinetics of this process [105]. Hill described dynamic instability as a two-phase macroscopic kinetic model, which has expanded our fundamental understanding of the process. Further development of theoretical models has more accurately captured biological phenomena, such as limiting MT growth rate based on the availability of free tubulin in the system, as the Freed model describes [72]. This type of model refinement allows theorists and biologists alike to confidently rely on theoretical model predictions to provide deep insight into dynamic biological systems.

Similar approaches have been applied to individual motor proteins, where understanding their movement and function provides valuable insight into their biochemical, biophysical, and biological properties and functions. Stochastic Monte-Carlo modeling is a common approach to simulate and study the activity of individual motor proteins, where a probability determines the outcome of an event taking place [227]. For motor proteins, this "event" is taking a step along a MT, simulating the chemical energy released by hydrolyzing ATP into mechanical energy. The first and most frequently modeled motor proteins are dynein and kinesin-1 [57, 96, 118, 227, 247, 275], although more recent studies explore the chemomechanical properties of additional kinesins, which is important to understanding their role(s) in mitosis [97, 276]. Importantly, the relationship between motor force and velocity has been informed by single molecule studies *in vitro* [237], allowing mathematicians to define a well-informed equation to capture this relationship. Our increasing knowledge of motor protein dynamics and function through combined experimental and

modeling approaches have allowed theorists to scale up from the molecular to the cellular level, and combine information and techniques to model the mitotic spindle.

1.5.2 Modeling spindle assembly and spindle function

Assembly of the mitotic spindle in prophase requires motor-driven centrosome separation (models of early centrosome separation and spindle assembly summarized in Tables 5 & 6 in the Appendix). One of the early models of spindle assembly and spindle elongation relied on the balance between HSET-dependent forces between spindle poles and dynein-dependent forces at the cell boundary [49]. These forces oppose each other, and Cytrynbaum, et al. found the required balance between these forces for a steady-state spindle length to be achieved. This model suggested biological experiments to test its hypotheses, which in turn allowed the authors to further develop and refine the model based off of experimental findings [50]. In the updated model, Cytrynbaum, et al. included a second force antagonistic to cortical dynein-dependent pulling; nuclear elasticity. Consideration of this force, along with additional assumptions, allowed the authors to make predictions about the MT and motor-independent forces impacting early centrosome separation and spindle formation.

In 2002, Nédélec created a model of MTs from two asters interacting via motor protein-derived forces and tested the behavior of the model when only certain forces are permitted [185] (Table 6 in the Appendix). In particular, he found that considering only inward or outward forces cause the asters to collapse or separate fully, respectively. His model suggested further that motor proteins with heterocomplexes, those that can move toward both the plus and minus end, allow a spindle-like structure to form. Nédélec's modeling approaches have since evolved into a sophisticated simulation software for cytoskeletal modeling, called Cytosim [186]. Cytosim is based in Langevin's equation, where for each object within the system, including dynamic filaments, motor, and non-motor protiens, an equation of motion is solved. The equation includes both active forces acting on each object

and Brownian motion resulting from random collisions within the system [186]. Many predictions about MT and spindle organization have been proposed based on results from Cytosim simulations [54, 109, 129, 149, 210, 259], and this will continue to be a valuable tool in generating experimentally testable predictions of dynamic cytoskeletal processes.

1.5.3 Limitations of non-mammalian models

Researchers have used mathematical and computational modeling to study the mitotic spindle of many model organisms, which have varying spindle structure and dynamics. For example, meiotic spindles of *Xenopus* egg extracts are a valuable tool in understanding motor and non-motor protein-dependent spindle organization because they lack centrosomes [103, 149]. However, this system also lacks astral MTs, so simulations in this system cannot be used to explore cortex-derived forces in mitotic spindle formation and function. Models in *Schizosaccharomyces pombe*, fission yeast, have the benefit of simplicity, where their two spindle pole bodies (SPB) are embedded in the nuclear envelope and each SPB has a constant number of 14 MTs (models summarized in Table 6 in the Appendix) [11, 61, 83, 135, 259]. Models in this system are therefore computationally inexpensive and easy to manipulate, however they have little relevance to mitotic progression in metazoans (animals). *Drosophila*, however, have mitotic spindles with similar structure and function to mammalian cells while still having a relatively simple genome that is easy to manipulate [22], making it an appealing model organism for both biological experimentation and mathematical modeling of the mitotic spindle. Furthermore, combined experimental and modeling approaches in *Drosophila* have provided insight into how ploidy, defined as the number of sets of chromosomes in a cell, impacts centrosome clustering in cells with CA (model summarized in Table 11 in the Appendix) [92].

While a valuable model organism, only 60% of human genes have homologs in *Drosophila* [171], and motor protein and MT properties can vary widely between species. As a result, it is important to consider and test functional properties of the mammalian mitotic spindle.

In expanding models to mammalian contexts, researchers can make predictions about how properties of the mitotic spindle impact its function. This becomes particularly relevant in cancer contexts, where improper formation and function of the mitotic spindle can lead to chromosome mis-segregation [224]. Unfortunately, few models specifically consider the mammalian mitotic spindle, but rather describe a general model unspecific to any one organism (models summarized in Tables 6 & 9) [36, 141–143]. While approaches and assumptions vary widely between models, many recent models are not informed or validated by experimental approaches. This reinforces the need for a comprehensive biophysical model capturing mammalian mitotic spindle formation and function paired with biological experimentation.

Mathematical and computational modeling continues to be an essential tool in understanding mitotic spindle formation, function, and dynamics. An extensive list of existing models, their major findings and limitations is in the Appendix (Chapter 9). In this text, I will describe a minimal biophysical model for mammalian spindle formation and maintenance. I describe experimental approaches to both inform the model and validate model predictions.

2 A Minimal Biophysical Model Captures Centrosome Movement and Bipolar Spindle Formation

2.1 Introduction

Mathematical and computational modeling of biological processes can bypass experimental limitations and provide a framework to identify and manipulate individual molecular components. An appealing candidate for such modeling is the process of cell division. Many models have been developed to understand early centrosome separation and spindle formation [36, 49, 61, 109, 135, 143, 149, 236], chromosome dynamics, [5, 27, 43, 54, 154, 268], and spindle elongation during anaphase [21, 129, 259] (expanded upon in Section 1.5 and summarized in Tables 5, 6, 7, 8, 9, 10, 11 in the Appendix). While varying widely in methods and biological motivation, computational force-balance models have been used to understand key mechanistic components that modulate positioning of spindle poles and bipolar spindle formation [68, 110, 142, 143, 185]. Due to the ambiguity surrounding the exact spatiotemporal distribution and motor force generation in cells, and the large number of MT-motor protein interactions [156, 180, 219], computational models generally simplify dynamics and focus on the role of a limited number of interactions. We too reduce the computational complexity of our model in two distinct ways. First, we omit chromosomes and chromosome-derived forces, as these structures are not required for bipolar spindle formation [26, 52, 157] (expanded upon in Section 2.6). Second, we simplify MT-motor interactions, where, rather than modeling each individual motor protein in time and space, we set a probability that a motor protein will stochastically bind and generate force based on its proximity to a MT (Fig.8) [142, 143].

In our simulations, the cell cortex is a rigid, circular boundary, with a diameter of 30 μm, capturing a mammalian cell that has rounded as it enters mitosis [10, 130, 136]. While calculations are performed in two dimensions, we assume a thin slice in the third

dimension, allowing MTs to intersect without a spatial restriction. We allow MT-motor protein interactions with Eg5 and HSET on antiparallel MTs, capturing the dominant roles of these proteins in mitosis, and with dynein at the cell cortex and spindle poles [67, 68, 147, 156, 219, 220, 251, 253]. Where available, experimentally defined parameters using mammalian cell culture were chosen from the literature, and all parameters described below are listed in Table 1. The model is benchmarked on previous modeling approaches that capture dynamic centrosome positioning and cell division [133, 134, 142, 143, 184]. In this chapter I will discuss how we model MTs and MT-motor protein interactions, and the forces governing centrosome movement and spindle formation. I will describe how we directly incorporate biological data to both inform and validate our biophysical model.

2.2 Model Details

2.2.1 Dynamic microtubules

MTs are elastic filaments oriented such that their plus-ends point outward while their minus ends remain anchored at the centrosome [84, 85, 176]. We consider MT minus-ends to remain embedded in the centrosome (c in Fig.7 A) to account for crosslinking proteins that maintain spindle-pole focusing throughout mitosis [91, 257].

MT plus-ends undergo dynamic instability [121], meaning that they are stochastically switching between states of growing (at a velocity v_g) and shrinking (at a velocity v_s if unbound or v_b if bound to cortical dynein). MTs undergo rescue (switch from shrinking to growing) at a rate k_1 and undergo catastrophe (switch from growing to shrinking) at a MT length-dependent rate k_2, defined as $k_{2_i} = sv_g\ell_i$, where s is a scaling factor, and ℓ_i is the length of the i^{th} MT [85]. Following a standard Monte Carlo method, where at each time step, Δt, we choose n_2 from a uniform distribution, $n_2 \in \mathcal{U}[0, 1]$, and the i^{th} growing MT undergoes catastrophe if $n_2 \leq k_2^*$, where $k_2^* = 1 - e^{-k_{2_i}\Delta t}$ [143]. Similarly, shrinking MT i will be rescued if $n_1 \leq k_1^*$ where $k_1^* = 1 - e^{-k_1\Delta t}$. Shrinking MTs that fail to undergo rescue depolymerize completely and are no longer considered in the system when

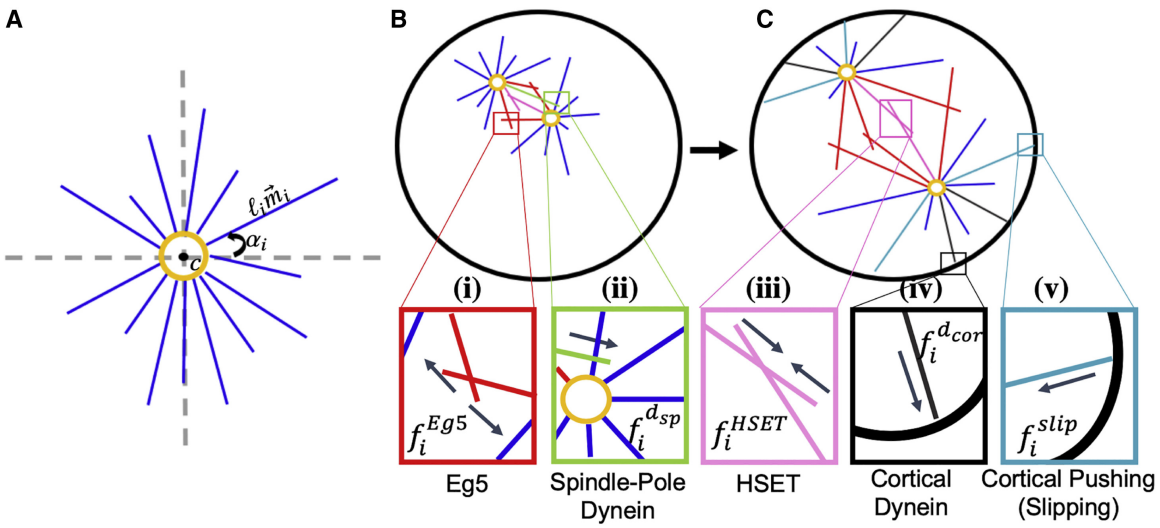

Figure 7: **MT-associated forces are involved in forming and maintaining a bipolar mitotic spindle**. (A) MTs are nucleated from and remain anchored at centrosome c. Each MT i is defined by an angle α_i, length ℓ_i and direction $\vec{m}_i$. A balance of pushing and pulling forces are required for proper centrosome separation in (B) and maintenance of spindle bipolarity in (C). (i) Eg5 generates an outward force at antiparallel MT overlap regions. (ii) Dynein localized to spindle poles binds to and pulls MTs from the opposing spindle pole. (iii) HSET generates an inward force at antiparallel MT overlap regions. (iv) Dynein localized to the cell cortex generates a pulling force on bound MTs. (v) MTs that continue to grow as they reach the cell cortex generate a pushing force. Arrows in (i)-(v) indicate the direction in which centrosome c will move in response to force f_i on MT i by motor M. Image from Mercadante, et al. (2021) [167].

$\ell_i \leq v_g \Delta t$.

Each MT i is nucleated from one of the two centrosomes at a rate MT_{nuc}, has an angle α_i, length ℓ_i, and is characterized by a unit direction vector $\vec{m}_i$ from the center of the centrosome to the MT plus-end (Fig.7 A). As MTs interact with each other or the cell boundary, $\vec{m}_i$ further defines the direction in which motor-dependent forces are generated on MT i, and therefore felt on centrosome c. While we do not account for physical bending of dynamic MTs, when defining the model terms and MT force generation by motor proteins, we account for the tendency of MT to bend, particularly at interpolar regions, and scale the force as needed (Eqs.(11), (12), Fig. 9 B).

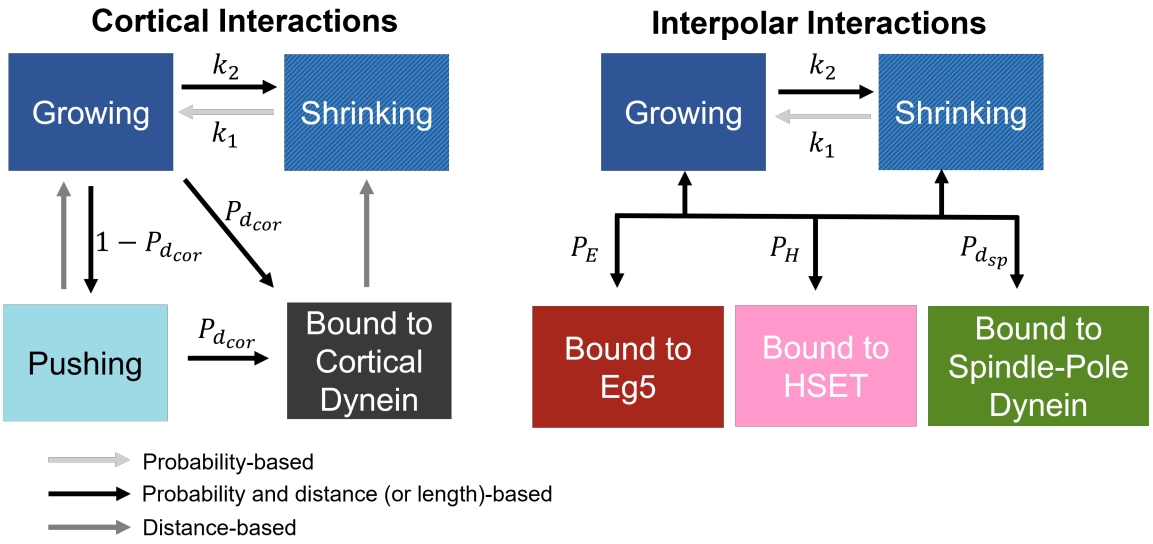

Figure 8: **MT dynamics and motor-derived forces are dependent on probabilities and/or distances.** MTs switch stochastically and constantly between states of growing and shrinking at a rate k_1 and MT length-dependent rate k_2, respectively. Cortical Interactions: If growing MTs are close to the cell cortex, they will either bind to cortical dynein, with probability $P_{d_{cor}}$, or continue to grow and push against the boundary with probability $1 - P_{d_{cor}}$. A pushing MT will grow but no longer generate force if the MT end is too far away from the boundary. A MT that is bound to cortical dynein shrinks with velocity v_b while bound. If the MT end is too far away from the boundary a MT bound to cortical dynein will switch to shrinking and shrink with velocity v_s. Interpolar Interactions: If growing MTs intersect with or are nearly parallel to MTs on the opposing centrosome, they will bind to Eg5 or HSET (with probabilities P_E and P_H, respectively. If growing MTs penetrate a radius around the opposing centrosome they will bind to spindle-pole-localized dynein with probability $P_{d_{sp}}$. All rates and probabilities are listed in Table 1.

2.2.2 Centrosome movement

We define five MT-derived forces that drive the movement of centrosome c within the confined cell boundary: pushing forces by MTs growing and slipping against the cell cortex ($\vec{F}_c^{slip}$), motor-dependent pulling forces by dynein at the cell cortex ($\vec{F}_c^{d_{cor}}$) or spindle poles ($\vec{F}_c^{d_{sp}}$), and Eg5- ($\vec{F}_c^{Eg5}$) or HSET- ($\vec{F}_c^{HSET}$) derived forces at interpolar MT overlap regions (Fig. 7 B,C (i)-(v)). Since exact amounts and distributions of motor proteins throughout the spindle have not been experimentally determined, and modeling individual molecular motors is computationally intensive, we use a simplified approach that has been

used previously to capture the effective overall force by motor proteins on each centrosome [142, 143].

The fluid dynamics inside of a single cell occurs at low Reynold's number, where viscous forces dominate [187, 198]. Reynold's number is calculated as the ratio between intertial and viscous forces, and is given by

$$Re = \frac{ul}{\mu}, \tag{1}$$

where u is the velocity, l is the length, and μ is the kinematic viscosity of the fluid. Here, we assume that the kinematic viscosity of the cytoplasm within the cell is similar to that of water at 37°C, $\mu = 7\text{x}10^5$ μm^2/sec. If we consider the movement of a centrosome surrounded by a dense network of MTs with average length 3 μm (having an average aster diameter 6 μm), and observe that the centrosome moves within the fluid at a velocity of $u \approx 0.5$ μm/sec, the Reynold's number is approximately $4\text{x}10^{-6}$. Given this condition of low Reynold's number, we consider the following force-balance equation for the movement of centrosome c in the overdamped limit:

$$\vec{0} = \vec{F}_c^{d_{cor}} + \vec{F}_c^{d_{sp}} + \vec{F}_c^{slip} + \vec{F}_c^{Eg5} + \vec{F}_c^{HSET} + \vec{F}_c^{r_{cent}} + \xi\vec{v_c}, \tag{2}$$

where $\vec{F}_c^{r_{cent}}$ prevents two centrosomes from occupying the same space (Eq. (14)). We solve a system of c equations for the velocity of each centrosome, $\vec{v_c}$, and use the velocity to determine the new location of each centrosome. Due to MT dynamics and stochastic force generation, a new set of forces in Eq.(2) are calculated at every time point, determining the corresponding centrosome velocity. The velocity is scaled by a constant drag coefficient, ξ, to account for the viscosity of the cytoplasm within the cell. The drag is calculated as $\xi = \mu/\sqrt{\gamma}$, where μ is the viscosity and γ is the permeability, approximated using the volume fraction of MTs in the system (Table 1) [151].

2.2.3 Cortical forces

Dynein is a minus-end directed motor that is localized at the cell cortex (cor) during mitosis where it binds to MT plus-ends, generates a pulling force on the MT, and contributes to a net force that drives the centrosome closer to the boundary [49, 122, 128, 133, 134, 191, 274], as illustrated in Fig. 7 C(iv). Cortical dynein is assumed to be uniformly distributed along the boundary and each MT plus-end within a distance $\mathcal{D}_{d_{cor}}$ to the boundary has a probability $P_{d_{cor}}$ of binding to dynein. Binding to dynein will occur if $n_d \leq P_{d_{cor}}$, where $n_d \in \mathcal{U}[0,1]$. The pulling force generated by cortical dynein on the i^{th} MT nucleated from the c^{th} centrosome follows a standard linear force-velocity relationship [237]:

$$f_i^{d_{cor}} = f_{0,d}\left(1 - \frac{\vec{v}_c \cdot \vec{m}_i}{v_{0,d}}\right), \tag{3}$$

where $f_{0,d}$ is the stall force of dynein, $v_{0,d}$ is the walking velocity of dynein, $\vec{v}_c$ is the velocity of centrosome c, and $\vec{m}_i$ is the unit vector in the direction of MT i. The total pulling force by cortical dynein on the c^{th} centrosome in the direction of the i^{th} MT is,

$$\vec{F}_c^{d_{cor}} = \sum_{i=1}^{N_{c,d_{cor}}} -\vec{m}_i \exp\left(-\frac{\ell_i}{K d_{cor}}\right) f_i^{d_{cor}}, \tag{4}$$

where $N_{c,d_{cor}}$ is the total number of MTs on centrosome c that bind to cortical dynein, ℓ_i is the length of MT i, d_{cor} is the minimal distance between centrosome c and the cell cortex, and K is a scaling factor. This force will pull the centrosome in the direction of $\vec{m}_i$, towards the cell cortex. MTs will stay bound to cortical dynein until the end of the MT is greater than a distance $\mathcal{D}_{d_{cor}}$ from the cell cortex, at which time it begins depolymerizing at velocity v_s. The exponential term accounts for a higher drag due to MT length, density, and proximity to the cell boundary (see details in Section 2.4).

Alternatively, if the random number, n_d, is greater than the probability of binding to dynein, $P_{d_{cor}}$, the MT instead continues to grow and slips along the boundary [23, 133]

(Fig.7 C(v)). For simplicity, we do not allow a MT to be bound to cortical dynein and grow/slip against the cortex simultaneously. The pushing force is described as:

$$f_i^{slip} = min\left(f_{stall}, \frac{\pi^2 \kappa}{\ell_i^2}\right), \tag{5}$$

where f_{stall} is the stall force of a MT and κ is the bending rigidity of the MT. This force is also dependent on MT length, ℓ_i, such that longer MTs are more likely to buckle than shorter MTs. The pushing force felt back on the c^{th} centrosome by $N_{c,slip}$ MTs is then:

$$\vec{F}_c^{slip} = \sum_{i=1}^{N_{c,slip}} f_i^{slip} \vec{m}_i. \tag{6}$$

We note that this force already accounts for length-dependence, and long MTs are unlikely to generate significant force because they are more likely to buckle. Therefore, we do not consider the additional exponential scaling in forces derived by MT pushing against the cell boundary. Pushing MTs also experience a slight angle change of θ and the corresponding unit direction vector $\vec{m}_i$ and angle α_i are then updated. A MT will stop pushing against the cell cortex if the end of the MT is greater than a distance $\mathcal{D}_{d_{cor}}$ from the cell cortex. Alternatively, if $n_d \leq P_{d_{cor}}$ and the end of the MT is within $\mathcal{D}_{d_{cor}}$ from the cell cortex, a pushing MT can then bind to cortical dynein.

2.2.4 Interpolar forces

Interpolar MTs can experience pushing or pulling forces by being bound to opposing MTs by either Kinesin-5 (Eg5, plus-end directed) or Kinesin-14 (HSET, minus-end directed), respectively (Fig. 7 B(i),C(iii)). Specifically, we define interpolar MTs as any MT having an angle within $\pi/2$ of the vector between the centrosomes, regardless of whether it is growing, shrinking, or bound to other motor proteins (Fig. 9 A). Forces from Eg5 are necessary for centrosome separation early in mitosis, as loss of Eg5 prevents centrosome separation and results in monopolar spindles [115, 156, 162, 219]. HSET is localized along

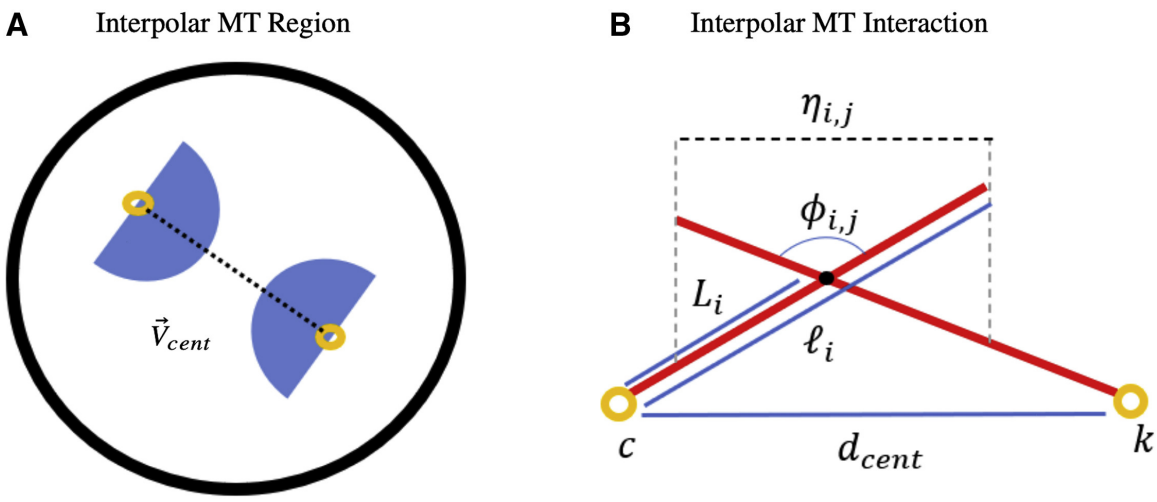

Figure 9: **Interpolar MTs.** (A) Schematic of interpolar MT region. Black dashed line indicates the vector between the centrosomes ($\vec{V}_{cent}$). Interpolar MTs are those that lie within the blue shaded regions. (B) Schematic of interpolar MT interaction. MTs i, j are nucleated from centrosomes c, k, respectively. Figure modified from Mercadante, et al. (2021) [167].

interpolar MTs and is involved in both antiparallel MT sliding and parallel MT bundling [220]. However, since we do not explicitly model crosslinking activity by motors or passive crosslinker proteins, we consider only HSET activity on antiparallel MTs. HSET that is bound to antiparallel MTs is antagonistic to Eg5 and contributes to spindle maintenance during mitosis [26, 181, 205].

Interpolar MTs i, j nucleated from centrosomes c, k, that are within a distance $\mathcal{D}_{Eg5}$ or $\mathcal{D}_{HSET}$ will have a probability of binding to Eg5 (P_E) and/or HSET (P_H) and generating force. Using a Monte Carlo Method, if a random number n_{Eg5}, n_{HSET} is less than P_E, P_H, binding of Eg5 and/or HSET occurs, respectively. We allow each MT from centrosome c to generate force on up to two MTs from centrosome k. MT interactions are considered to be those that intersect or are antiparallel and colinear within an angle $\theta \in [0, \pi/36)$. We determine a point of intersection, $\mathbf{P}$, of line segments $\mathbf{P_a} = \mathbf{P1} + t(\mathbf{P2} - \mathbf{P1})$ and $\mathbf{P_b} = \mathbf{P3} + u(\mathbf{P4} - \mathbf{P3})$ by solving for the point where $\mathbf{P_a} = \mathbf{P_b}$ (Fig. 10). That is, solving $x_1 + t(x_2 - x_1) = x_3 + u(x_4 - x_3)$ and $y_1 + u(y_2 - y_1) = y3 + u(y_4 - y_3)$. Solving for t and u as

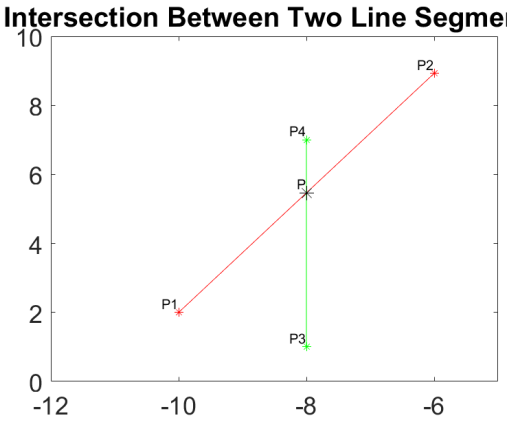

Figure 10: **Point of intersection between two line segments.** Two line segments in two dimensions, defined by points $\mathbf{P1} = (x_1, y_1)$, $\mathbf{P2} = (x_2, y_2)$, $\mathbf{P3} = (x_3, y_3)$, $\mathbf{P4} = (x_4, y_4)$. The intersection point, $\mathbf{P} = (x, y)$, is represented by a black '*'.

$$t = \frac{(x_4 - x_3)(y_1 - y_3) - (y_4 - y_3)(x_1 - x_3)}{(y_4 - y_3)(x_2 - x_1) - (x_4 - x_3)(y_2 - y_1)}, \tag{7}$$

$$u = \frac{(x_2 - x_1)(y_1 - y_3) - (y_2 - y_1)(x_1 - x_3)}{(y_4 - y_3)(x_2 - x_1) - (x_4 - x_3)(y_2 - y_1)}, \tag{8}$$

we can substitute these values solve for the coordinates (x, y) of point P. Therefore,

$$x = x_1 + t(x_2 - x_1), \tag{9}$$

$$y = y_1 + u(y_2 - y_1). \tag{10}$$

If $0 < t < 1$ and $0 < u < 1$, a point of intersection exists. If MTs do not intersect, but are close to antiparallel, they can also have motors bind and generate force. In this case, $t = 1, u = 1$ in the above calculations.

The force on each MT by either Eg5 or HSET follows Eq. 3 with stall forces $f_{0,Eg5}$, $f_{0,HSET}$ and walking velocities $v_{0,Eg5}$, $v_{0,HSET}$, respectively. As MTs nucleated from both centrosomes are bound, we consider the net velocity of each centrosome in the force-velocity equation. The net velocity of centrosome c is therefore calculated as $\vec{v}_c = \vec{v}_{net} - v_f$ where $\vec{v}_{net}$ is the relative velocity between centrosomes c and k, and v_f is the poleward flux, the constant depolymerization of MT minus-ends on interpolar MTs [173, 260]. The force felt on centrosome c due to Eg5 and HSET motors bound to MTs i and j from centrosomes

c and k, respectively, is

$$\vec{F}_c^{Eg5} = \sum_{i=1}^{N_{c,Eg5}} -\vec{m}_i a(1+O_{i,j})C\exp\left(-\frac{L_i}{Kd_{cent}}\right) f_i^{Eg5}, \tag{11}$$

$$\vec{F}_c^{HSET} = \sum_{i=1}^{N_{c,HSET}} \vec{m}_i a(1+O_{i,j})C\exp\left(-\frac{L_i}{Kd_{cent}}\right) f_i^{HSET}. \tag{12}$$

L_i is the distance between the centrosome c to the point where the motor binds to the i^{th} MT, d_{cent} is the distance between centrosomes c and k, and C is a constant scaling factor to account for both passive crosslinkers at antiparallel MT overlap regions and motor-dependent crosslinking activity by HSET and Eg5 [61, 135, 178, 193, 205, 221]. The sensitivity of the model (defined by bipolar spindle length) to parameter C is shown in the Appendix (Chapter 9), Table 12. If the angle of intersection between MTs i and j, $\phi_{i,j} \in [90°, 120°]$, then $a = 1$ and if $\phi_{i,j} > 120°$, then $a = 2$; this allows interpolar MTs that are closer to antiparallel to generate more force. $O_{i,j}$ is the overlap distance of interpolar MTs i and j and is calculated as the minimum of ℓ_i, ℓ_j, or $\eta_{i,j}$, calculated as the law of cosines between the two MTs (Fig. 9 B). For each interpolar interaction, the same equations are solved to calculate the force on centrosome k, using L_j in the exponential scaling term and $\vec{m}_j$, the unit direction vector of MT j, to determine the direction of the force. We determine the 2 MTs on centrosome k that MT i from centrosome c interacts with by the two largest exponential scaling factors within Eqs.(11,12). In Fig. 13 (C) in Section 2.4 we plot the relationship between L_i and the exponential scaling term, showing a decrease in force scaling with increased distance from the centrosome to motor-derived force.

2.2.5 Spindle-pole dynein

In addition to its localization at the cell cortex, dynein is highly localized to spindle poles (sp) during mitosis (Fig.7 B(ii)), where it is necessary for the maintenance of MT minus-end focusing and spindle pole integrity [78,91,241]. We allow MTs nucleated from centro-

some c to have a probability $P_{d_{sp}}$ of binding to dynein anchored to MTs near centrosome k if they get within a distance, $\mathcal{D}_{d_{sp}}$, from the center of centrosome k. The force $f_i^{d_{sp}}$ by each interaction of MT i with dynein localized at spindle poles is the same as Eq.(3). The force on centrosome c by dynein localized at spindle poles is calculated by:

$$\vec{F}_c^{d_{sp}} = \sum_{i=1}^{N_{c,d_{sp}}} -\vec{m}_i \exp\left(-\frac{\ell_i}{K d_{cent}}\right) f_i^{d_{sp}} \tag{13}$$

where $f_i^{d_{sp}}$ is calculated using Eq.(3) and is scaled to account for MT length, density, and proximity to the other centrosome (see details in Section 2.4). For each MT i bound to dynein from centrosome c, an equal and opposite force is felt on centrosome k.

2.2.6 Repulsive force

We consider a repulsive force between centrosomes to be activated if the distance between centrosomes, $d_{cent} < \mathcal{D}_r$ (Table 1). The force applied to centrosome c if this distance argument is achieved is:

$$\vec{F}_c^{r_{cent}} = \frac{\vec{V}_{cent} R}{(1 + d_{cent})}, \tag{14}$$

where $\vec{V}_{cent}$ is the unit vector between centrosomes c and k (Fig. 9), d_{cent} is the distance between both centrosomes and R is a scaling factor.

2.3 Model Initialization and Algorithm

The model is initialized (at time $t = 0$) with 300 MTs with random lengths between 0 and 0.5 μm. MTs are randomly distributed amongst the centrosomes. MT angles are random between 0 and 2π. Initial centrosome position is random within 7.5 μm from the cell center (see Section 2.7 for details). Calculations are performed to determine the proximity of the MT end to the cell boundary and MT interactions at interpolar regions. Distance and probability arguments described in previous sections determine if a MT changes state or

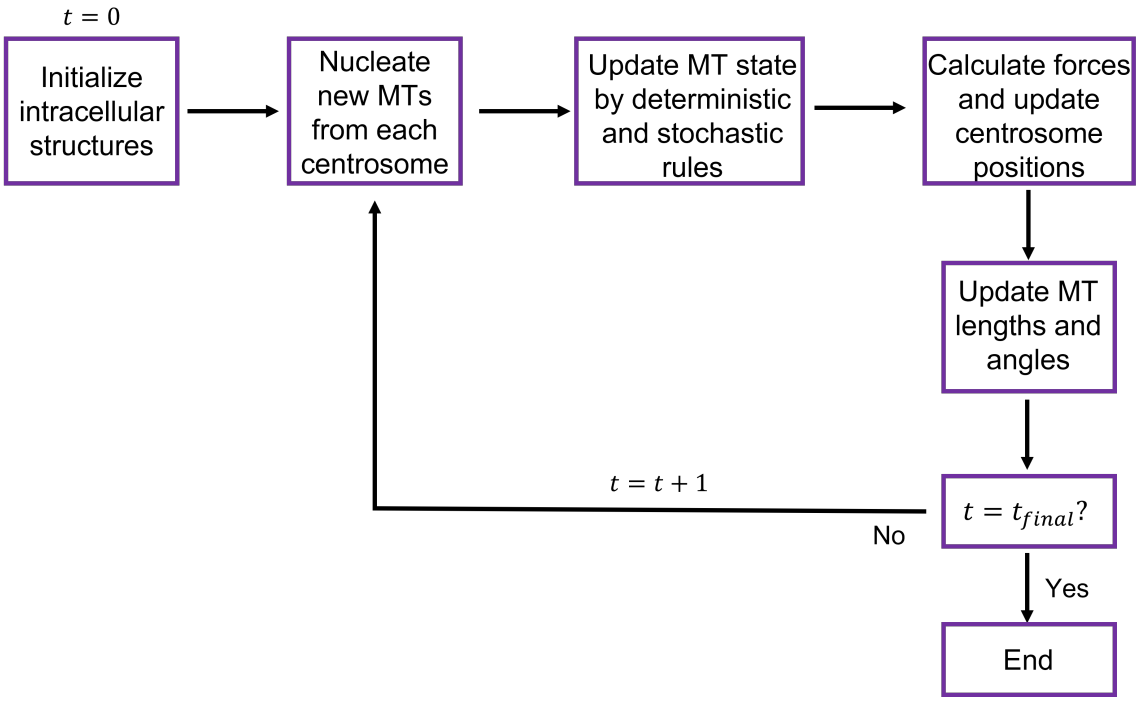

Figure 11: **Algorithm to determine stochastic MT dynamics, force generation, and centrosome positioning** We initialize intracellular structures (MTs, centrosomes) at time $t = 0$. We nucleate new MTs from each centrosome at a rate MT_{nuc}. We update MT state and determine motor interactions based on stochastic and deterministic rules as described in Fig. 8. We calculate forces based on equations described previously and the position of each centrosome by Eq.(2). MT lengths and angles are updated based on their state. We iterate on time until $t = t_{final}$.

generates force (Fig. 8). Force generated by MTs is calculated and summed to determine the total force on each centrosome. Centrosome position is updated by Eq. (2). MT lengths are updated based on their state, as described in Section 2.2.1. MT angles are additionally updated for MTs pushing against the cell boundary. We check the time t, if $t = t_{final}$ we complete the simulation, if $t < t_{final}$ we move to step $t = t + 1$ and generate new MTs. This procedure is summarized in the schematic in Fig. 11.

2.4 Exponential Length Scaling on Forces Captures Increased Drag

While the force by each motor population, dynein, Eg5, and HSET, is consistent on every MT they are bound to, we carefully consider how each force is felt by the centrosome

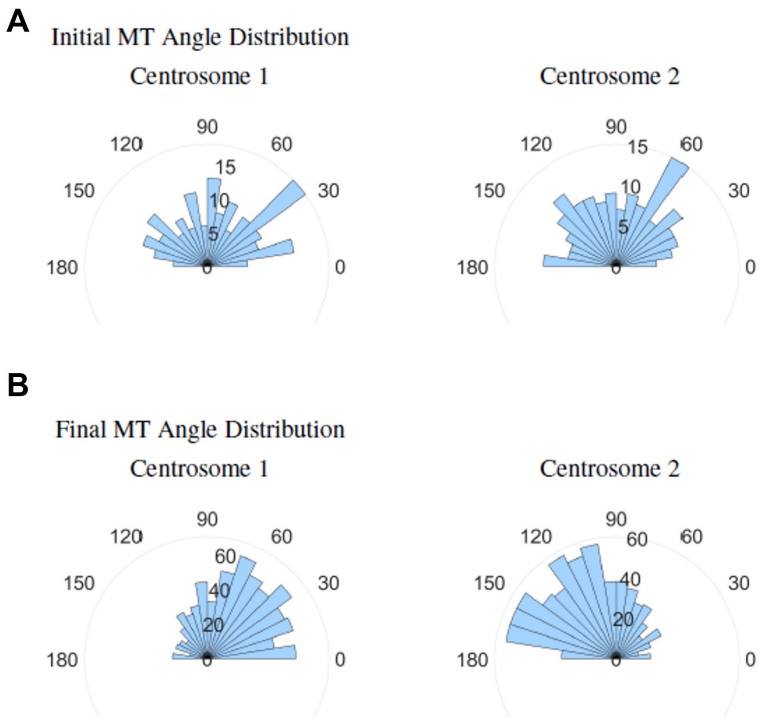

Figure 12: **Distribution of MT angles.** Representative histograms depicting the random initial (A, $t = 20$ sec) and final (B, $t = 25$ min) MT angle distribution (in degrees) with respect to $\vec{V}_{cent}$ on both centrosomes from a single simulation. Figure from Mercadante, et al. (2021) [167].

center, and therefore contributes to centrosome movement. Stoke's Law states that the drag on a spherical object is dependent on the viscosity of the fluid and the radius of the sphere when in free space. However, it is well established that the drag on a sphere increases when it is centered inside a larger sphere [99]. In this model, however, rather than a sphere, we have a centrosome with an attached radial array of MTs that are asymmetrically distributed and changing over time (Fig. 12 B). Our system is dynamic, with changing MT number, MT lengths, and centrosome position at every time step. Studies have explored the drag on a symmetric and centered MT aster, where drag was an increasing function of MT volume fraction [184]. However, they do not consider multiple asters, or how asters interact with each other. Further theoretical studies reveal that confinement and proximity to a boundary increases drag, but does not explore drag on non-solid objects [3]. While these studies do not capture the effective drag on two asymmetric asters interacting with each other within a cell, they do provide insight into how forces should be scaled to account for this geometry.

We account for dynamic changes in drag by scaling motor-derived forces exponentially,

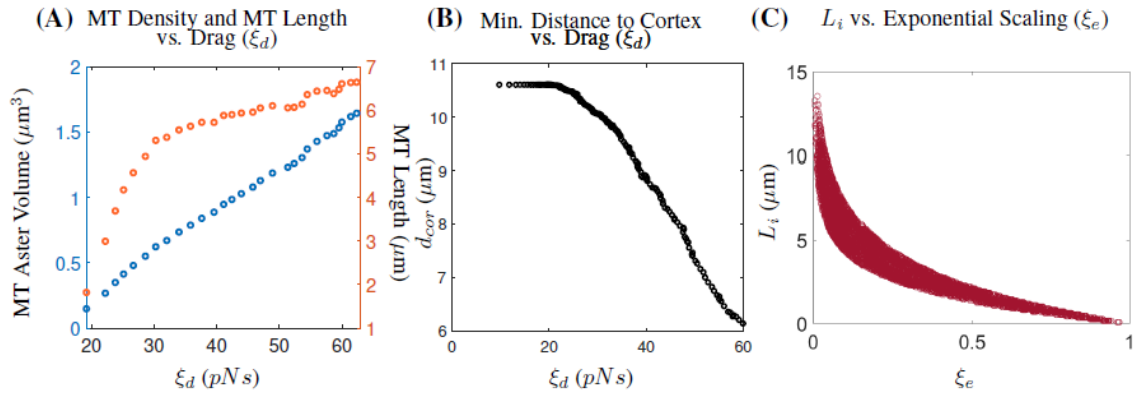

Figure 13: **Exponential length scaling on forces captures increased drag due to MT length and MT density** (A) Scatter plot of a dynamic drag coefficient (ξ_d) (Eq.(15)) versus MT density (aster volume) and MT length from a single simulation of spindle formation up to $t = 5$ min. (B) Scatter plot of a dynamic drag coefficient (ξ_d) (Eq. 15) versus centrosome distance to the cell cortex. (C) Scatter plot of the exponential length scaling of motor-derived interpolar forces ξ_e (Eq.(16)) and the distance from the centrosome to the point of force application for all MTs bound to Eg5 and/or HSET (L_i). Figure from Mercadante, et al. (2021) [167].

with a strong dependence on the proximity of the centrosome to the point where the force is applied. We confirm that this scaling is appropriate by comparing it directly to previously described hydrodynamic drag terms [3, 184]. We define a dynamic drag term, benchmarked on previously published results [3, 184], which is dependent on MT aster size, MT density, and location within the cell. This term is calculated as:

$$\xi_d = \frac{6\pi\mu r_c \omega}{1 - \left(\frac{d_{cor}}{r}\right)^2}, \tag{15}$$

where μ is the viscosity of the cytoplasm (Table 1), r_c is the effective radius of the MT aster, calculated as the average length of MTs nucleated from centrosome c, ω is the volume fraction of MTs nucleated from centrosome c, d_{cor} is the minimal distance from the centrosome center to the cell cortex, and r is the radius of the cell (Table 1). We show that this drag coefficient increases as MT length and MT aster volume (MT density) increase (Fig. 13 A). Furthermore, ξ_d increases as the centrosome distance to the cell cortex decreases (Fig. 13 B). Since MTs and forces are dynamic in our model, rather than applying

a uniform drag coefficient on the centrosome, we define an exponential scaling term that is specific to each MT-motor interaction. We define this term as:

$$\xi_e = exp\left(\frac{\ell}{Kd}\right), \tag{16}$$

which considers ℓ, the distance from the centrosome center to the point where the force is applied, and d, the distance between the centrosome center and the object it is interacting with (either the cell boundary or the opposing centrosome). These terms account for the dynamic changes in drag described previously. K is a constant parameter that was chosen to match experimental results of bipolar spindle length, and model sensitivity (defined by bipolar spindle length) to this parameter is in the Appendix (Chapter 9, Table 12). To observe how this term impacts how force is felt by the centrosome center, we plot L_i, the distance from the centrosome to the point where Eg5 and/or HSET bind, with ξ_e. We see that forces generated when L_i is large are scaled significantly by a small ξ_e, while when L_i is small, i.e. when the centrosome is close to where the force is being applied, ξ_e approaches 1 (Fig. 13 C). d_{cent}, the distance between centrosomes, ranges from 4-15 μm. Overall, this exponential term accounts for the increased drag that the centrosome experiences as MTs become longer and more dense during mitotic progression.

2.5 Centrosome Centering During Interphase is Driven By MT-Cortex Derived Forces

Centrosomes have important roles throughout the cell cycle. Proper centrosome positioning in both interphase and mitosis is critical for its function. It has been well documented that the centrosome is localized in the center of the cell during interphase; the time between successive mitotic divisions when only one centrosome is present. This phenomenon has been largely attributed to MT arrangement, MT dynamics, dynein-dependent forces, actomyosin contractility, and external cues [23, 139, 254]. Researchers have used *in vitro*

Table 1: Parameter values for model results presented in Chapters 2, 3. All parameter values without reference are approximated to match biological results.

Parameter	Value	Description	Reference
Microtubules			
v_g	0.183 μms^{-1}	MT growth velocity (+ ends)	[195, 274]
v_s	0.3 μms^{-1}	MT shrinking velocity (+ ends)	[274]
v_b	0.057 μms^{-1}	MT shrinking velocity (+ ends) bound to cortical dynein	[133]
k_1	0.167 s^{-1}	Rescue frequency	[125, 274]
κ	10 pNμm^2	Bending rigidity	[120, 133, 142]
f_{stall}	5 pN	Stall force of MTs	[152]
MT_{nuc}	2 s^{-1}	MT nucleation rate per centrosome	[196]
θ	10π/180	Slipping MT angle change	
M	6000 μm	Maximum sum of MT lengths	
Motor Proteins			
Dynein			
$f_{0,d}$	3.6 pN	Stall force of dynein	[62]
$v_{0,d}$	0.86 μms^{-1}	Walking velocity of dynein	[62, 250]
$P_{d_{cor}}$	0.5	Probability of binding to cortical dynein	
$P_{d_{sp}}$	0.1	Probability of binding to spindle pole dynein	
$\mathcal{D}_d$	4$v_g(dt)$ μm	Distance required for binding to dynein	
$\mathcal{D}_{d_{sp}}$	1 μm	Distance required for binding to dynein at spindle poles	
Kinesin-5 (Eg5)			
$f_{0,Eg5}$	1.5 pN	Stall force of Eg5	[221]
$v_{0,Eg5}$	0.2 μms^{-1}	Walking velocity of Eg5	[141]
P_E	0.5	Probability of binding to Eg5	
Kinesin-14 (HSET)			
$f_{0,HSET}$	1.1 pN	Stall force of HSET	[210]
$v_{0,HSET}$	0.2 μms^{-1}	Walking velocity of HSET	[141]
P_H	0.5	Probability of binding to HSET	
$\mathcal{D}_{Eg5,HSET}$	$v_g dt$ μm	Distance required for binding to Eg5 or HSET	
Other			
r	15 μm	Radius of the cell	
c_r	0.3 μm	Radius of a centrosome	
$\mathcal{D}_r$	2 μm	Distance for repulsive forces	
K	0.25	MT length-dependent scaling factor	
C	0.1	Antiparallel crosslinking scaling factor	
s	0.15 μm^{-1}	Scaling for catastrophe frequency	
R	1 μm	Scaling for repulsive forces	
μ	0.7 pNsμm^{-2}	Viscosity of the cytoplasm	[151]
ξ	20.6 pNs	Drag coefficient	

approaches that mimic the confined geometry of a cell to study centrosome positioning during interphase. For example, Laan et. al. [133] use a microfabricated chamber with a centrosome and discretely localized dynein motors bound to the chamber to analyze the impact of dynein-derived forces on centrosome movement. This system simulates an interphase cell with a single centrosome, where MT dynamics and dynein-dependent forces have been shown to largely be responsible for centrosome centering within a cell [133].

To confirm that our model captures appropriate centrosome dynamics in interphase, we observed centrosome movement over time in 50 independent simulations of a single centrosome with varying concentrations of cortical dynein, as has been experimentally tested *in vitro* [133]. The initial number of MTs and the length distribution of MTs was similar in all simulations. Initially, centrosomes were randomly positioned with $x, y \in [0, 15]$. We find that a centrosome efficiently centers with our "intermediate" dynein concentration ($P_{d_{cor}} = 0.5$); centering 85% of the time (Fig. 14 (B)). Centering is defined by the centrosome achieving a distance of at least 4 μm from the center of the cell.

Altering cortical dynein concentration also impacts centrosome centering efficiency. Increasing dynein concentrations ($P_{d_{cor}} = 0.75$) prevents centrosome centering since there is an increase in pulling force towards the cell boundary (Fig.14 C). Additionally, high cortical dynein increases the average centrosome velocity. Alternatively, preventing MT binding to cortical dynein ($P_{d_{cor}} = 0$) improved centering efficiency, with centrosomes centering 100% of the time (Fig. 14 A). Additionally, both the maximum centrosome velocity and the average centrosome velocity is increased compared to the intermediate dynein case (Fig.14 B,D). These results are consistent with [133], who show that, with moderate MT lengths, MT centering is most efficient with no dynein and least efficient with high dynein. Together these results indicate that our model is capturing appropriate centrosome movement and velocity driven by MT-cortex derived forces.

2.6 Spindle Formation Occurs Independently of Stable Microtubule Interactions with Chromosomes

Proper formation of the mitotic spindle is required for accurate chromosome segregation. While the molecular regulation of segregation onset is dependent on stable MT attachments

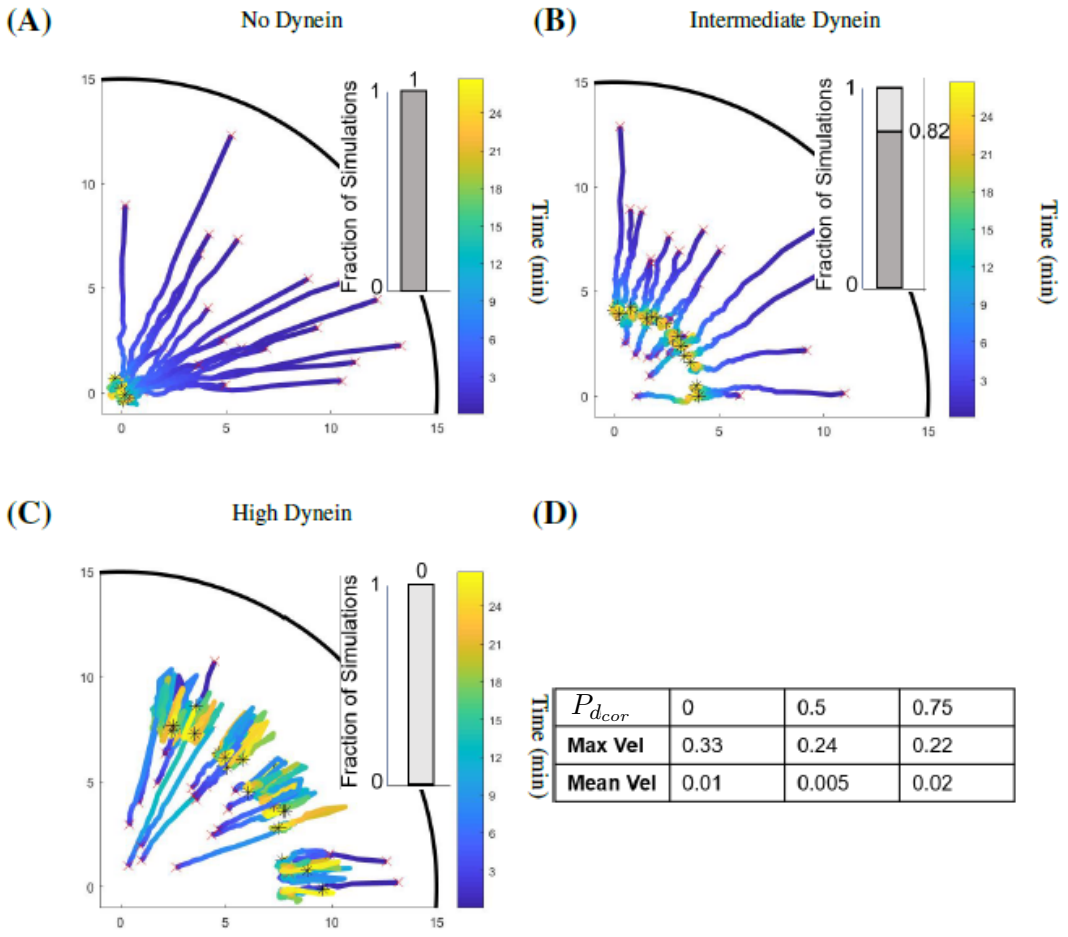

$P_{d_{cor}}$	0	0.5	0.75
Max Vel	0.33	0.24	0.22
Mean Vel	0.01	0.005	0.02

Figure 14: **MT interactions with the cell cortex regulate centrosome movement and positioning.** (A,B,C) Centrosome movement traces from independent simulations of a single centrosome over time from $t = 0$ to $t = 30$ min (colorbar) with no MT binding to cortical dynein ($P_{d_{cor}} = 0$), intermediate cortical dynein ($P_{d_{cor}} = 0.5$), and high cortical dynein ($P_{d_{cor}} = 0.75$), respectively. Bar plots represent the fraction of simulations with the centrosome centered at the final time point where the dark gray bar represents centered centrosomes and the light gray bar represents un-centered centrosomes. The red 'x' is the initial centrosome position in the simulation and the black asterisk is the final centrosome position. (D) Table showing the average maximum and mean centrosome velocities in the three represented conditions. All averages were calculated from 50 simulations.

to chromosomes [280], chromosomes are dispensable for early bipolar spindle assembly [26, 52, 157]. Hence, we develop a minimal computational model to analyze centrosome movement and mammalian mitotic spindle formation in the absence of chromosomes.

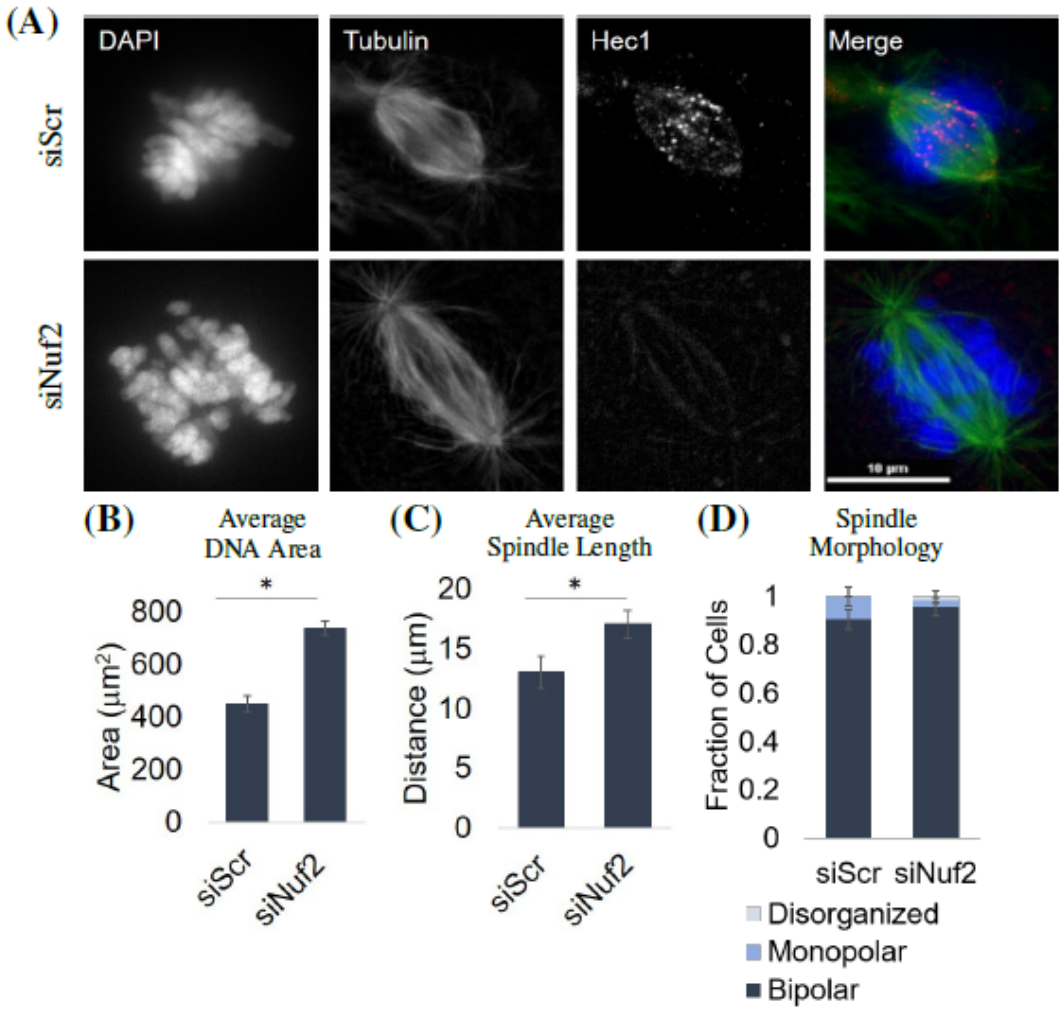

Figure 15: **Stable end-on kinetochore attachments are not required for bipolar spindle formation.** (A) Fixed-cell imaging of RPE cells stained for DAPI (DNA), Tubulin (MTs), and Hec1 (Ndc80 complex) in the control (siScr) and knockdown (siNuf2) condition. (B) Quantification of the average DAPI area in the control (siScr) and knockdown (siNuf2) condition. (C) Quantification of the average spindle length in the control (siScr) and knockdown (siNuf2) condition. (D) Quantification of the average fraction of cells with bipolar, monopolar, or disorganized spindles. All averages calculated from at least 30 cells from 3 biological replicates. Error bars are standard deviation. *$p<0.05$ indicates statistical significance. Figure from Mercadante, et al. (2021) [167].

To inform our model and better define the extent to which stable microtubule attach-

ments to chromosomes are dispensable for bipolar spindle structure, we use immunofluorescence imaging approaches to observe cells depleted of Nuf2 (siNuf2), a component of the Ndc80 complex which is responsible for MT attachments to kinetochores (Fig.15 A) [249, 263, 264]. While it has been established that a bipolar spindle can form in the absence of stable MT attachments to kinetochores [52, 157], performing these experiments in house provides valuable data that can be used to inform and validate our model. We use RPE cells for mitotic analysis, which are a well characterized, diploid, immortalized mammalian cell line. We stained mitotic cells with DAPI to label chromatin and α-tubulin to label MTs. We used siRNA sequences to specifically target Nuf2 to prevent protein translation and then assessed mitotic spindle structure; Nuf2 depletion was confirmed by qPCR (Fig.20 C). We further confirm loss of Nuf2 through immunofluorescent imaging of Hec1, a co-subunit of the Ndc80 complex. Consistent with previously described work [26, 52, 157], we find that Nuf2 depletion leads to a marked decrease in Hec1 localization at kinetochores, dispersion of chromosomes throughout the cell, and an increase in spindle length (centrosome-to-centrosome distance) compared to the control condition, indicating failure to form stable MT attachments to kinetochores (Fig.15 B,C). Despite these differences, spindle morphology remains largely bipolar in the Nuf2 depleted condition, with more than 90% of cells achieving bipolarity (Fig.15 D). Spindle morphology was characterized as bipolar, monopolar, or disorganized, where monopolar spindles were characterized by spindle length being less than half the average bipolar spindle length, and disorganized spindles had indistinguishable spindle poles. These data confirm that kinetochores and kinetochore-derived forces are not required for bipolar spindle formation and maintenance.

2.7 A Biophysical Model Captures Bipolar Spindle Formation and Maintenance

The positioning of the two mitotic centrosomes is essential for proper and error-free cell division. To confirm that our model captures bipolar spindle formation and maintenance, and

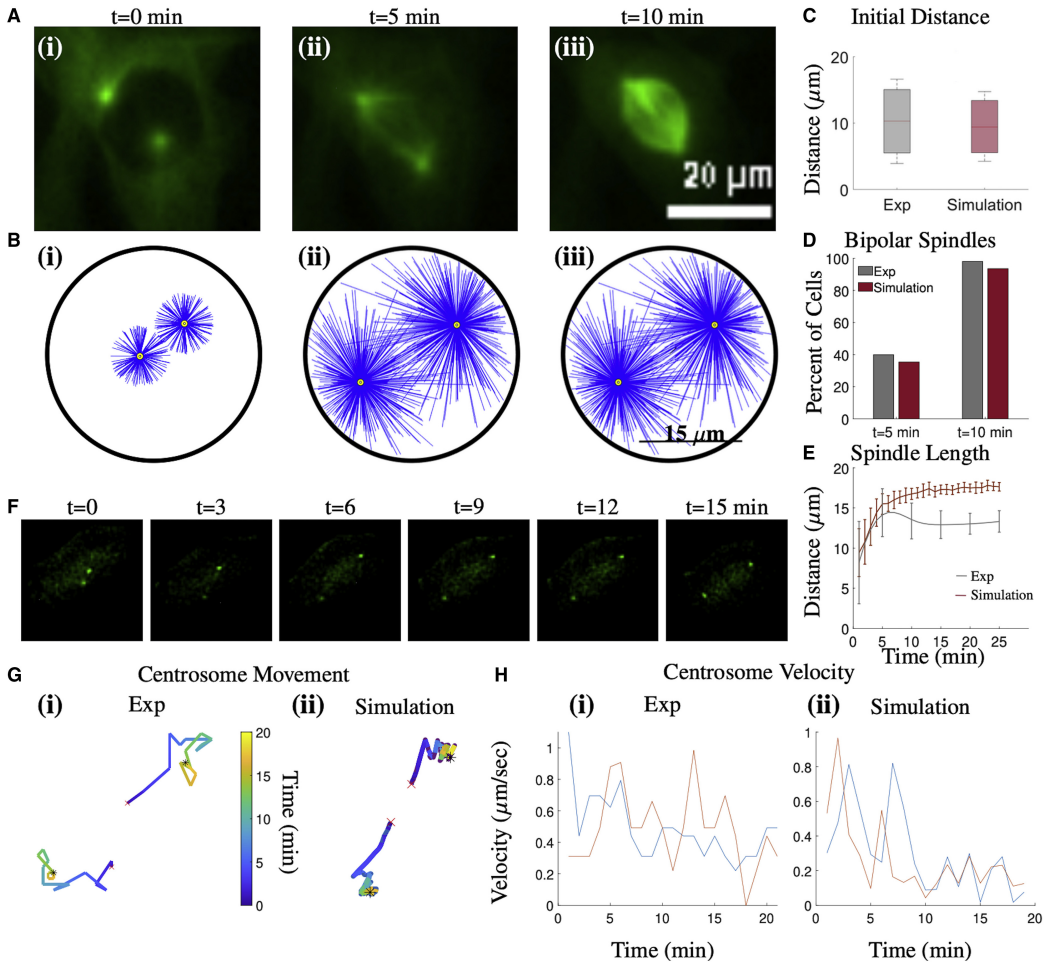

Figure 16: **Stochastic force-balance model captures centrosome movement and bipolar spindle formation.** (A) Still frames from live-cell imaging of RPE cells expressing tubulin-EGFP from the time point before nuclear envelope breakdown (NEB) at $t = 0$ min in (i) to spindle bipolarity at $t = 10$ min in (iii). (B) Still frames from a single simulation showing initial centrosome positioning at $t = 0$ min in (i) to spindle bipolarity at $t = 10$ min in (iii). The corresponding simulation is shown in Movie M1 in the Supporting Material. (C) Distributions of initial distance between spindle poles from live-cell imaging (Data) and simulations (Sim). (D) Plot of the fraction of cells (Data) and simulations (Sim) that achieve bipolarity by 5 and 10 min. (E) Plot of the spindle length over time from live-cell imaging (Data) and simulations (Sim). Error bars are standard deviation. Biological data are captured at 5 min increments; a cubic spline is used to generate the curve. All averages for (C)-(E) calculated from at least 40 cells and 30 simulations. (F) Still frames from live-cell imaging of RPE cells expressing GFP-centrin. (G) (i) Experimental traces of centrosome movement from the movie shown in (F), where color denotes time (min). (G) (ii) Traces of centrosome movement from a single simulation, where the two lines correspond to the two centrosomes, and color denotes time (min). Red 'x' is initial centrosome position, black asterisk is final centrosome position. (H) (i) Centrosome velocities over time from movie shown in (F). (H) (ii) Centrosome velocities over time from simulation shown in (G)(ii). Each line is a centrosome. Figure from Mercadante, et al. (2021) [167].

to validate model outputs, we performed live-cell imaging of RPE cells stably expressing an α-tubulin-EGFP transgene (Fig.16 A) or a GFP-tagged centrosome marker (GFP-centrin) (Fig.16 F). Spindle MTs are anchored at centrosomes by crosslinking and motor proteins to form spindle poles, allowing analyses of either spindle pole or centrosome position to be used to quantify centrosome movement in space and time. We used RPE cells expressing α-tubulin-EGFP to inform initial conditions of the model (Fig.16 A). We quantified intracentrosomal distance just prior to nuclear envelope breakdown (NEB), defined as the first point in time at which GFP-tubulin is no longer visibly excluded from the nuclear region. This analysis reveals a wide distribution, with initial centrosome distances ranging between 3.9 and 16.6 μm (Fig.16 C). To mirror this distribution of centrosome positions in our model, we initialize centrosomes to be randomly placed at least 7.5 μm from the center of the cell, achieving a range of distances between 4.2 and 14.75 μm (Fig.16 C).

Live-cell imaging was used to monitor centrosome movement and spindle bipolarity, capturing centrosome separation at early time points (Fig.16 E,F,G(i)) until an eventual bipolar spindle is achieved and maintained at an average spindle length of 12 μm (Fig.16 E). Image analyses further reveal that 40% of cells achieve spindle bipolarity by 5 min and 96% by 10 min (Fig.16 D). Quantification of bipolar spindle length from live-cell imaging is consistent with fixed-cell image analysis of RPE cells with stable MT-chromosome attachments in Fig.15. By tracking individual centrosome positions in time, we calculate that centrosome velocity is less that 0.1 μm/sec (Fig.16 H(i)). While mitotic progression has been well characterized, performing this analysis provides data to directly integrate and compare with our model.

We have parameterized our model such that mitotic timing, bipolar spindle length, and centrosome velocity closely match our experimental measurements. Where available we used parameters that have been well established (summarized in Table 1), and where necessary we have defined and optimized new parameters to closely capture biological phenomena (see Appendix (Chapter 9), Tables 12,13). Centrosomes are initialized within a 7.5μm

radius from the cell center to capture the distribution of centrosome positioning at mitotic entry in cells (Fig. 16 C). Late time points of our model resemble a bipolar spindle with asymmetrically distributed MTs, with an increased density towards the center of the spindle structure (Fig.16 B(iii), Fig.12 D). MTs in the interpolar region (the region between poles) are interacting and generating force (Eqs.(11),(12)), allowing the maintenance of this bipolar configuration. Model analysis shows that 35% of simulations achieve spindle bipolarity by 5 min and 95% by 10 min (Fig.16 D). Furthermore, an average bipolar spindle length of 17 μm is achieved (Fig.16 E). While this is a longer spindle length than that seen in control RPE cells, it is consistent with measured spindle lengths from RPE cells depleted of Nuf2 which, like our model, lack kinetochore-driven forces (Fig.15 C). Centrosome movement and velocity, quantified by centrosome movement from simulations, similarly resembles biological results in single cells (Fig.16 G,H). These results suggest that our parameterized model closely captures the dynamics of mitotic progression, which we use as our base case for results discussed in Chapter 3.

3 Modeling Reveals Cortical Dynein-Dependent Fluctuations in Bipolar Spindle Length

3.1 Introduction

Discerning the distinct role(s) of motor-dependent forces on mitotic progression has been challenging as some mitotic motors have two or more regions of localization and/or functions that are independently regulated in the cell [200, 220]. Dynein, for example, is localized to and interacts with MTs at spindle poles, kinetochores, and the cell cortex (expanded upon in Section 1.3) [200]. Cell biological approaches can be limited in their ability to selectively perturb one localization or function of this important motor. In the biophysical model described in Section 2.2, we consider cortical- and spindle pole-localized dynein independently, allowing us to assess the force generation of each population separately. The model also explores temporal changes in motor-dependent forces and their impact of spindle dynamics. Analysis of such forces through mitotic progression allows us to answer outstanding questions regarding the balance of forces during cell division.

Using a combined experimental-modeling approach, we explore the impact of cortical dynein activity on spindle bipolarity and test how force perturbations impact bipolar spindle length in the absence of cortical dynein. Experimentally, we use siRNA-mediated gene silencing to directly target the localization of dynein at the cell cortex, then used fixed and live-cell imaging to elucidate the impact of cortical dynein activity on spindle dynamics. We directly compare our experimental results to novel predictions made by our model regarding the forces required for spindle dynamics.

3.2 Motor Protein Perturbations Alter Spindle Bipolarity

The mitotic spindle has been extensively studied, and our understanding of the force requirements for spindle bipolarity has been determined primarily through experimental ma-

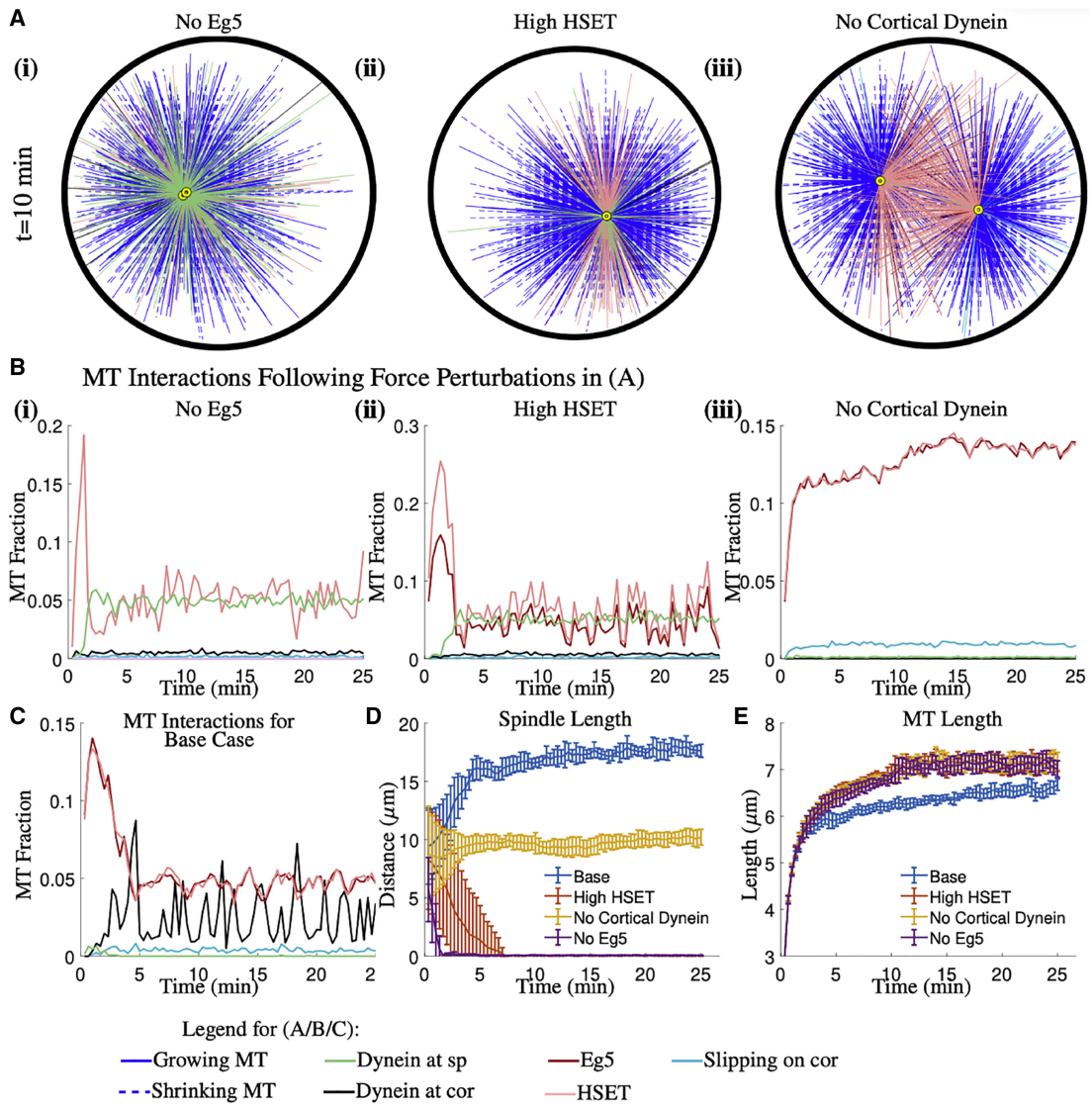

Figure 17: **Motor perturbations impact spindle bipolarity.** (A) Still frame from a simulation at t=10 min with: (i) no Eg5 binding, (ii) high HSET binding, or (iii) no cortical dynein binding. Colors indicate the force generated by each MT, defined in the legend. (B) Plot of the average percent of MTs in each force-generating state over time with: (i) no Eg5 binding, (ii) high HSET binding, or (iii) no cortical dynein binding, and (C) the base case. (D) Plot of the average distance between spindle poles over time for the base case and each single force perturbation. (E) Plot of the average length of MTs over time. All averages are of 10 simulations and error bars shown correspond to standard deviation. Figure from Mercadante, et al. (2021) [167].

nipulation of force-generating motor proteins. While informative, biological assays can induce potential off-target effects and impact multiple cellular processes. In contrast, mathematical and computational modeling allows for the specific modulation of individual motor

populations and affords temporal control of such perturbations to defined stages of mitosis. Therefore, to determine how motor proteins considered in our model (described in Chapter 2.2) impact spindle bipolarity, we independently perturbed motor function of Eg5, HSET, and cortical dynein. We accurately reflect perturbed motor activity by altering the binding probability of the motor β from the base case of $P_\beta = 0.5$ (Table 1). All other parameters remain unchanged from the base case, allowing us to specifically determine the impact of altered motor activity on spindle bipolarity.

Biological data indicates that loss of Eg5 activity results in failed centrosome separation and the formation of a monopolar spindle [115, 156, 162, 181, 219]. To determine if our model is able to capture this phenomenon, we simulate loss of Eg5 activity by setting the probability of Eg5 binding to MTs (P_E) to zero. Our simulations with loss of Eg5 activity result in failure to establish a bipolar spindle (Fig.17 A(i),D), and maintained spindle collapse through the duration of the simulation. Consistent with the requirement of Eg5 for centrosome separation and early bipolar spindle formation in cells, our simulations with no Eg5 activity show that centrosomes collapse to a monopolar spindle is immediate, with a monopolar spindle being formed in less than 2 min (Fig.17 D). Analysis of the fraction of MTs bound to motor proteins over time reveals that HSET activity remains unchanged from the base condition (Fig.17 B(i),C). However, spindle pole-localized dynein becomes relevant with loss of Eg5, where it helps to maintain close proximity of centrosomes following spindle pole collapse (Fig.17 B(i),C).

Biological results also show that high HSET activity increases the frequency of monopolar spindles [222, 277, 278]. To test that our model accurately reflects this role of HSET activity, we mimic HSET overexpression by setting the probability of binding to MTs (P_H) equal to one. Consistent with published biological data, our model captures monopolar spindle formation with high HSET activity (Fig.17 A(ii),D). We observe that monopolar spindle formation occurs almost immediately, with all simulations having a fully collapsed spindle by t=5 min (Fig.17 D). Similar to the condition with no Eg5, the fraction of MTs

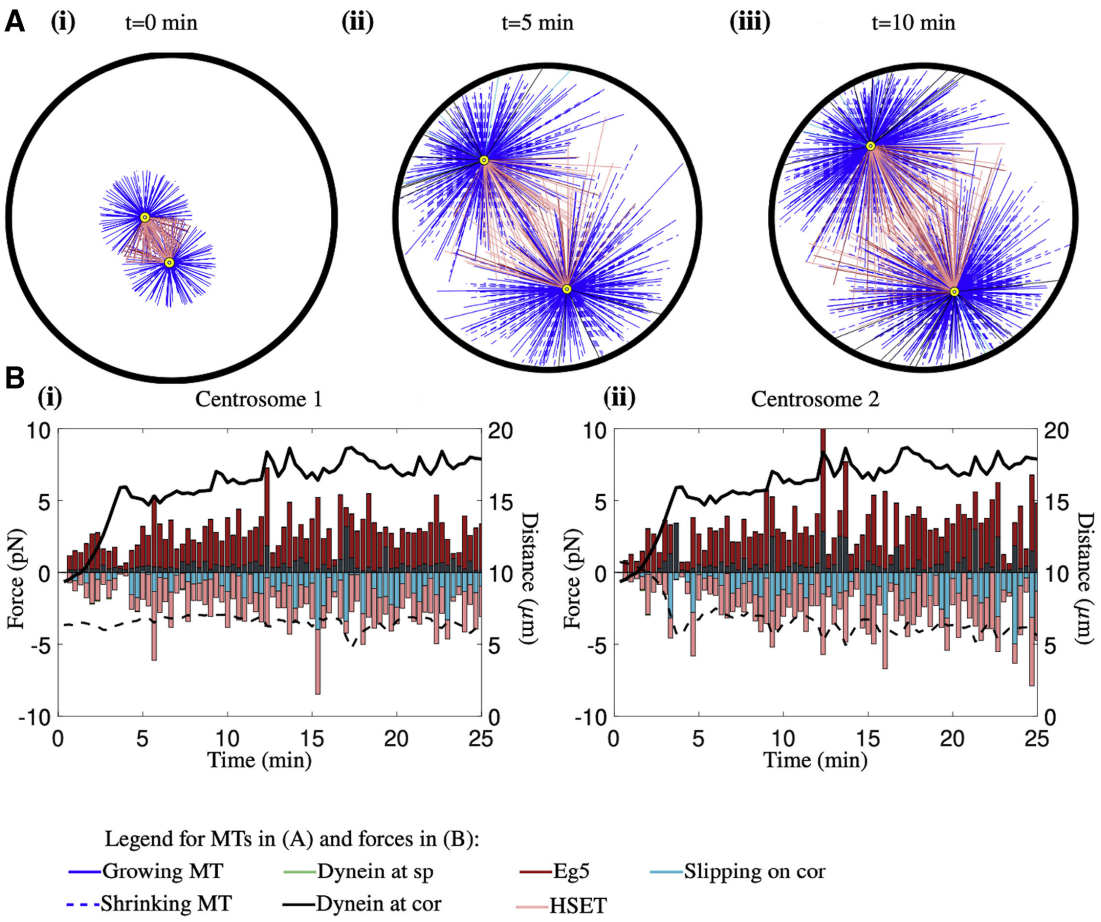

Figure 18: **Forces are dynamic over time, enabling the formation and maintenance of a bipolar spindle.** (A) Still frames from a simulation from initial centrosome positioning (i) to spindle bipolarity (iii). MT color represents its "state", defining the force that it generates. (B,C) Force plots of centrosome "1" and centrosome "2" in the direction of the vector between the two centrosomes, where a positive force brings centrosomes together and negative force pushes centrosomes apart. Black solid line shows spindle length over time and black dashed line shows the absolute minimum centrosome distance to the cell cortex over time. Figure from Mercadante, et al. (2021) [167].

bound to spindle pole-localized dynein is increased with high HSET activity compared to the base condition (Fig.17 B(ii),C). These results suggest that spindle pole dynein is similarly important in maintaining a monopolar spindle when HSET activity is high.

Due to the multiple functions of dynein at spindle poles, kinetochores, and the cell cortex [78, 91, 122, 128], biological approaches have been unable to discern the specific role of cortical dynein in bipolar spindle formation. To address this limitation, cortical dynein activity was depleted in our model by setting the probability of binding to MTs

(P_d) to zero. Our simulations indicate that specific loss of cortical dynein results in shorter bipolar spindles, decreased from 17 μm in the base case to 10 μm (Fig.17 A(iii),D). We additionally see a greater than 2-fold increase in MTs bound to Eg5 and/or HSET when cortical dynein activity is absent compared to the base case, where the percent of MTs bound to both Eg5 and HSET increases from 6% in the base case to 15% in the absence of cortical dynein (Fig.17 B(iii),C).

None of the single motor protein perturbations described have a significant impact on average MT length compared to the base condition (Fig.17 E). As such, the changes in bipolar spindle length following perturbations to motor activity are strictly a result of altered forces on the centrosomes and not a consequence of limitations imposed by altered MT lengths. Combined, these results indicate that our model both captures known changes in bipolar spindle length following loss of Eg5 or overexpression of HSET, and demonstrates a decrease steady-state spindle length following loss of cortical dynein.

3.3 Cortical Dynein is a Primary Regulator of Bipolar Spindle Length

Our biophysical model used to describe and explore the dynamics of bipolar spindle formation and maintenance has the benefit of discretely defined MTs, each of which can generate force depending on its length and position relative to other intracellular components (detailed in Chapter 2.2, Fig.18 A). To explore how the magnitude and direction of forces on centrosomes change during spindle formation, we assessed each component of the force over time with respect to $\vec{V}_{cent}$, the unit vector between centrosomes (Fig.9 A) (using the projection of the total forces in the direction of $\vec{V}_{cent}$). We considered a positive force to be one that increases spindle length (i.e. Eg5/cortical dynein) and a negative force to be one that decreases spindle length (i.e. HSET/dynein at spindle poles/pushing on the cell cortex).

To visualize how forces contribute to spindle dynamics, force plots for each centrosome were overlaid with curves for spindle length and the minimal centrosome distance to the

cell cortex over time (Fig.18 B(i)-(ii)). In our base case, where we have no perturbed motor activity, we find dynamic and reproducible force-dependent changes in spindle length. Our analysis shows that forces driving centrosome movement are dominated by Eg5 at early time points (t<5 min), consistent with the known biological role of Eg5 in mitosis [113, 117, 242]. While averaging over many simulations of the base case show that a stable bipolar spindle length of 17μm is achieved (Fig. 16 E, Fig. 43 B in the Section 9), analysis of individual simulations indicate that this is a quasi steady-state, where rather than remaining constant, fluctuations in bipolar spindle length occur. Observing how forces change over time reveals that these fluctuations coincide with increased cortical dynein-derived force (Fig. 18 B). These data implicate cortical dynein in orchestrating dynamic changes to bipolar spindle length during mitosis.

3.4 Cortical Dynein Drives Fluctuations in Spindle Length After Spindle Bipolarity is Achieved

To define the forces required for fluctuations in bipolar spindle length we explored the consequences of perturbing cortical dynein pulling forces. To mimic loss of cortical dynein activity we altered $P_{d_{cor}}$, the probability of MTs binding to dynein at the cell cortex. As $P_{d_{cor}}$ is reduced, bipolar spindle length decreases from 17.9 μm when $P_{d_{cor}} = 0.5$ to 15.6 μm when $P_{d_{cor}} = 0.3$, and 10.3 μm when $P_{d_{cor}} = 0$ (Fig. 19 A), implicating cortical dynein in the regulation of steady-state bipolar spindle length.

To define a time-dependent relationship between bipolar spindle length and cortical dynein binding and pulling forces, we performed quantitative time-series analyses. The data is represented as a kymograph, a graphical representation of position over time, where the y-axis represents time (Fig. 19 B). In each plot, $x = 0$ is the center of the cell and $x = -15$, $x = 15$ are the cell boundaries. Red asterisks indicate centrosome position at 20 sec time intervals. We used peak prominence [161], defined as the vertical distance between the height of a peak and its lowest contour line, as a readout of significant changes in

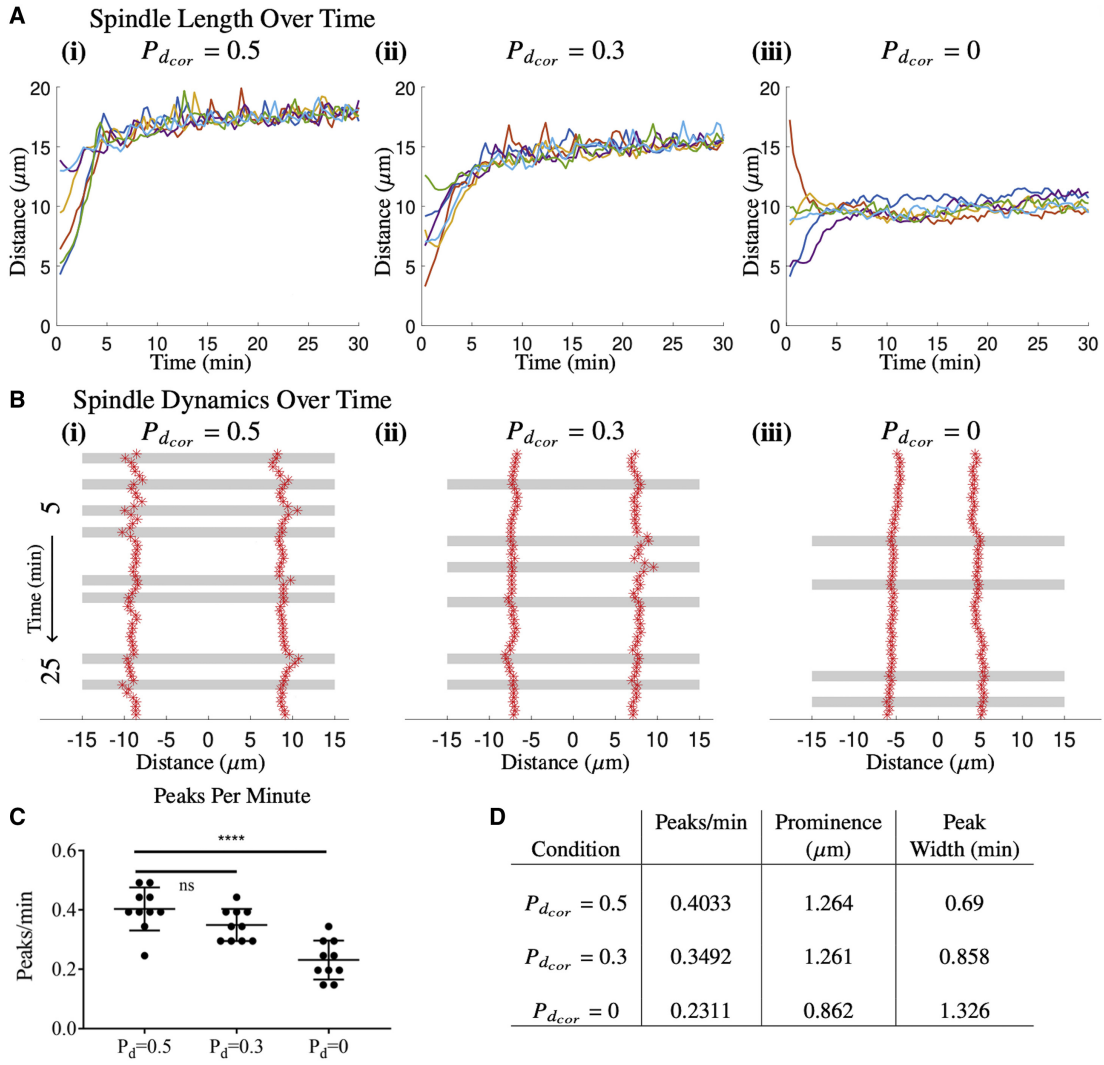

D

Condition	Peaks/min	Prominence (μm)	Peak Width (min)
$P_{d_{cor}} = 0.5$	0.4033	1.264	0.69
$P_{d_{cor}} = 0.3$	0.3492	1.261	0.858
$P_{d_{cor}} = 0$	0.2311	0.862	1.326

Figure 19: **Cortical dynein regulates spindle length and bipolar spindle dynamics.** (A) Curves of spindle length over time for 10 simulations with a dynein binding probability of 0.5 in (i), 0.3 in (ii), and 0 in (iii). (B) Representative kymograph of a single simulation with dynein binding probability 0.5 in (i), 0.3 in (ii), and 0 in (iii) from 5 to 25 minutes. Red asterisks are centrosome position plotted every 20 seconds, gray bars indicate prominent peaks in spindle length. (C) Plot of the number of peaks per minute from 10 simulations with dynein binding probability 0.5, 0.3, and 0. Each dot is a simulation, error bars are mean and SD. ****p<0.0001, ns indicates not significant. (D) Table showing average number of peaks per minute, average peak prominence, and average peak width over 10 simulations for each condition with dynein binding probability 0.5, 0.3, or 0. Significance was determined by a one-way ANOVA with Dunnett's test for multiple comparisons (****<0.001, ns indicates not significant). Figure from Mercadante, et al. (2021) [167].

spindle length. Peaks identified as significant had a prominence greater than the minimum average standard deviation within spindle length traces between the conditions $P_{d_{cor}} = 0.5$,

$P_{d_{cor}} = 0.3$, and $P_{d_{cor}} = 0$. As shown in Fig. 19 B, C, D, we find that fluctuations in bipolar spindle length have both decreased frequency (peaks/min), decreased amplitude (prominence), and increased duration (width) when cortical dynein activity is decreased. Specifically, we see a 14% and 43% decrease in the number of peaks per minute from the base condition when $P_{d_{cor}} = 0.3$, and $P_{d_{cor}} = 0$, respectively. Furthermore, we see a 32% decrease in peak prominence when $P_{d_{cor}} = 0$, although we see no change when $P_{d_{cor}} = 0.3$, and a 24% and 92% increase in peak width when $P_{d_{cor}} = 0.3$, and $P_{d_{cor}} = 0$, respectively. Together, this data suggests that reduced cortical dynein activity reduces the frequency, amplitude, and duration of bipolar spindle length fluctuations.

3.5 Loss of Cortical Dynein Activity Disrupts Spindle Dynamics *in vivo*

To determine if cortical dynein activity similarly impacts bipolar spindle length in cells we performed fixed-cell imaging and analysis of pole-to-pole distance in RPE cells depleted of Nuf2. We disrupted cortical dynein activity via short-term chemical inhibition (Dynarrestin) or siRNA-mediated depletion of Afadin, a protein involved in localizing NuMA-dynein complexes to the cell cortex [28, 107]. Duration and concentration of Dynarrestin treatment was optimized to preferentially impair cortical dynein activity as previously described [107]. Afadin depletion was validated by qPCR (Fig.20 D) and disruption of cortical dynein localization was confirmed by reduced cortical NuMA staining intensity (Fig.20 A,B).

Consistent with our modeling results, fixed-cell imaging reveals that average bipolar spindle length is reduced from 13 μm to 11.1 μm and 9.6 μm in Nuf2 depleted cells following disruption of cortical dynein activity by Afadin depletion or Dynarrestin treatment, respectively (Fig. 21 A,B). Similar results were observed in control cells with functional kinetochore attachments following treatment with Dynarrestin, with a reduction from 11.05 μm to 8.9 μm (Fig. 22 A,B). While spindle length with Afadin depletion alone remains

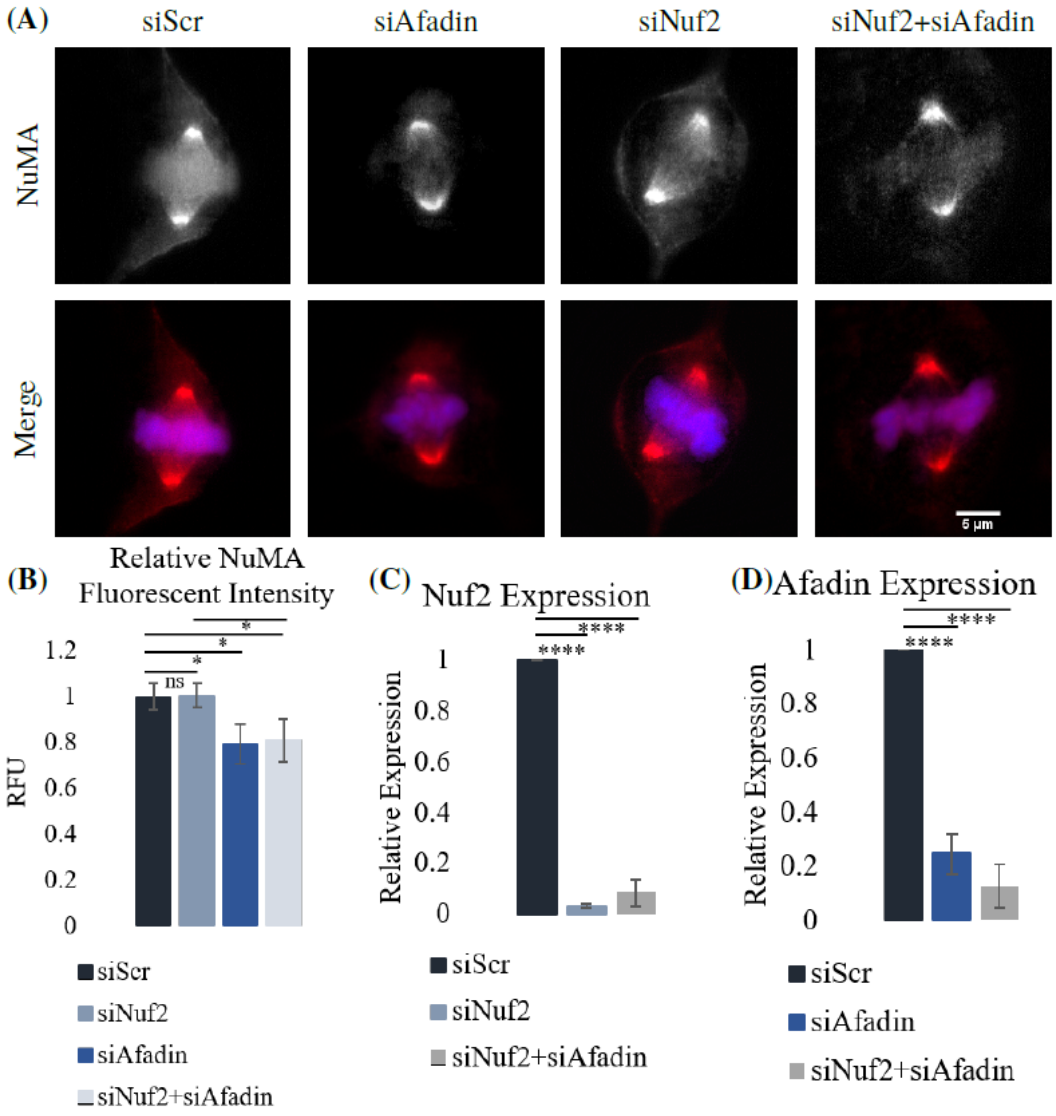

Figure 20: **Loss of Afadin disrupts cortical NuMA localization during mitosis.** (A) Immunofluorescent imaging of RPE cells following knockdown of Nuf2 and/or Afadin by siRNA. (B) Relative fluorescent intensity (RFU) of cortical-to-cytoplasmic NuMA. At least 20 cells were quantified for each condition from 3 independent replicates. (C) Quantification of Nuf2 RNA expression by qPCR. (D) Quantification of Afadin RNA expression by qPCR. Each condition was normalized to a control (siScr) and data is averaged over 3 independent replicates. Error bars are standard deviation. Significance was determined by a one-way ANOVA with Dunnett's test for multiple comparisons
(*$<$0.05, ****$<$0.001, ns indicates not significant). Figure from Mercadante, et al. (2021) [167].

comparable to the control (siScr), depletion of Afadin in the absence of Nuf2 shows a decrease in spindle length that is not statistically different than what is seen following Dynar-

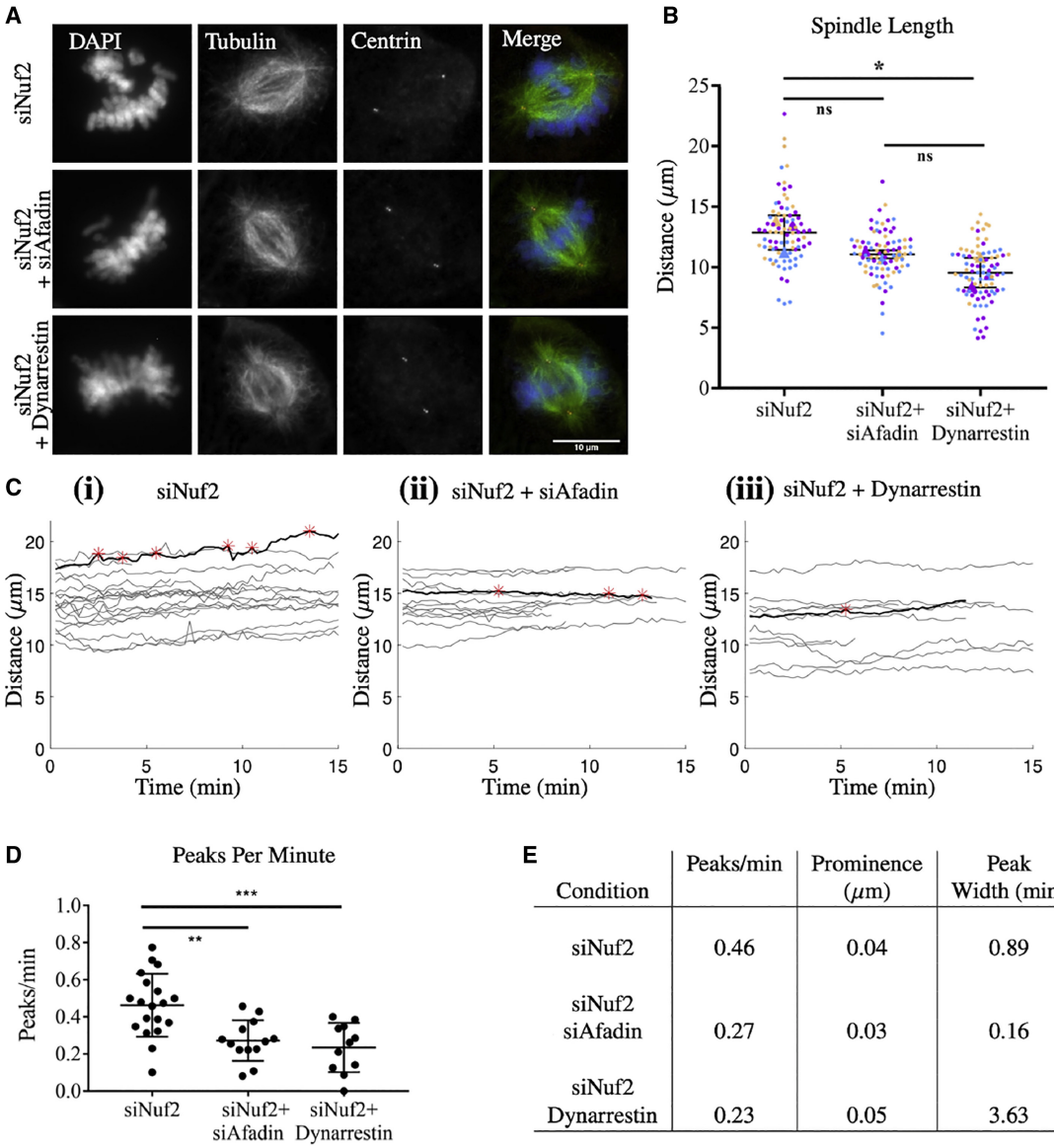

E

Condition	Peaks/min	Prominence (µm)	Peak Width (min)
siNuf2	0.46	0.04	0.89
siNuf2 siAfadin	0.27	0.03	0.16
siNuf2 Dynarrestin	0.23	0.05	3.63

Figure 21: **Fixed- and live-cell imaging captures dynein-dependent changes in bipolar spindle length and spindle dynamics.** (A) Fixed cell imaging of RPE cells stained for DAPI (DNA), Tubulin (MTs), and Centrin (centrosomes) in siNuf2, siNuf2+siAfadin, and siNuf2+Dynarrestin conditions. (B) Quantification of bipolar spindle length in siNuf2, siNuf2+siAfadin, and siNuf2+Dynarrestin conditions. Quantification performed on at least 25 cells from each condition for 3 biological replicates. Each color indicates a replicate and the average for each replicate is represented by a triangle of the same color. (C) Traces of spindle length over time of individual RPE cells expressing a GFP-centrin tag for siNuf2 (i), siNuf2+siAfadin (ii), and siNuf2+Dynarresetin (iii) conditions. Red asterisks represent significant peaks on the curve shown in black. (D) Quantification of the average number of peaks per minute in siNuf2, siNuf2+siAfadin, and siNuf2+Dynarrestin conditions. Significance determined by one-way ANOVA. (E) Table showing the average number of peaks per minute, the average peak prominence, and average peak width from each condition. At least 10 cells were captured and quantified for each condition. All error bars are SD. Significance was determined by a one-way ANOVA with Dunnett's test for multiple comparisons

(*p<0.05, **p<0.01, ***p<0.001, ns indicates not significant). Figure modified from Mercadante, et al. (2021) [167].

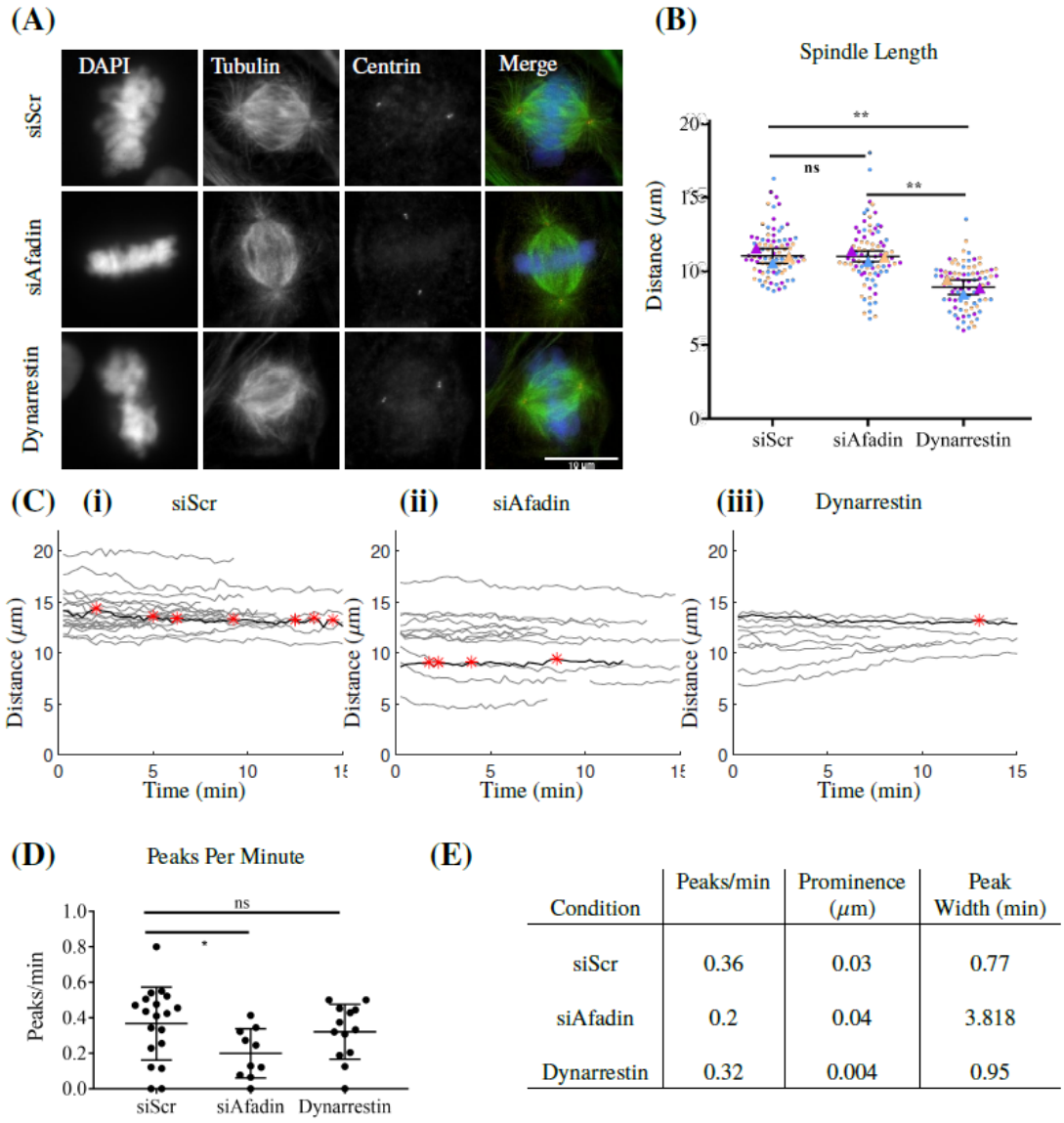

Condition	Peaks/min	Prominence (μm)	Peak Width (min)
siScr	0.36	0.03	0.77
siAfadin	0.2	0.04	3.818
Dynarrestin	0.32	0.004	0.95

Figure 22: **Fixed and live-cell imaging captures dynein-dependent changes in bipolar spindle length and spindle dynamics.** (A) Fixed cell imaging of RPE cells stained for DAPI (DNA), Tubulin (MTs), and Centrin (centrosomes) in siScr, siAfadin, and Dynarrestin conditions. (B) Quantification of bipolar spindle length in siScr, siAfadin, and Dynarrestin conditions. Quantification performed on at least 25 cells from each condition for 3 biological replicates. Each color indicates a replicate and the average for each replicate is represented by a triangle of the same color. (C) Traces of spindle length over time of individual RPE cells expressing a GFP-centrin tag for siScr (i), siAfadin (ii), and Dynarresetin (iii) conditions. Red asterisks represent significant peaks for the curve shown in black. (D) Quantification of the average number of peaks per minute in siScr, siAfadin, and Dynarrestin conditions. Significance determined by one-way ANOVA. (E) Table showing the average number of peaks per minute, the average peak prominence, and average peak width from each condition. At least 10 cells were captured and quantified for each condition. All error bars are SD. Significance was determined by a one-way ANOVA with Dunnett's test for multiple comparisons
(*p<0.05 indicates statistical significance, ns indicates not significant). Figure from Mercadante, et al. (2021) [167].

restin treatment (Fig. 21 B), (Fig. 22 A,B). These data raise the possibility that kinetochore MT attachments may stabilize spindle length in the absence of Afadin, thereby limiting the impact of decreased cortical dynein on bipolar spindle length.

To test whether fluctuations in bipolar spindle length could be observed in cells, we next performed live-cell imaging of RPE cells expressing GFP-centrin. Similar to the analysis performed on simulations, significant peaks were determined by peak prominence. In our analysis, prominent peaks were those having a prominence greater than the minimum average standard deviation within spindle length traces from the following six conditions: siScr, siAfadin, Dynarrestin treated, siNuf2, siNuf2 + siAfadin, siNuf2 + Dynarrestin treated. Consistent with our simulations, we observe an average of 0.36 peaks/min in control cells (siScr) and 0.46 peaks/min in cells depleted of Nuf2 (siNuf2) that lack stable chromosome attachments (Fig.21 C,D,E, Fig.22 C,D,E). We used Afadin depletion (siAfadin) or Dynarrestin treatment, as described previously, to determine if loss of cortical dynein activity impacts spindle length fluctuations. In Nuf2 depleted cells, we see a significant 41% and 50% decrease in the average number of peaks per minute with Afadin depletion and Dynarrestin treatment, respectively (Fig.21 C,D,E). We also see a significant 44% decrease in the number of peaks per minute in the absence of Afadin alone (Fig.22 C,D,E). These results are consistent with our model, where loss of cortical dynein decreases the number of peaks per minute by 43% (Fig.19 C,D). However, we do not see a significant decrease with Dynarrestin treatment, indicating a possibility of drug-induced alterations to spindle structure or stability following extended treatment through the duration of imaging. Together, model predictions and biological results implicate cortical dynein activity in spindle length fluctuations during mitosis.

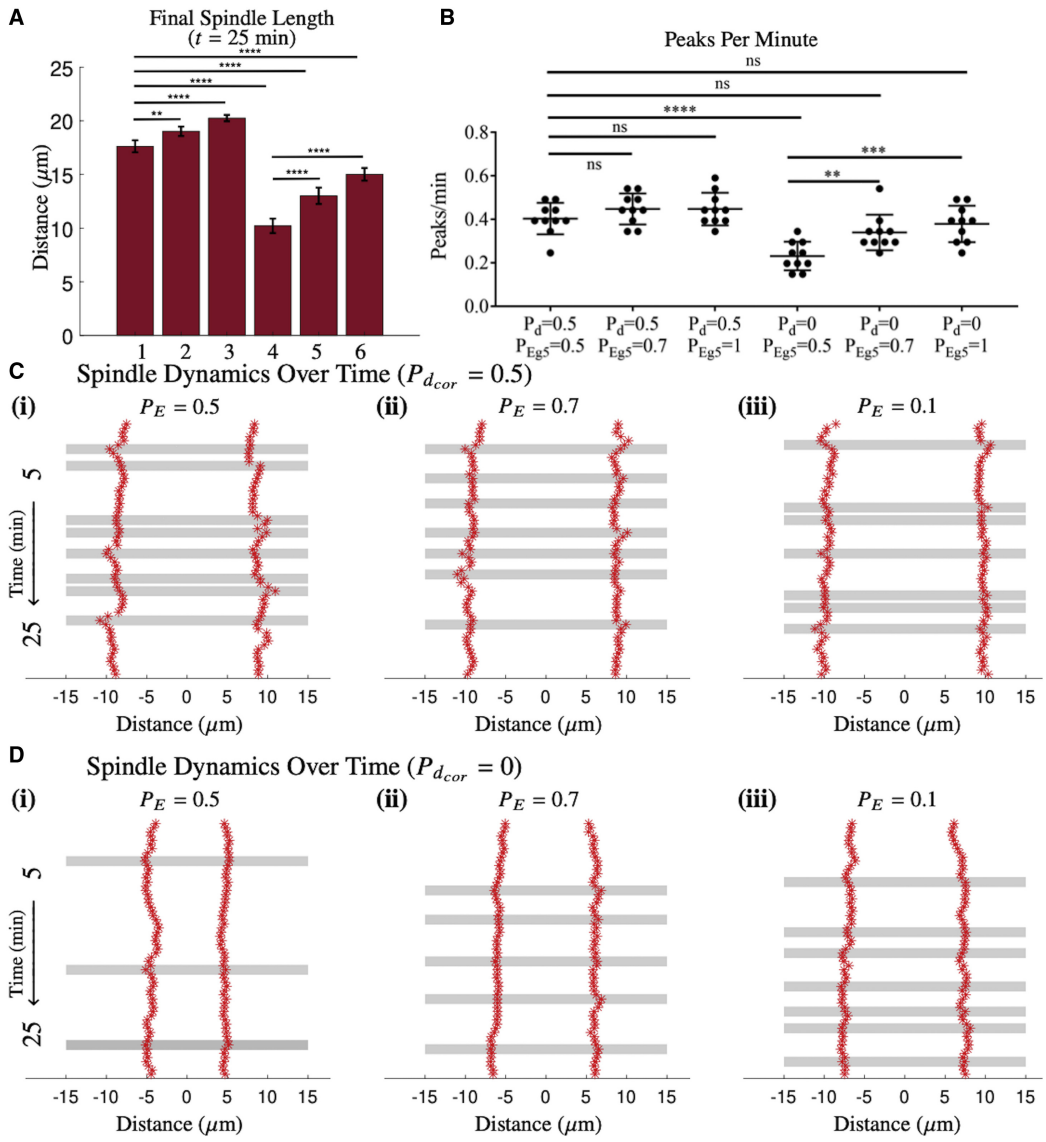

E

Condition	$P_{d_{cor}} = 0.5$ $P_E = 0.5$	$P_{d_{cor}} = 0.5$ $P_E = 0.7$	$P_{d_{cor}} = 0.5$ $P_E = 1$	$P_{d_{cor}} = 0$ $P_E = 0.5$	$P_{d_{cor}} = 0$ $P_E = 0.7$	$P_{d_{cor}} = 0$ $P_E = 1$
Peaks/min	0.4033	0.4475	0.4475	0.2311	0.3393	0.3787
Prominence (μm)	1.264	1.173	1.106	0.862	0.8994	0.9471
Peak Width (min)	0.69	0.69	0.79	1.326	0.965	0.94

Figure 23: **High Eg5 activity rescues spindle length fluctuations in the absence of cortical dynein.** (A) Bar graph of final spindle length from 10 simulations for each condition: (1) $P_{d_{cor}} = 0.5$, $P_E = 0.5$, (2) $P_{d_{cor}} = 0.5$, $P_E = 0.7$, (3) $P_{d_{cor}} = 0.5$, $P_E = 1$, (4) $P_{d_{cor}} = 0$, $P_E = 0.5$, (5) $P_{d_{cor}} = 0$, $P_E = 0.7$, (6) $P_{d_{cor}} = 0$, $P_E = 1$. (B) Quantification of the number of peaks per minute from 10 simulations for each condition. Each dot is a simulation. (C/D) Representative kymographs of varied Eg5 binding probabilities, in the presence (C) or absence (D) of cortical dynein. Gray bars indicate prominent peaks in spindle length. (E) Table of the average number of prominent peaks, peak prominence, and peak width for each condition. All data averaged over 10 simulations. All error bars are SD. Significance was determined by a one-way ANOVA with Dunnett's test for multiple comparisons

(**p<0.01, ***p<0.001, ****p<0.0001, ns indicates not significant). Figure from Mercadante, et al. (2021) [167].

3.6 Modeling Reveals That High Eg5 Activity Rescues Spindle Length Fluctuations in the Absence of Cortical Dynein

To further define the relationship between MT-derived forces and the maintenance of spindle bipolarity in the presence or absence of cortical dynein, we increased Eg5 activity thereby increasing the outward force on each centrosome (i.e. pushing away from each other). We find that increasing Eg5 activity, by increasing the binding probability of Eg5 to MTs (P_E), significantly increases bipolar spindle length, regardless of cortical dynein activity (Fig. 23 A). However, reduced spindle length seen in the absence of cortical dynein is not restored with high Eg5 activity (Fig. 23 A(1),(6)), suggesting that cortical dynein pulling force, independent of Eg5 activity, is important in establishing and maintaining bipolar spindle length.

To determine if Eg5 activity impacts spindle fluctuations in bipolar spindle length, we quantified the number of peaks per minute in simulations with increased Eg5 activity with and without cortical dynein. We find that in simulations with cortical dynein activity, increased Eg5 activity, either at intermediate ($P_E = 0.7$) or high ($P_E = 1$) levels, does not significantly impact the number of peaks per minute (Fig. 23 B,C,E). However, in the absence of cortical dynein activity, increased Eg5 activity rescues spindle length fluctuations to levels that are not significantly varied from the base condition (Fig. 23 B,D,E). Increased Eg5 activity does not, however, restore reduced peak prominence nor increased peak width in the absence of cortical dynein (Fig. 23 E). These results suggest that Eg5 activity cooperates with cortical dynein-derived forces to maintain fluctuations in bipolar spindle length.

3.7 Cortical Dynein is Required for Spindle Bipolarity When HSET Activity is High

HSET overexpression is prominent in many cancer contexts where its expression corresponds with increased cell proliferation [123, 192]. This relationship with proliferation is

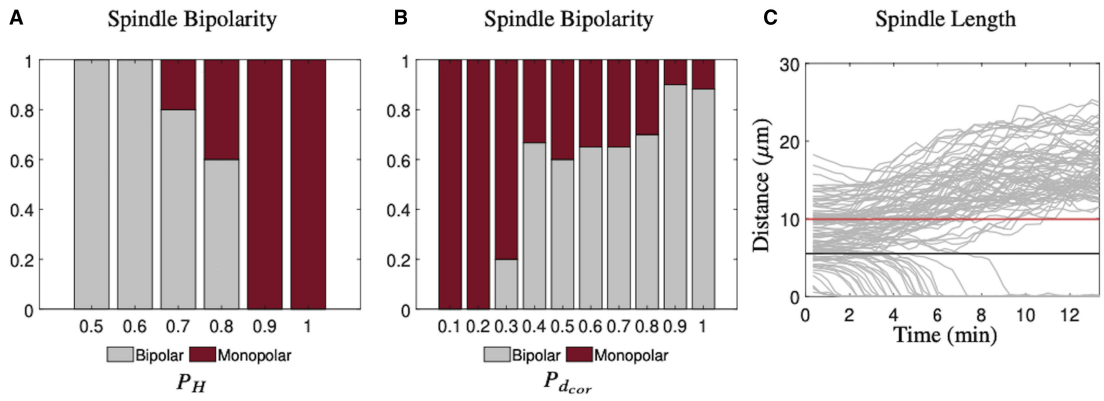

Figure 24: **High cortical dynein activity promotes spindle bipolarity in the presence of high HSET.** (A) Fraction of simulations that form a bipolar spindle with varying levels of HSET $P_{d_{cor}} = 0.5$. (B) Fraction of simulations that form a bipolar spindle in the presence of high HSET ($P_H = 0.8$) with varying levels of cortical dynein. (C) Plots of spindle length over time of simulations with high HSET ($P_H = 0.8$) and varying levels of cortical dynein that have simulations that form a bipolar spindle ($0.3 < P_{d_{cor}} \leq 1$). Red line is the average initial distance of centrosomes that separate (9.95 μm) and black line is the average initial distance of centrosomes that collapse (5.4 μm). Data from 20 simulations for each condition. Figure from Mercadante, et al. (2021) [167].

independent of centrosome number, though in cancer contexts where centrosome number is amplified, HSET is additionally required to cluster extra spindle poles into a bipolar structure [34, 79, 81, 131, 183, 199]. We have confirmed that our model captures spindle-pole collapse in the context of high HSET activity (Fig. 17 A (ii), D). We then sought to further understand the sensitivity of spindle bipolarity to HSET activity. To test this, we incrementally increased the HSET binding probability in our model from its base level of $P_H = 0.5$. Our simulations indicate that spindle bipolarity is sensitive to HSET activity, such that the incidence of spindle pole collapse increases with high HSET activity, with only 40% of simulations forming a bipolar spindle when $P_H = 0.8$ and 0% when $P_H = 0.9$ or $P_H = 1$ (Fig. 24 A). To determine the force requirements for bipolar spindle formation in the presence of high HSET ($P_H = 0.8$), we explored a range of increasing cortical dynein activity and found that spindle bipolarity is rescued by cortical dynein activity in a concentration-dependent manner, with 90% of simulations forming a bipolar spindle when $P_{d_{cor}} = 0.9$ or $P_{d_{cor}} = 1$ (Fig. 24 B).

Work from other groups indicates that HSET-dependent motor activity is a dominant force in centrosome clustering once centrosomes reach a critical distance of 7-8 μm from each other, whereas centrosome pairs are not impacted by HSET activity when they are 11-12 μm apart [207]. Consistent with this, we find that centrosomes collapse when they are, on average, initially 5.4 μm apart, and instead form a bipolar spindle when initial centrosome distance is, on average, 9.95 μm apart. Together, these results indicate that high cortical dynein activity and/or a large initial centrosome distance promotes bipolar spindle formation in the presence of high HSET.

4 Cortical Dynein Drives Centrosome Clustering and Bipolar Divisions in Cells with Supernumerary Centrosomes

4.1 Introduction

Alterations to spindle structure, such as those resulting from aberrations to centrosome number, impact the ability of chromosomes to segregate properly [1, 34]. Importantly, aberrations to centrosome number is a hallmark of cancer, and the continued proliferation of cancer cells with centrosome amplification (CA), defined as having more than the normal complement of two centrosomes, contributes to tumor heterogeneity, drug resistance, and cancer progression [81, 89, 160]. Cancer cells with CA divide efficiently by clustering their extra centrosomes into a functional bipolar spindle [131, 137, 183, 199, 207]. Therefore, targeting centrosome clustering to promote multipolar divisions resulting in nonviable daughter cells is a promising therapy for cancers with a high frequency of CA [81]. The motor protein HSET, along with proteins involved in cell-cell junctions, cortical contractility, and kinetochore-MT interactions have been characterized as potential targets to limit centrosome clustering in cancer cells [102, 131, 132, 207].

Based on the known roles of cortical dynein in spindle positioning and orientation, and our previous finding that dynein activity impacts spindle dynamics, we hypothesize that cortical dynein activity may contribute to centrosome clustering in cells with CA. Here, we use a combined experimental-modeling approach to explore the impact of cortical dynein on centrosome clustering. Modeling results suggest that uniformly distributed cortical dynein localization, similar to that considered in Chapters 2 and 3, is not sufficient to cluster centrosomes. By observing the localization of cortical NuMA in fixed cells with CA, we determine that cortical NuMA/dynein localizes asymemtrically, similar to cells with two centrosomes [122]. From this finding we hypothesize that asymmetric localization of dynein contributes to centrosome clustering by pulling centrosomes close together. By

allowing MTs to bind to cortical dynein in only a quadrant of the cell boundary in simulations, we find that centrosome movement is responsive to dynein activity, and centrosomes cluster toward the region of active cortical dynein. Additionally, we show that asymmetric dynein localization that is dynamic in time aids centrosome clustering but is insufficient to maintain clustering. Simulations further reveal a decrease in clustering efficiency in the absence of cortical dynein activity. Immunofluorescent imaging and spindle assessment in cells with CA confirms this model prediction, where loss of cortical dynein significantly disrupts centrosome clustering. Together, the results presented in this Chapter suggest that targeting cortical dynein localization and activity may be an appealing approach to prevent centrosome clustering.

4.2 Uniformly Distributed Cortical Dynein Activity Reduces Centrosome Clustering

To assess the dynamics and force requirements of centrosome clustering in cells with CA, we optimized and expanded our previously published model of bipolar spindle formation and function to have four centrosomes [167]. Updated parameter values were chosen to match experimental results and are listed in Table 2; all other parameters remain unchanged from those listed in Table 1. Our previous model assumed uniformly distributed cortical dynein localization, where MTs had an equal probability of binding to dynein anywhere on the cell boundary (Fig. 25 A,B) [167]. By visualizing where MTs bind to cortical dynein, we confirm that they bind everywhere on the cell boundary (Fig. 25 C). By assessing centrosome movement and spindle morphology in simulations with four centrosomes, we find that no centrosomes cluster under this condition (Fig. 25 D). By visualizing and quantifying the distance between centrosome pairs for each simulation, we find that centrosomes separate and remain at a distance greater than 5 μm for the entirety of the simulation (Fig. 25 E). This phenotype is consistent across 10 simulations with four centrosomes and uniformly distributed cortical dynein activity, where 0% of simulations form a clustered bipolar spin-

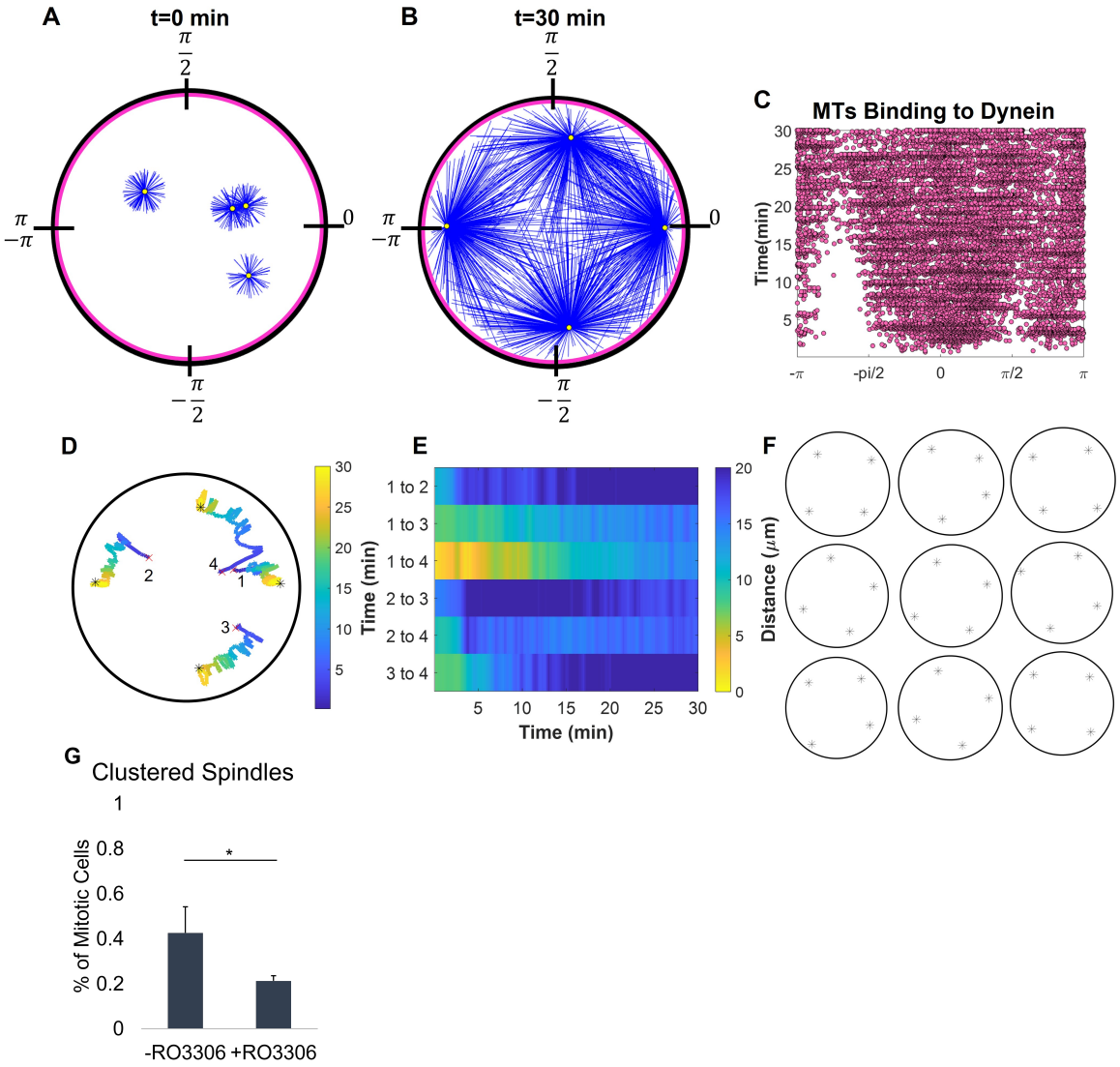

Figure 25: **Uniformly distributed cortical dynein localization disrupts centrosome clustering.** (A) Still frame of the initial time point (t=0 min) from a simulation with four centrosomes with cortical dynein localized uniformly on the cell boundary. Pink circle represents region of dynein activity. (B) Still frame of the final time point (t=30 min) from a simulation with four centrosomes with cortical dynein localized uniformly on the cell boundary. Pink circle represents region of dynein activity. (C) Plot of MTs binding to cortical dynein on the boundary of the cell ($[-\pi, \pi]$) from the simulation shown in A/B/C. Each dot is a MT binding to dynein. Time is on the y-axis, starting at time $t = 0$ at $y = 0$. (D) Traces of centrosome movement over time from the simulation shown in A/B. Red 'x' is initial centrosome position, black '*' is the final centrosome position, colorbar is time (min). (E) Heat map representing the distance between each centrosome pair over time from the simulation shown in A/B/C/D. Colorbar is distance (μm). (F) Still frames of final centrosome position (represented by black '*') from 9 simulations. Clustered spindles are represented with a red square. (G) Quantification of the percent of mitotic cells with clustered spindles in tetraploid RPE p53-/- cells with and without treatment with RO-3306. Quantification performed on at least 50 cells per condition from 3 biological replicates, errors bars are SD. Significance was determined by student's t-test (*p<0.05).

dle (Fig. 25 F).

Cortical dynein localization and activity is regulated by kinase-dependent phosphorylation of NuMA, such that inhibition of the kinases Cdk1 or Plk1 increase cortical NuMA localization in mitotic cells [127,214,216]. To test the impact of increased NuMA localization in cells with extra centrosomes, we performed fixed-cell imaging and analysis in cells with CA. To induced CA in cells, we inhibited cytokinesis via treatment with the actin assembly inhibitor dihydrocytochalasin B (DCB) in RPE cells lacking p53 (p53-/-), resulting in tetraploid cells with four centrosomes (Fig. 33 C). By assessing the percent of mitotic cells with clustered spindles, we see a significant decrease in clustering efficiency following treatment with the Cdk1 inhibitor RO-3306 (Fig. 25 G). Together, these data suggest that uniformly distributed cortical dynein localization is insufficient to cluster centrosomes and reduces clustering efficiency in cells.

4.3 Cortical Dynein Localizes Asymmetrically in Cells with Supernumerary Centrosomes

To determine the localization of cortical dynein in cells with CA, we assessed the localization of its binding partner NuMA using fixed-cell imaging and analysis. We found that 50% of mitotic cells have visible cortical NuMA (data not shown), and cells with visible or non-visible cortical NuMA was were easily identified. As such, we only assessed cells with visible cortical NuMA, similar to previous approaches [216]. By analyzing NuMA localization in fixed RPE cells with two centrosomes, we find that cortical NuMA localizes asymmetrically, consistent with previous findings [122, 216]. We found that nearly 90% of mitotic cells with visible cortical NuMA with two centrosomes (-DCB) have increased cortical NuMA localization behind 1 pole (Fig. 26 A,B). To determine the localization of cortical dynein in cells with CA, we assessed mitotic cells with visible cortical NuMA in tetraploid RPE p53-/- cells with four centrosomes (+DCB) (Fig. 26 C). We find that 95% of mitotic cells with clustered spindles, those having two spindle poles with one or more

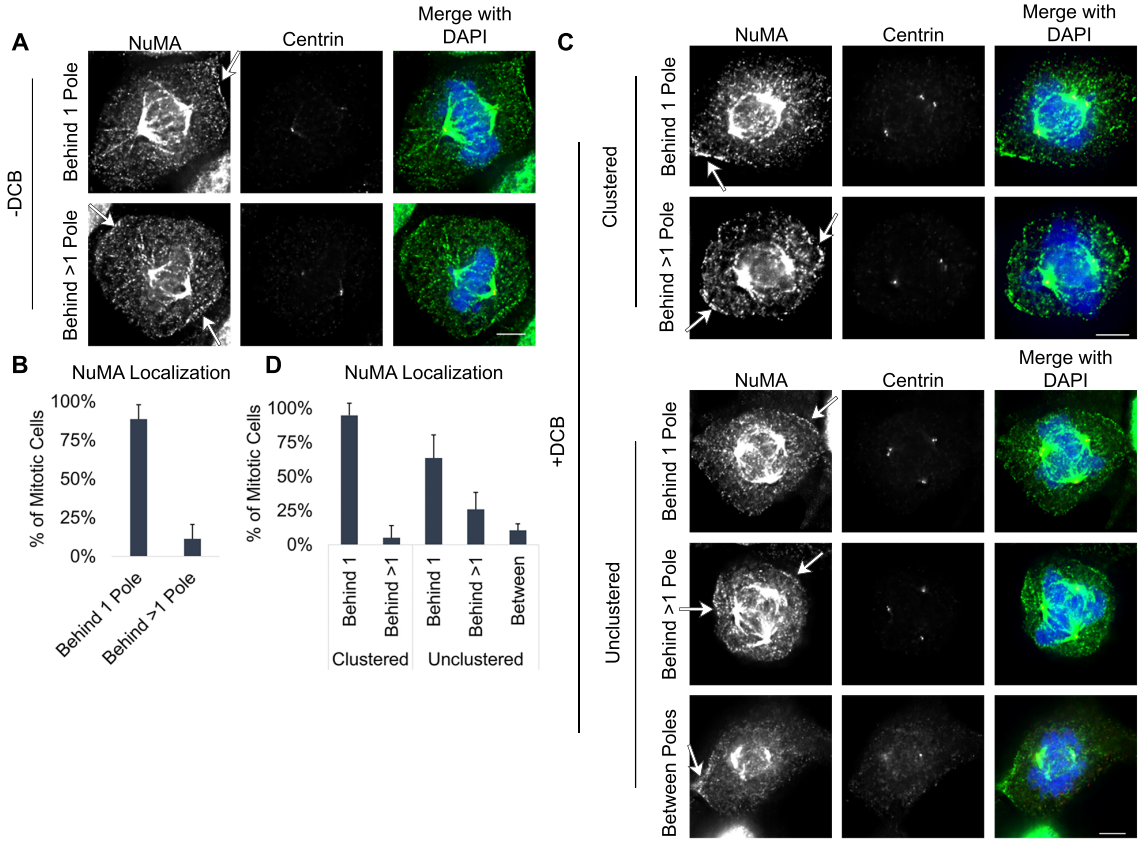

Figure 26: **Cortical dynein localizes asymmetrically in cells with CA.** (A) Fixed-cell images of RPE cells with two centrosomes (-DCB) in mitosis. (B) Quantification of NuMA localization in mitotic RPE cells with two centrosomes (-DCB) with visible cortical NuMA. (C) Fixed-cell images of tetraploid RPE p53-/- cells with four centrosomes (+DCB) in mitosis with clustered or unclustered spindles. (D) Quantification of NuMA localization in mitotic tetraploid RPE p53/- cells with four centrosomes (+DCB) with visible cortical NuMA. All scale bars are 5 μm. White arrows indicate visible cortical NuMA. All quantification was performed on at least 50 cells per condition from 3 biological replicates. Error bars are SD.

centrosome at each pole, have increased NuMA localization behind 1 spindle pole (Fig. 26 D). Similarly, the majority (65%) of mitotic cells with unclustered spindles, those having more than two spindle poles with one or more centrosome at each pole, have increased cortical NuMA localization behind 1 pole. The remaining mitotic cells with unclustered spindles have increased localization behind more than 1 or between spindle poles (Fig. 26 D). These results suggest that, similar to normal cells, cortical NuMA localization is largely

asymmetric in cells with CA.

4.4 Centrosome Movement is Responsive to Cortical Dynein Activity

To determine if cortical dynein localization contributes to centrosome movement and clustering, we leveraged the strength of our model to specify a region of cortical dynein on the cell boundary. Here we assume that localization and activity are synonymous, allowing us to modulate the region to which MTs can bind to cortical dynein to simulate asymmetric localization in cells. We allowed MTs to bind to cortical dynein, with probability $P_{d_{cor}}$, in the upper right quadrant of the cell (Fig. 27 A,B; Fig. 28 A,B). We set a small probability ($P_{d_{cor}} = 0.01$) of binding everywhere else on the cell boundary under the assumption that cortical dynein is unlikely to be entirely absent from this region. Since dynein localizes asymmetrically in cells with two centrosomes, we verified that a bipolar spindle still forms and is maintained with this defined region of asymmetric dynein in our simulations (Fig. 27 A,B). By assessing the region on the boundary where MTs bind to cortical dynein, we confirm that they primarily bind within the region $[0, pi/2]$ (Fig. 27 D; Fig. 28 D). Indeed, we confirm that a bipolar spindle forms with asymmetric dynein localization in simulations with 2 centrosomes (Fig. 27 C,E,F). Furthermore, fluctuations in bipolar spindle length, as described in Chapter 3, are still observed (Fig. 27 E). We find that the spindle orients along the axis where dynein is localized, consistent with previous findings that cortical dynein regulates bipolar spindle orientation (Fig. 27 D). This trend is consistent across 5 simulations with unique initial positions (Fig. 27 F).

To understand the impact of asymmetric cortical dynein localization on centrosome movement and centrosome clustering, we ran simulations with four centrosomes (Fig. 28 A,B). Under the condition of asymmetric dynein localization, we find that centrosomes cluster toward the region of the cell boundary where cortical dynein is localized (Fig. 28 B,C). Once again we confirm that MTs are primarily binding to the region where the probability of binding to dynein is highest, within $[0, pi/2]$ on the cell boundary (Fig. 28 D). By

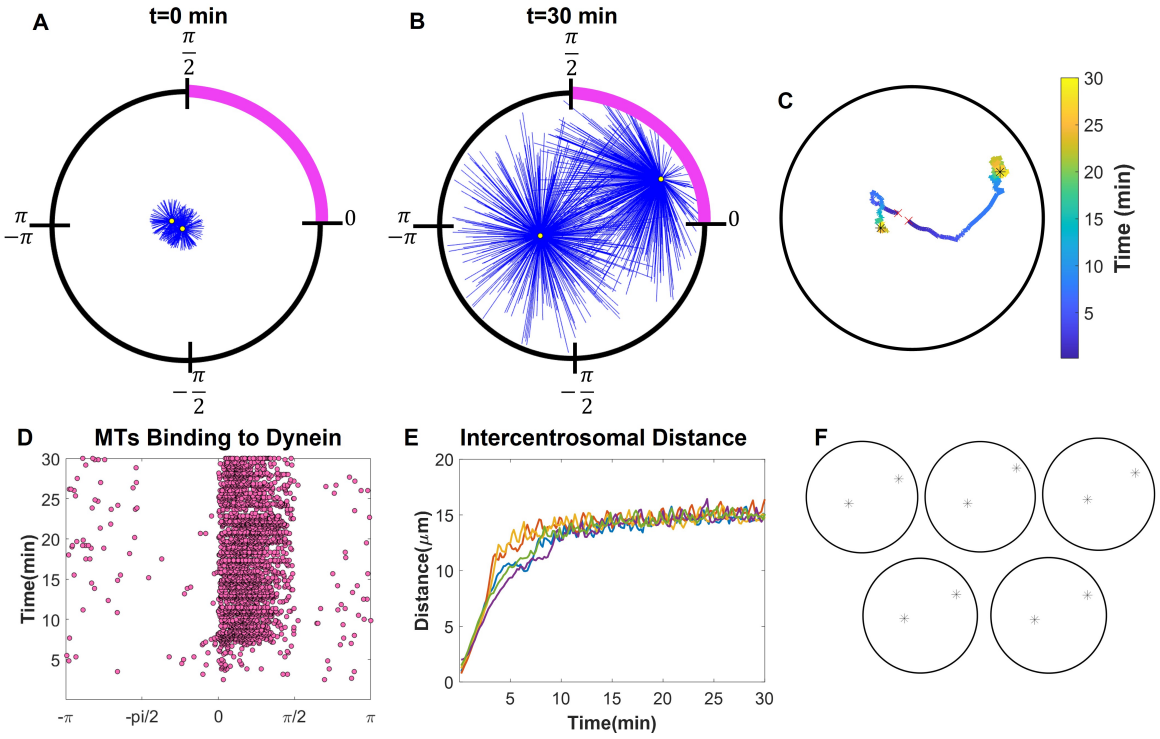

Figure 27: **Asymmetric dynein guides spindle orientation.** (A) Still frame of the initial time point (t=0 min) from a simulation with two centrosomes with cortical dynein localized asymmetrically on the cell boundary. Pink arc represents region of dynein activity. (B) Still frame of the final time point (t=30 min) from a simulation with two centrosomes with cortical dynein localized asymmetrically on the cell boundary. Pink arc represents region of dynein activity. (C) Plot of intercentrosomal distance (spindle length) from 5 simulations with two centrosomes. Each line is a simulation. (D) Still frames of final centrosome position (represented by black '*') from 5 simulations.

visualizing and quantifying the distance between centrosome pairs for each simulation, we find that once two centrosomes cluster together (achieve a distance less than 5 μm), they remain clustered (Fig. 28 E, Fig. 30 A). By assessing the final distance between centrosome pairs from 10 simulations, we find that 60% of simulations formed clustered bipolar spindles, where clustered spindles achieved a distance of less than 5 μm between at least two centrosome pairs (Fig. 28 F). In the remaining 40% of simulations, the spindle remains multipolar. However, in these simulations, two centrosomes cluster together toward the region of active cortical dynein while the other two centrosomes remain unclustered (Fig. 28 F). Together these results suggest that centrosome movement and clustering is responsive

to cortical dynein activity.

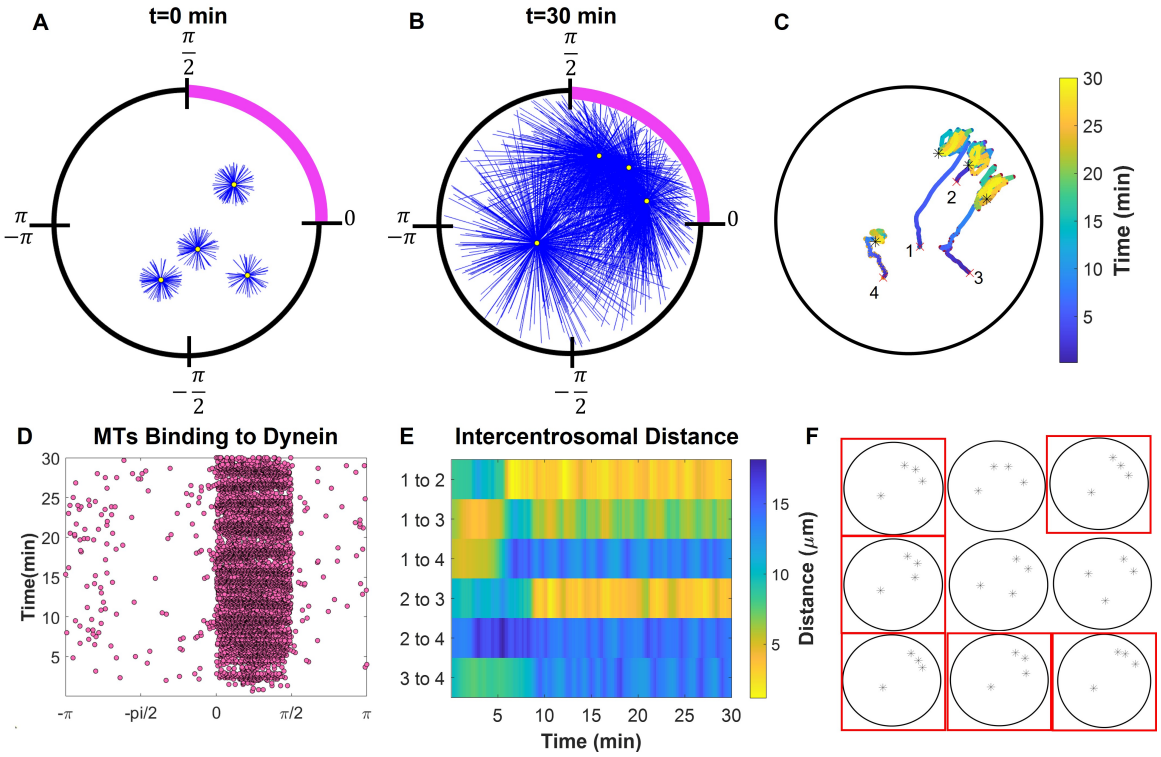

Figure 28: **Centrosome movement and clustering is responsive to cortical dynein activity.** (A) Still frame of the initial time point (t=0 min) from a simulation with four centrosomes with cortical dynein localized asymmetrically on the cell boundary. Pink arc represents region of dynein activity. (B) Still frame of the final time point (t=30 min) from a simulation with four centrosomes with cortical dynein localized asymmetrically on the cell boundary. Pink arc represents region of dynein activity. (C) Traces of centrosome movement over time from the simulation shown in A/B. Red 'x' is initial centrosome position, black '*' is the final centrosome position, colorbar is time (min). (D) Plot of MTs binding to cortical dynein on the boundary of the cell ($[-\pi, \pi]$) from the simulation shown in A/B/C. Each dot is a MT binding to dynein. The region represented in pink in A and B is $[0, \pi/2]$. Time is on the y-axis, starting at time $t = 0$ at $y = 0$. (E) Heat map representing the distance between each centrosome pair over time from the simulation shown in A/B/C/D. Colorbar is distance (μm). (F) Still frames of final centrosome position (represented by black '*') from 9 simulations. Clustered spindles are represented with a red square.

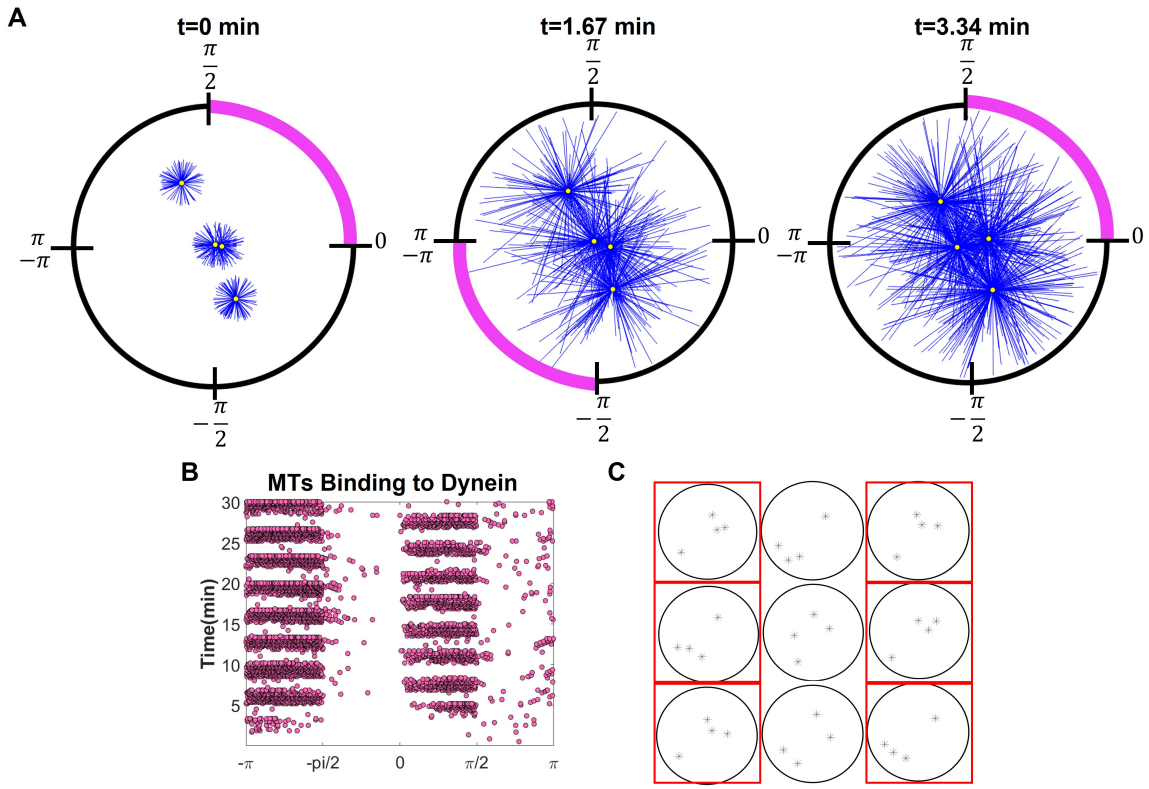

Figure 29: **Dynamic dynein aids centrosome clustering.** (A) Still frame of three time points ($t = 0, 1.67, 3.34$) from a simulation with four centrosomes with dynamic and asymmetric cortical dynein with dynein oscillations occurring with period $T = 1.67$ min. Pink arc represents region of dynein activity. (B) Plot of MTs binding to cortical dynein on the boundary of the cell ($[-\pi, \pi]$) from the simulation shown in A. Each dot is a MT binding to dynein. The regions represented in pink in A are $[0, \pi/2]$ and $[-\pi, -\pi/2]$. (C) Still frames of final centrosome position (represented by black '*') from 9 simulations. Clustered spindles are represented with a red square.

4.5 Dynamic Cortical Dynein Localization Aids Centrosome Clustering

Asymmetric cortical dynein localization is dynamic in human cells with two centrosomes [122]. To recapitulate this characteristic in our model, and determine its impact (if any) on centrosome clustering, we make asymmetric cortical dynein activity dynamic in time. Specifically, we allow MTs to bind to cortical dynein on one quadrant of the cell boundary (with probability $P_{d_{cor}}$) for a set period of time (defined by period value T) (Fig. 29 A). Then, the region of dynein activity shifts to the opposing quadrant for an equal period of

time, T (Fig. 29 A). We set a small probability ($P_{d_{cor}} = 0.01$) of binding everywhere else on the cell boundary. These oscillations in dynein activity continue with a period T until the final time points ($t = 30$ min) is achieved. By assessing the region on the boundary where MTs bind to cortical dynein, we confirm that they primarily bind within the region with active cortical dynein and that this region changes in time with period T (Fig. 29 B). We find that when $T = 1.67$ min, 70% (7/10) simulations form clustered bipolar spindles, i.e. two centrosome pairs achieve a distance of less than 5 μm during the simulation.

To determine if clustering is sensitive to the parameter T, we tested varying values and assessed centrosome movement and intercentrosomal distances (Fig. 30, Fig. 31). We tested varying periods of dynein oscillations by changing the parameter T ($T = 1.67, 3.33, 5, 10, 15$ min) to determine if an optimal period contributes to centrosome clustering. With a low period ($T = 1.67$ min), corresponding to short, rapid oscillations in dynein activity, we find that 70% of simulations form a clustered bipolar spindle (Fig. 29 C, Fig. 30 B). By observing the intercentrosomal distances over time under this condition, we see rapid oscillations in the distance between centrosomes (Fig. 30 B (bottom)). These oscillations correspond with changes in dynein localization (indicated by alternating black/gray lines). Specifically, we see that when dynein is active in a region, centrosomes near that region move closer together. Similarly, when dynein is removed from that region, centrosomes move apart from each other. This trend is consistent in all conditions with dynamic dynein localization, and the duration of centrosome clustering corresponds with the defined period parameter, T (Fig. 30 B,C, Fig. 31). Importantly, this is not seen when asymmetric dynein localization is static in one region (Fig. 30 A), suggesting that intercentrosomal distance is dependent on cortical dynein activity.

Previously published work suggests that cortical dynein oscillations occur on the order of 5-10 minutes in cells with two centrosomes [122]. We see a drastic increase to 100% of simulations achieving centrosome clustering when $T = 5$ min or $T = 10$ min. By observing intercentrosomal distances over the entirety of the simulation, we see that all

simulations in these conditions have time frames in which they achieve clustering, indicated by two pairs of centrosomes achieving a distance of 5 μm (Fig. 31 A,B). However, this clustering is not maintained and becomes disrupted once cortical dynein activity is removed (shifts positions) (Fig. 31 A,B). This characteristic is also seen when $T = 15$ min (Fig. 31 C). Together, these results suggest that dynamic and asymmetric cortical dynein contributes to centrosome clustering but is not sufficient to maintain clustering. Other physical and mechanical characteristics within the spindle, such as MT attachments to kinetochores or non-motor crosslinking activity, may be required to maintain centrosome clustering in the absence of cortical dynein.

Table 2: Updated parameter values for model results presented in Chapter 4. All parameters are approximated to match biological results.

Parameter	**Value**	**Description**
$P_{d_{sp}}$	0.3	Probability of binding to spindle pole dynein
P_H	0.7	Probability of binding to HSET
$\mathcal{D}_r$	2 μm	Distance for repulsive forces
K	0.35	MT length-dependent scaling factor
C	0.01	Antiparallel crosslinking scaling factor
s	0.075 μm^{-1}	Scaling for catastrophe frequency
R	1 μm	Scaling for repulsive forces
ξ	41.2 pNs	Drag coefficient

4.6 Loss of Cortical Dynein Disrupts Centrosome Clustering

To determine if centrosome clustering is dependent on cortical dynein activity, we remove dynein activity within the model by setting the probability of binding, $P_{d_{cor}} = 0$ (Fig. 32 A,B). By visualizing centrosome movement in simulations with no cortical dynein, we see an increased distance between the centrosomes and the cell boundary compared to Fig. 25 D and Fig. 28 C (Fig. 32 C). This is indicative of a lack of pulling forces toward the cell boundary. Additionally, by quantifying the distance between centrosome pairs over time, we find that in the absence of cortical dynein, centrosomes never cluster (Fig. 32 D). Out of

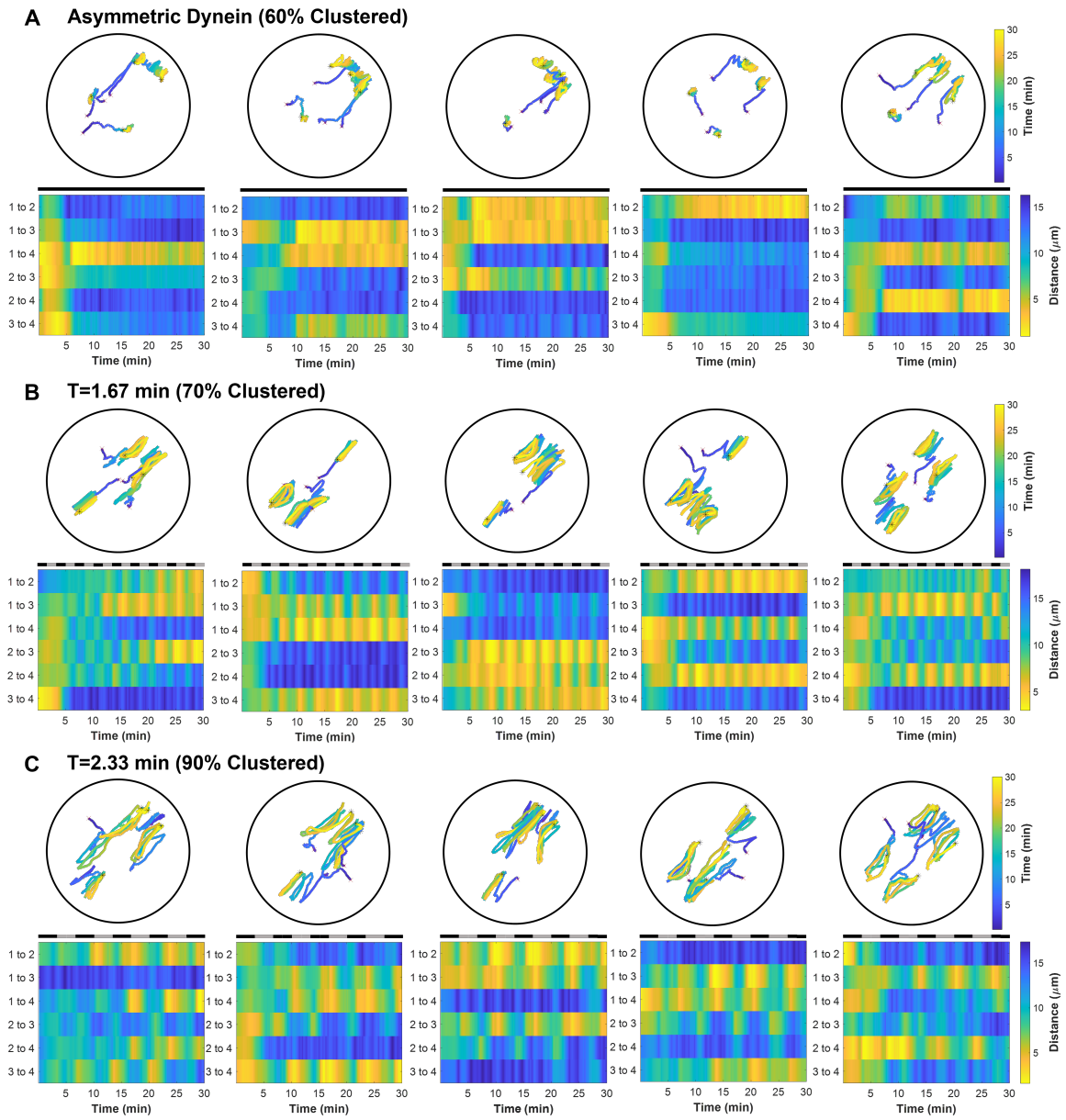

Figure 30: **Asymmetric and static dynein sustains centrosome clustering.** Traces of centrosome movement (top) and heat map of intercentrosomal distances (bottom) over time from 5 simulations with static asymmetric dynein (A), or dynamic asymmetric dynein that oscillates with period $T = 1.67$ min (B) or $T = 3.33$ min (C). In centrosome movement traces, the red 'x' indicates initial centrosome position and the black '*' indicates the final centrosome position. Above the intercentrosomal distance heat map, the black and gray bars indicate changes in dynein positioning. Black indicates dynein localization in the top right quadrant while gray indicates dynein localization in the bottom left quadrant. Clustered spindles were characterized as those having a final intercentrosomal distance of 5 μm or less between two pairs of centrosomes at the final time point. Percent clustered spindles per condition based off of 10 simulations with unique initial centrosome positioning.

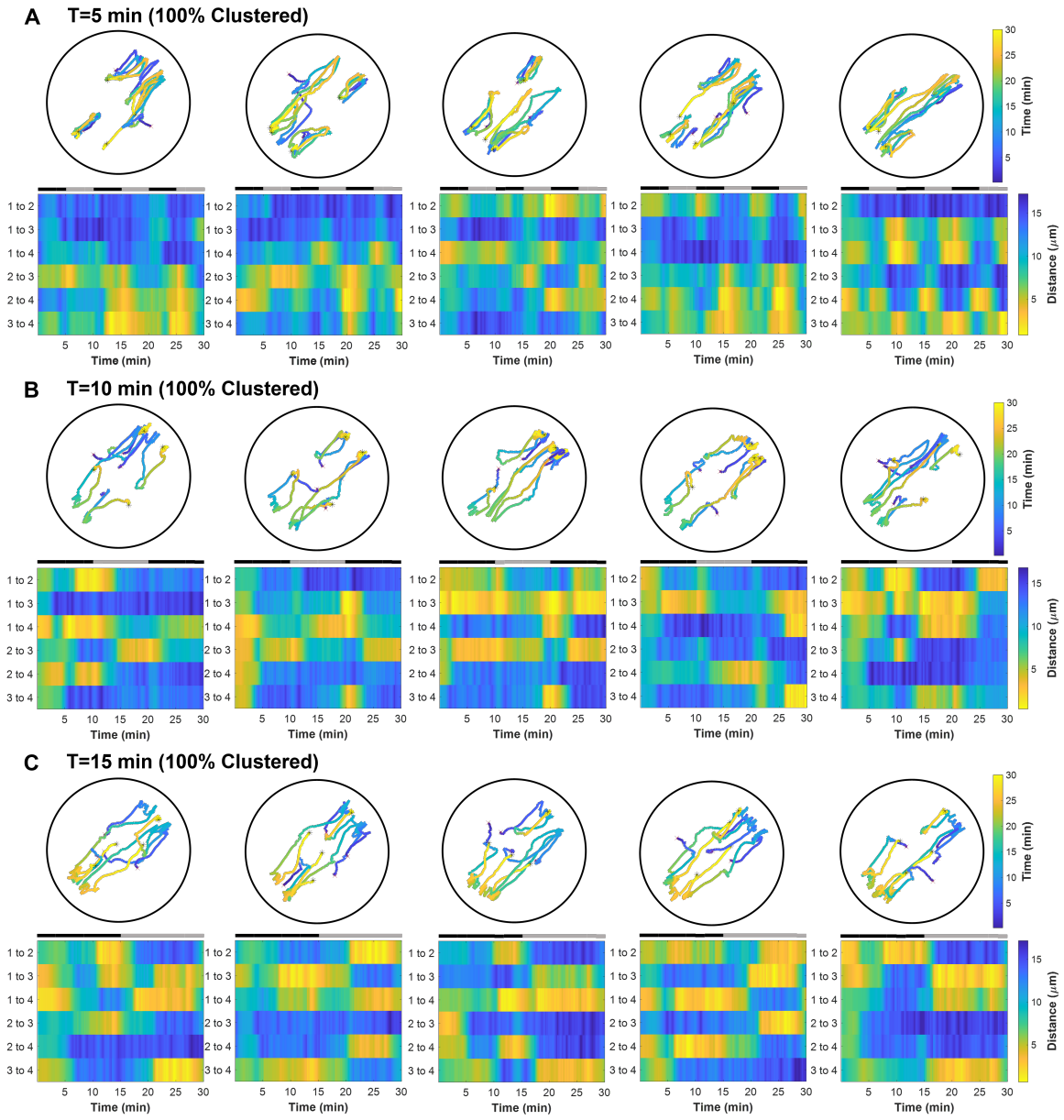

Figure 31: **Dynamic dynein activity is not sufficient to sustain centrosome clustering.** Traces of centrosome movement (top) and heat map of intercentrosomal distances (bottom) over time from 5 simulations with dynamic asymmetric dynein that oscillates with period $T = 5$ min (A), $T = 10$ min (B), or $T = 15$ min (C). In centrosome movement traces, the red 'x' indicates initial centrosome position and the black '*' indicates the final centrosome position. Above the intercentrosomal distance heat map, the black and gray bars indicate changes in dynein positioning. Black indicates dynein localization in the top right quadrant while gray indicates dynein localization in the bottom left quadrant. Clustered spindles were characterized as those achieving an intercentrosomal distance of 5 μm during the simulation. Percent clustered spindles per condition is based off of 10 simulations with unique initial centrosome positioning.

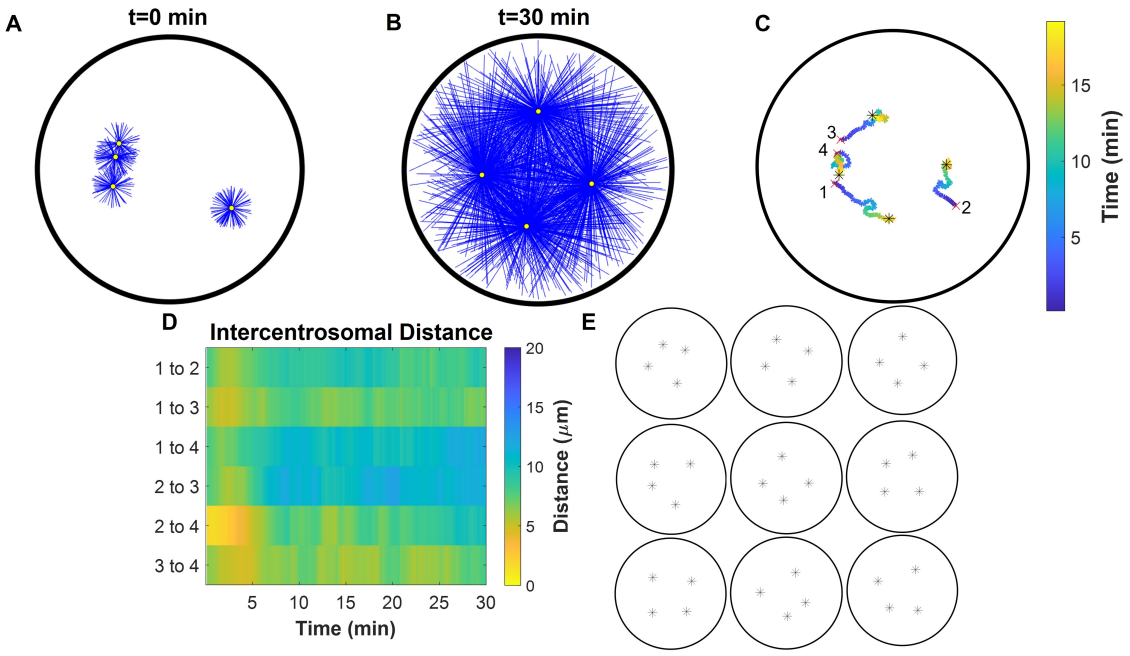

Figure 32: **Centrosome clustering efficiency is reduced following loss of cortical dynein.** (A) Still frame of the initial time point (t=0 min) from a simulation with four centrosomes with no cortical dynein. (B) Still frame of the final time point (t=30 min) from a simulation with four centrosomes with no cortical dynein. (C) Traces of centrosome movement over time from the simulation shown in A/B. Red 'x' is initial centrosome position, black '*' is the final centrosome position, colorbar is time (min). (D) Heat map representing the distance between each centrosome pair over time from the simulation shown in A/B/C/D. Colorbar is distance (μm). (F) Still frames of final centrosome position (represented by black '*') from 9 simulations.

10 simulations, none achieve a clustered bipolar spindle, as defined by achieving a distance of less than 5 μm between at least two centrosome pairs (Fig. 32 E). These results suggest that cortical dynein activity contributes to centrosome clustering.

We sought to confirm the prediction by our model that cortical dynein contributes to centrosome clustering in cells. To do this, we analyzed spindle morphology in a panel of cell lines that have either chemically induced or naturally arising CA. To induce CA we used two distinct mechanisms. First, we use an RPE cell line expressing a doxycyline-regulated construct that causes overexpression of Polo-like kinase 4 (Plk4ind) (Fig. 33 A). Overexpression of Plk4 leads to centriole over-duplication, resulting in cells with more than the normal complement of two mitotic centrosomes (Fig. 33 A). Second, as described pre-

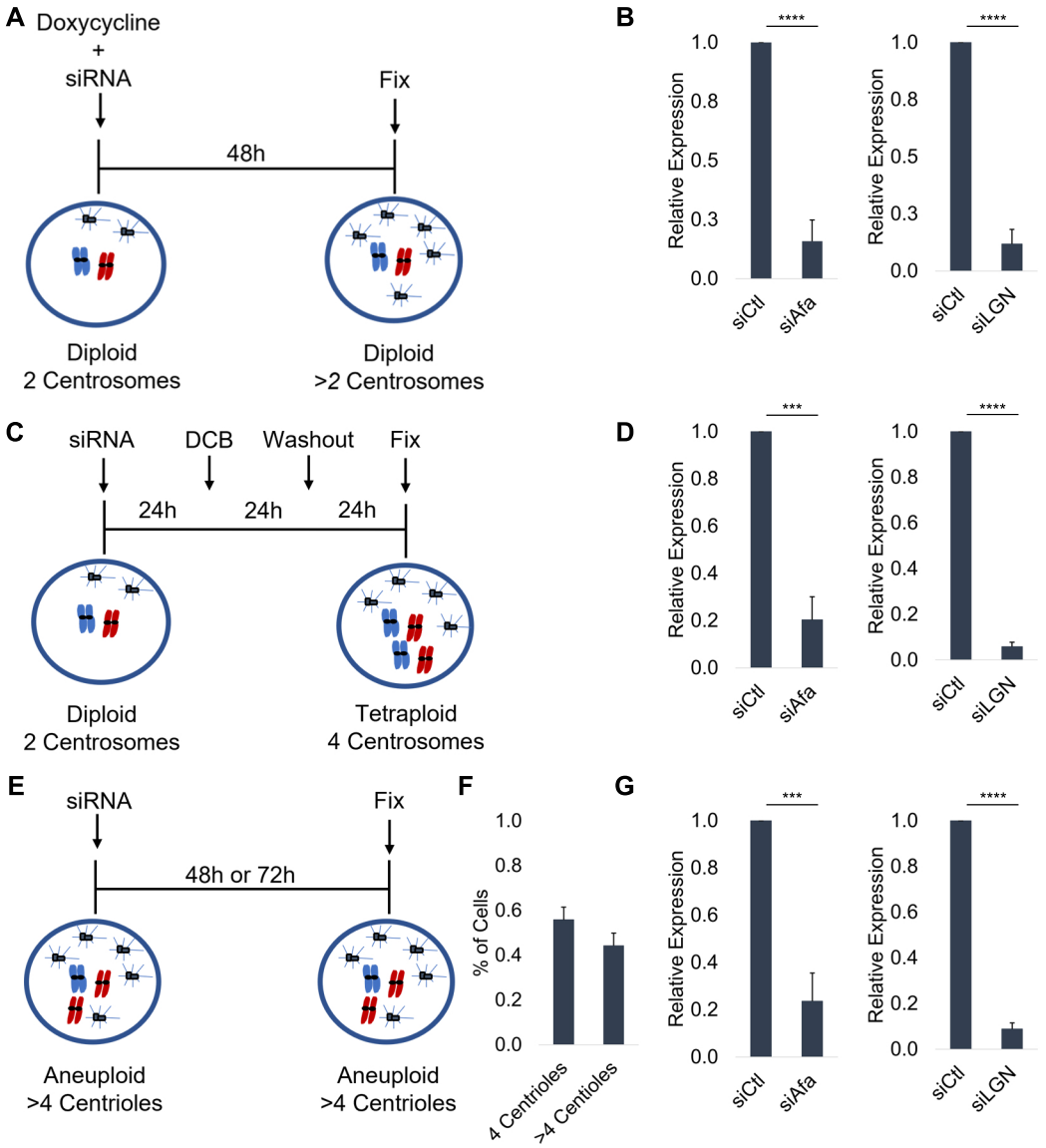

Figure 33: **Experimental systems and validation of knockdown.** (A) Schematic of experimental mechanism to induce centrosome amplification in RPE PLK4ind cells. (B) Quantification of gene expression following 48 h siRNA-mediated knockdown of Afadin or LGN in RPE PLK4ind cells. (C) Schemitic of experimental mechanism to induce centrosome amplification and tetraploidy in RPE p53-/- cells. (D) Quantification of gene expression following 72 h siRNA-mediated knockdown of Afadin or LGN in RPE p53-/- cells. (E) Schematic of experimental setup in MDA-MB-231 cells with centrosome amplification. (F) Quantification of the percent of cells with 4 or >4 centrioles. (G) Quantification of gene expression following 72 h or 48 h siRNA-mediated gene silencing of Afadin or LGN, respectively. Quantification from 3 biological replicates, errors bars are SD. Significance was determined by student's t-test (***p<0.001,****p<0.0001).

viously, we induce cytokinesis failure in RPE p53-/- cells, resulting in tetraploid cells with four centrosomes (Fig. 33 C). Finally, we use MDA-MB-231 cells, a well characterized breast cancer cell line with CA. Indeed, we find that nearly 50% of mitotic MDA-MB-231 cells have CA (have >4 centrioles) (Fig. 33 E,F).

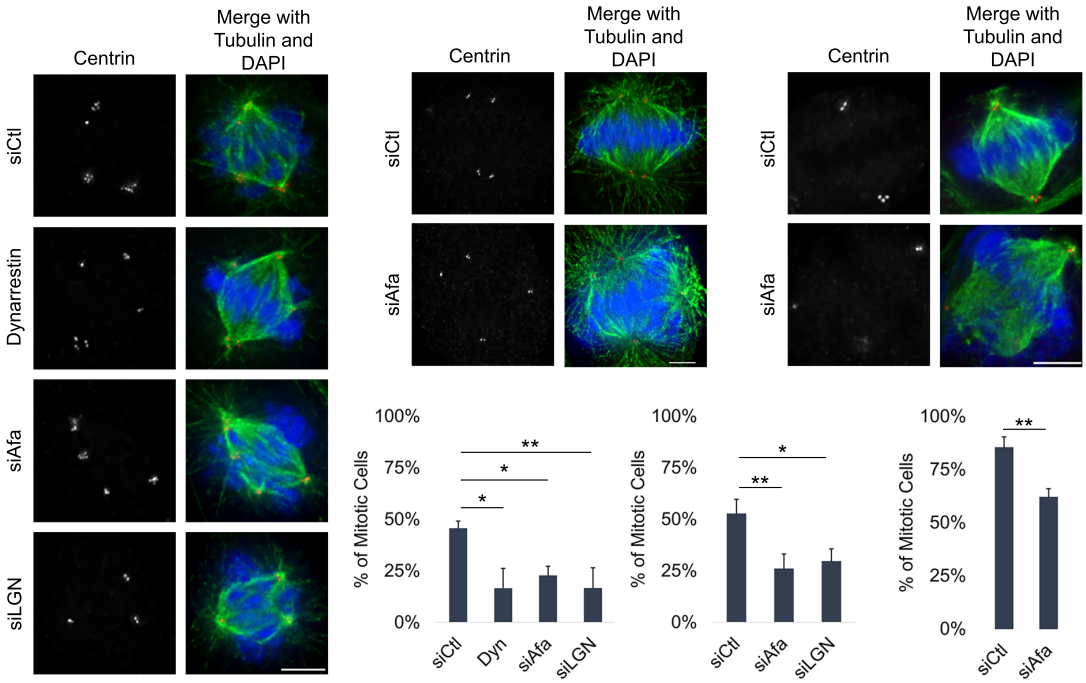

Figure 34: **Loss of cortical dynein disrupts centrosome clustering.** (A) Fixed-cell images of RPE PLK4ind cells following short-term dynein inhibition with dynarrestin or loss of Afadin or LGN. (B) Quantification of the percent of mitotic cells with clustered spindles in RPE Plk4ind cells. (C) Fixed-cell images of RPE p53-/- cells following loss of Afadin or LGN. (D) Quantification of the percent of mitotic cells with clustered spindles in RPE p53-/- cells. (E) Fixed-cell images of MDA-MB-231 cells following loss of Afadin. (F) Quantification of the percent of mitotic cells with clustered spindles in MDA-MB-231 cells. All scale bars are 5 μm. All quantification was performed on at least 50 cells per condition from 3 biological replicates. Error bars are SD. Significance was determined by student's t-test when comparing two conditions and a one-way ANOVA with Dunnett's test for multiple comparisons when comparing multiple conditions to one control (*p<0.05,**p<0.01).

To determine the impact of cortical dynein activity on centrosome clustering in cells

with CA, we disrupted cortical dynein localization via short-term dynein inhibition or siRNA-mediated depletion of Afadin or LGN in RPE Plk4ind cells (Fig. 33 B,D,G). Short-term treatment with the dynein inhibitor Dynarrestin (Dyn) has been shown to disrupt cortical dynein localization while maintaining its localization at spindle poles, allowing it to maintain its function in spindle formation and maintenance [107, 167]. Dynein inhibition results in a drastic decrease in clustered spindles, with 50% of spindles clustering in the control condition (siCtl) and 20% in the dynein inhibited condition (Fig. 34 A,B). However, short-term dynein inhibition with Dynarrestin has been shown to additionally disrupt dynein's localization and function at kinetochores, impacting chromosome movement and alignment [107]. To ensure that the unclustered phenotype that we see following dynein inhibition is not a result of disruption to kinetochore-derived forces that contribute to clustering, we specifically impacted cortical dynein localization via depletion of Afadin or LGN using siRNA specific to either gene. Both of these proteins have known roles in recruiting and anchoring the NuMA/dynein/dynactin complex to the actin cytoskeleton during mitosis, and loss of either one of these proteins efficiently disrupts mitotic cortical NuMA/dynein localization and activity [28, 53, 56, 122, 269]. We find that loss of cortical dynein via Afadin (siAfa) or LGN (siLGN) knockdown results in a similar spindle phenotype to Dynarrestin treatment, with about 50% less clustered spindles than the control condition (Fig. 34 A,B).

To determine if loss of centrosome clustering is dependent on the number of centrioles in the cell or DNA content, we perform similar analysis in tetraploid cells with four centrosomes (RPE p53-/-) and cancer cells with CA (MDA-MB-231). We find that loss of cortical dynein has a similar impact in each of these cell lines, with a significant decrease in clustered spindles following siAfa or siLGN treatment (Fig. 34 C,D,E,F). These results suggest that cortical dynein contributes to centrosome clustering, and this activity is independent of centrosome number in cells with CA or DNA content.

4.7 Cortical Dynein Suppresses Multipolar Divisions in Cells with Supernumerary Centrosomes

Prolonged mitosis following treatment with the proteosome inhibitor MG132 improves centrosome clustering efficiency [207]. To determine if cortical dynein-independent mechanisms are sufficient to cluster centrosomes in the absence of cortical dynein, we arrest RPE Plk4ind cells in mitosis via MG132 treatment following siAfa or siLGN treatment. We find that while the percent of cells with clustered spindles significantly increases in the control condition (siCtl) following 30 minutes or 1 hour of MG132 treatment, mitotic arrest does not impact the ability for centrosomes to cluster in the absence of cortical dynein (Fig. 35 A,B). These data suggest that dynein-independent mechanisms are not sufficient to cluster centrosomes during prolonged mitosis.

To assess the fate of mitotic cells following loss of cortical dynein activity, we performed time-lapse live-cell imaging in RPE Plk4ind cells stably expressing fluorescently-tagged tubulin (EGFP-tub) (Fig. 35 C) [166]. Analysis of single cells progressing through mitosis reveals that loss of cortical dynein via LGN depletion does not significantly impact the duration of mitosis in cells with extra centrosomes (Fig. 35 D). Analysis of mitotic fate, characterized as bipolar or multipolar cytokinesis, reveals that the vast majority of cells with CA undergo a bipolar division after forming a functional bipolar mitotic spindle (Fig. 35 E). However, loss of cortical dynein reduces the ability of cells undergo a bipolar division by 50%, where the majority of cells instead undergo a multipolar division and result in 3 or more daughter cells (Fig. 35 C,E). Fixed-cell analysis of tetraploid cells with four centrosomes (RPE p53-/-) reveals similar results, with a significant decrease in bipolar anaphase or telophase cells (Fig. 35 F,G). Together these results suggest that cortical dynein promotes centrosome clustering and bipolar divisions in cells with CA.

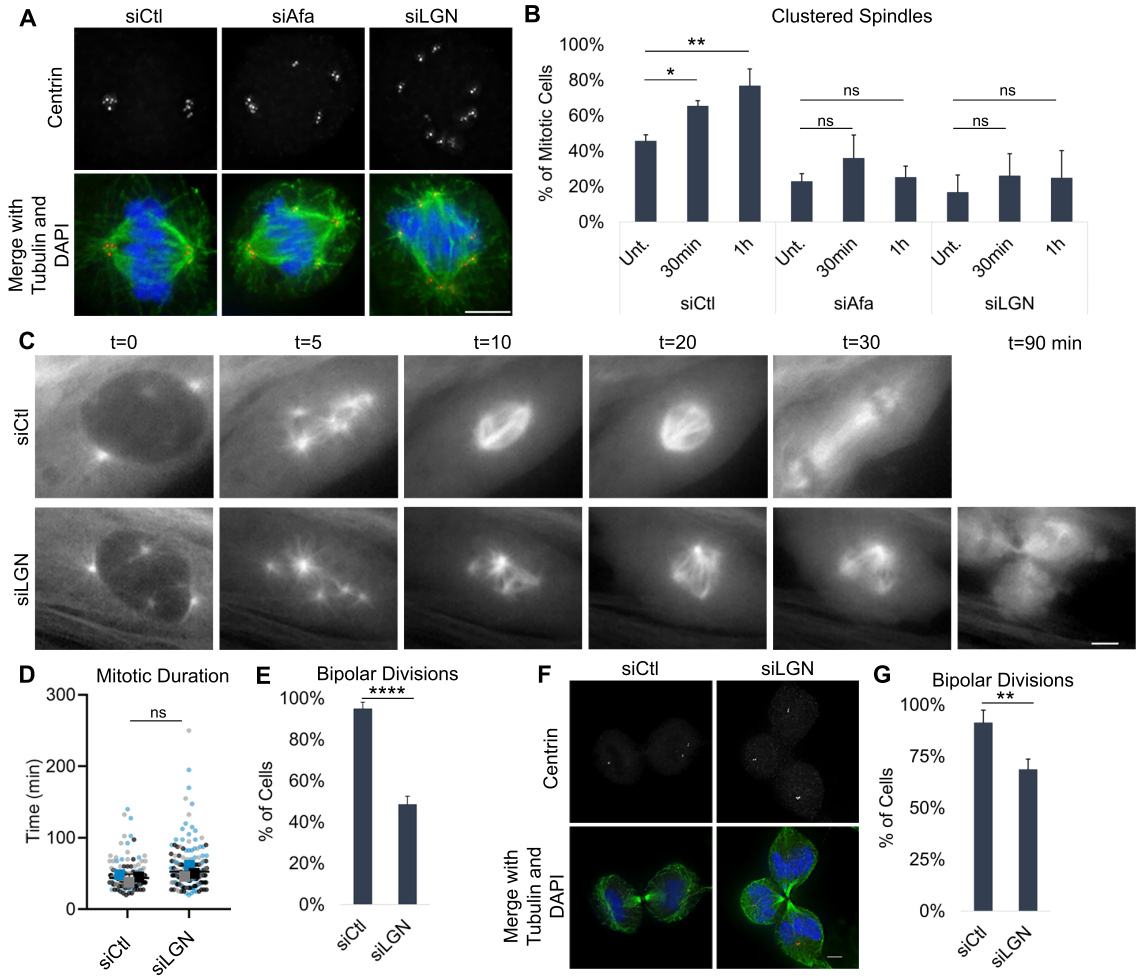

Figure 35: **Cortical dynein suppresses multipolar divisions in cells with supernumerary centrosomes.** (A) Fixed-cell images of RPE Plk4ind cells treated with MG132 for 1 h. (B) Quantification of the percent of mitotic cells with clustered spindle in RPE Plk4ind cells following treatment with MG132 for 30 min or 1 h. The Unt. condition is the same data shown in Fig. 34 B. (C) Still frames from live-cell imaging of RPE Plk4ind cells expressing EGFP-tubulin. (D) Quantification of mitotic duration, each dot is a cell. t=0 is the time point just prior to nuclear envelope breakdown, characterized by loss of EGFP exclusion from the nucleus. The final time point was characterized by rapid elongation of the spindle in anaphase B. (E) Quantification from live-cell imaging of the percent of RPE Plk4ind cells that undergo a bipolar division. (F) Fixed-cell images of RPE p53-/- cells in telophase. (G) Quantification from fixed-cell imaging of the percent of cells undergoing a bipolar division in RPE p53-/- cells. Mitotic fate (bipolar vs. multipolar) was characterized by the number of cytokinetic furrows. All scale bars are 5 μm. All quantification was performed on at least 50 cells per condition from 3 biological replicates. Error bars are SD. Significance was determined by student's t-test when comparing two conditions or a one-way ANOVA with Dunnett's test for multiple comparisons when comparing multiple conditions to one control

(*p<0.05, **p<0.01, ****p<0.001, ns indicates not significant).

5 Cortical Dynein Influences Chromosome Alignment and Segregation

5.1 Introduction

Building the mitotic spindle is required for chromosome alignment and segregation. Alignment is largely dependent of MT binding and force generation at kinetochores. The MT-kinetochore interface is incredibly complex, but MT attachment is dependent on the Ndc80 complex [38–40]. However, it is well established that a bipolar spindle can form in the absence of MT attachments to kinetochores, although this significantly disrupts chromosome alignment and segregation [26, 52, 157]. Furthermore, defects in chromosome alignment impact the localization of the dynein/NuMA/LGN complex to the cell cortex, where close proximity of chromosomes to the cell boundary prevents binding [122, 239]. Our analysis of spindle dynamics following loss of cortical dynein in cells shows a more robust impact on spindle length fluctuations in cells lacking Nuf2 than in cells with robust MT attachments (Fig. 21 B,D,E, Fig. 22 B,D,E). We find also that short term dynarrestin treatment, which has been shown to partially disrupt kinetochore attachments [107], has a similar impact on cells regardless of Nuf2 activity (Fig. 21 B,D,E, Fig. 22 B,D,E).

Additionally, we find that asymmetric and dynamic cortical dynein is insufficient to maintain centrosome clustering in cells with CA, suggesting that other force-derived mechanisms may be important for sustained clustering. As the major force-generating component within the spindle, MT attachments to kinetochores are an appealing candidate for this activity. Together, these results suggest a complex force-balance relationship between cortical and chromosome-derived forces and provide motivation for modeling chromosomes and MT-chromosome interactions.

To explore these forces further, the model described in Section 2.2 can be extended to include chromosomes. In this chapter, we present biological results exploring the impact

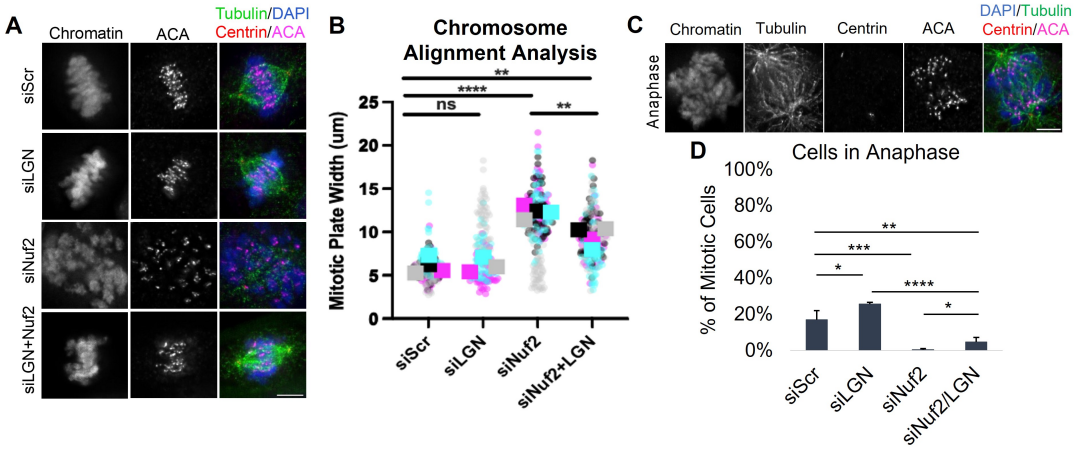

Figure 36: **Loss of cortical dynein promotes chromosome alignment and anaphase onset in the absence of Nuf2.** (A) Fixed-cell images of RPE cells in mitosis. (B) Quantification of mitotic plate width in RPE cells. Each dot is a cell with the color representing a biological replicate; squares are the average from the respective replicate. (C) Fixed-cell images of RPE cells in different stages of mitosis. (D) Quantification of the percent of mitotic cells in each stage of mitosis. Scale bars are 5 μm. All quantification was performed on at least 50 cells per condition from 3 biological replicates. Error bars are SD. Figure modified from Kylie Belanger's MQP (2022).

of loss of cortical dynein on cells lacking MT attachments to kinetochores and preliminary modeling approaches to simulate chromosomes. The biological results presented in this chapter were completed by Kylie Belanger as part of her Major Qualifying Project (MQP), and the modeling work was performed in collaboration with Samantha Mora as a summer Research Experience for Undergraduates (REU).

5.2 Loss of Cortical Dynein Improves Chromosome Alignment and Segregation in the Absence of Nuf2

To explore the impact of cortical dynein-derived forces on chromosome alignment and segregation in the absence of Nuf2, we performed fixed-cell imaging and analysis of cells

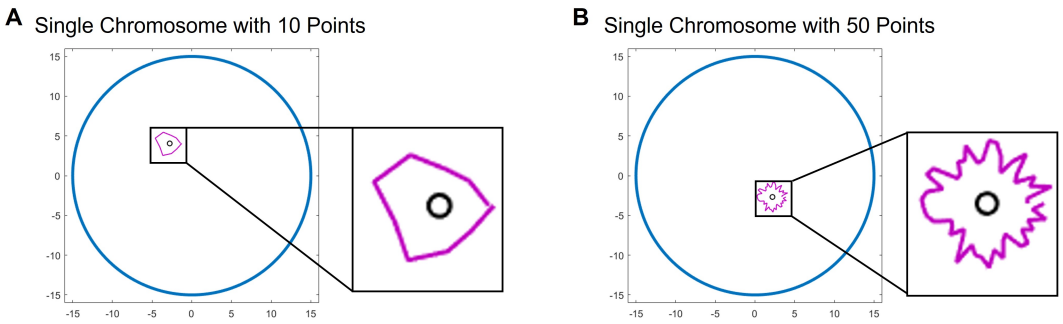

Figure 37: **Chromosomes are defined by a number of n points.** (A) Image of a single chromosome created by 10 points. (B) Image of a single chromosome created by 50 points. The black circle represents the kinetochore.

lacking cortical dynein and/or Nuf2 (Fig. 36 A). To quantify chromosome alignment, we measure the mitotic plate width in cells. This was calculated as the distance between the farthest kinetochores on each side of the spindle midzone. We found that chromosome dispersion following loss of Nuf2 (siNuf2) was partially rescued with the additional loss of cortical dynein (siNuf2/siLGN), with a decrease in metaphase plate width from 12.26 to 9.29 μm, respectively (Fig. 36 B). To determine if improved chromosome alignment following loss of cortical dynein in the absence of Nuf2 impacts chromosome segregation, we assessed the percent of cells progressing through anaphase in each of these conditions (Fig. 36 C,D). Quantification of the percent of mitotic cells in anaphase significantly increased following loss of cortical dynein in the absence of Nuf2 (Fig. 36 D). Together, these data suggest that loss of cortical dynein impacts chromosome alignment and segregation in the absence of stable end-on attachments to kinetochores. These results further suggest that modeling chromosomes may elucidate force-related mechanisms involved in chromosome alignment with and without cortical dynein.

5.3 Modeling Chromosomes as Rigid Polygons

In addition to biological experimentation, modeling approaches can be leveraged to assess the impact of cortical dynein on MT attachments to chromosomes and chromosome dy-

namics. The model described in Chapter 2.2 can be extended to include chromosomes or chromosome-like structures and their associated forces. As described previously in Chapter 2.2, fluid dynamics within the cell are characterized by a low Reynold's number [187, 198]. This property is maintained when considering chromosomes and chromosome-derived forces, with an approximated Reynold's number of 5x10^{-6}. This is calculated using Eq. 1 with a chromosome diameter $l = 1.4\mu$m and velocity $v = 0.1\mu$m/sec. Since this Reynold's number is on the same order of magnitude as that calculated for centrosome movement, all model parameters match those listed in Table 1 with additional chromosome-related parameters listed in Table 3. Our preliminary approach to modeling chromosomes and MT-chromosome interactions considered chromosomes as rigid blobs (to simulate compact chromosomes in mitosis) with a circular kinetochore region in the center of each blob (Fig. 37). The chromosome shape and structure was defined by a number of n points having random distance $d \in [1, 2]$ μm from the center of the structure. While calculations are performed in two dimensions, we assume a thin slice in the third dimension to allow MTs to interact with the chromosomes without spatial restrictions. The kinetochore is defined as a circular region with a radius of 0.3 μm located in the center of each chromosome. We identified MTs interacting with the chromosome using the MATLAB function "inpolygon", which determines if a set of points is inside or on the edge of a defined region. We allowed only MTs whose end point falls on the boundary or within the polygonal region to generate force, since we are only considering end-on MT attachments (Fig. 38).

MTs that interact with the chromosome can either bind and generate force, simulating MT binding to chromokinesins, or push against the chromosome if binding does not occur. Binding to chromokinesins is determined by MT intersection with the polygonal chromosome and a binding probability (P_{chr}), similar to MT-motor interactions described in Section 2.2. The force by each chromokinesin is calculated as:

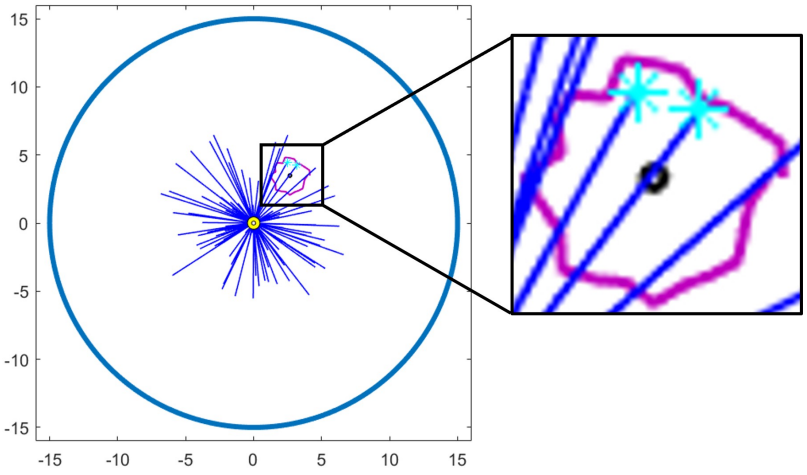

Figure 38: **Identification of MTs Intersecting with Chromosomes.** Image of MTs nucleated from a single centrosome interacting with a single chromosome (purple structure). The end of the MT that interacts with the chromosome is labeled with a blue '*'. The black circle represents the kinetochore.

$$f_i^{chr} = f_{0,chr}\left(1 - \frac{\vec{v}_c \cdot \vec{m}_i}{v_{0,chr}}\right), \tag{17}$$

where $f_{0,chr}$ is the stall force of chromokinesin, $v_{0,chr}$ is the walking velocity of chromokinesin, $\vec{v}_c$ is the velocity of centrosome c that MT i is nucleated from, and $\vec{m}_i$ is the unit vector in the direction of MT i. The total force by MTs nucleated from centrosome c binding to chromokinesins on the k^{th} chromosome in the direction of the i^{th} MT is,

$$\vec{F}_k^{chr} = \sum_{i=1}^{N_{k,chr}} \vec{m}_i \exp\left(-\frac{\ell_i}{K d_{chr}}\right) f_i^{chr}, \tag{18}$$

where $N_{k,chr}$ is the total number of MTs on centrosome c that bind to chromokinesins on chromosome k, ℓ_i is the length of MT i, d_{chr} is the minimal distance between centrosome c and the chromosome k, and K is a scaling factor (Table 1). This force will push the centrosome in the opposite direction of $\vec{m}_i$, away from the chromosome. MTs will stay bound to chromokinesins and continue to grow at a velocity v_g until the MT either undergoes catastrophe and begins shrinking or the end of the MT end is no longer inside the polygonal chromosome, at which time it will unbind. As described earlier, the exponential term accounts for a higher drag due to MT length, density, and proximity between centrosome c and chromosome k (see details in Section 2.4).

A slipping force, F_k^{slip}, similar to the cortical slipping force described in Section 2.2, is applied to MTs that interact with the chromosome but do not bind. The force-balance equation for the movement of chromosome k in the overdamped limit is:

$$\vec{0} = \vec{F}_k^{chr} + \vec{F}_k^{slip} + \vec{F}_k^{r_{cent}} + \vec{F}_k^{r_{chr}} + \xi\vec{v_k}, \tag{19}$$

where $\vec{F}_k^{r_{chr}}$ prevents two chromosomes from occupying the same space and $\vec{F}_k^{r_{cent}}$ is a repulsive force between chromosome k and centrosome c, similar to that described between centrosomes in Section 2.2. We solve a system of k equations for the velocity of each chromosome, $\vec{v}_k$, and use the velocity to determine the new location of each chromosome. An equal and opposite force is applied to the centrosome from which MT i is nucleated and the chromosome on which it binds, and the associated centrosome-chromosome forces are added to Eq. 2.

In addition to translational movement, chromosomes experience a rotational force that is dependent on the angle at which MT i interacts with the chromosome. For each MT i bound to chromokinesins on chromosome k, we calculate the rotational velocity as:

$$\vec{R}_k^{chr} = \sum_{i=1}^{N_{k,chr}} \vec{r}_i \times f_i^{chr}\vec{m}_i, \tag{20}$$

where $\vec{r_i}$ is the normal vector from the end of the MT to the center of chromosome k. We solve a similar equation for MTs slipping on chromosome k:

$$\vec{R}_k^{slip} = \sum_{i=1}^{N_{k,slip}} \vec{r}_i \times f_i^{slip}\vec{m}_i. \tag{21}$$

We solve for the rotational velocity, $\vec{\alpha}_k$ of each chromosome k by:

$$\vec{0} = \vec{R}_k^{chr} + \vec{R}_k^{slip} + \zeta\vec{\alpha_k}, \tag{22}$$

where ζ is the rotational drag on chromosome k.

Table 3: Chromosome-related model parameters. All parameters without reference were approximated to match biological results.

Parameter	Value	Description	Reference
$f_{0,chr}$	1 pN	Stall force of chromokinesin (kid)	[19]
$v_{0,chr}$	0.063 μm/s	Walking velocity of chromokinesin (kid)	[19]
P_{chr}	0.5	Probability of binding to chromokinesin	Approximated
ζ	10 pNs	Rotational drag coefficient	Approximated

5.4 Chromosomes Become Positioned Near the Boundary of the Cell Without Kinetochore Interactions

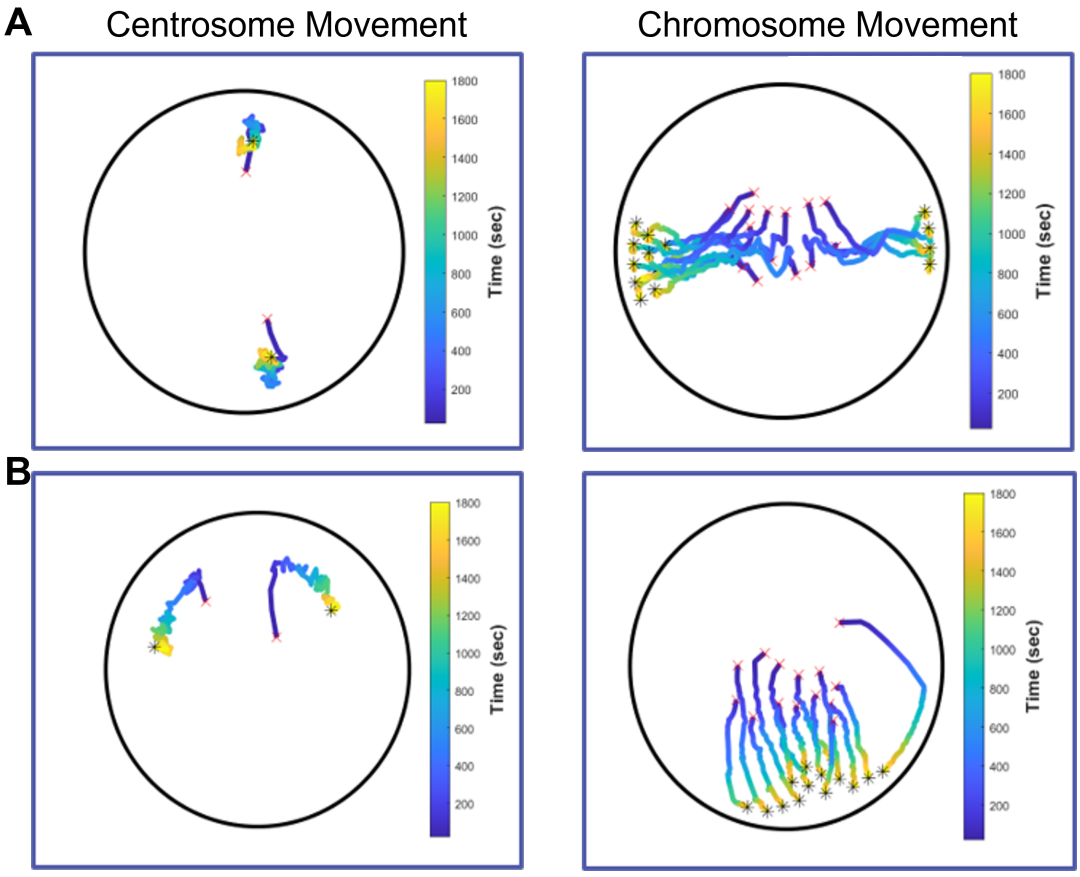

Figure 39: **Chromosomes become positioned near the cell boundary in the absence of kinetochore attachments.** (A) Traces of centrosome movement (left) and chromosome movement (right) over time from a single simulation. (B) Traces of centrosome movement (left) and chromosome movement (right) over time from a single simulation. Red 'x' represents initial centrosome or chromosome position, black '*' represents final centrosome or chromosome position. Colorbar is time (min).

Chromosome alignment is dependent on MT attachments to kinetochores, as loss of kinetochore attachments result in misalignment and a wide distribution of chromosomes throughout the cell during mitosis (Fig. 15 A,B). The inability of chromosomes to align in the absence of kinetochore attachments prevents satisfaction of the SAC and progression into anaphase. By modeling chromosomes and MT interactions with chromosome arms, but not kinetochores, we find a similar result (Fig. 39). Specifically, we find that chromosomes become distributed away from the center of the cell and become oriented towards the cell boundary (Fig. 39). Furthermore, we find that chromosomes become positioned away from centrosomes within the cell in the absence of kinetochore attachments, suggesting that centrosome positioning dictates chromosome movement and positioning (Fig. 39). Together, these results provide insight into centrosome-dependent chromosome positioning in the absence of kinetochore attachments. In the future, this model can be used to test the impact of cortical dynein-derived forces on chromosome alignment in the absence of kinetochore attachments.

6 Discussion and Future Directions

By leveraging our knowledge of the mitotic spindle, in combination with mathematics and the laws of physics, we have built a model to simulate the formation and function of the spindle. Our model has both validated experimental findings and made novel predictions about spindle dynamics, proving it to be a valuable and cost-effective approach to studying the dynamic process of mitosis.

6.1 Cortical Dynein Impacts Spindle Dynamics

6.1.1 Cortical dynein activity regulates bipolar spindle length and spindle dynamics

Cortical dynein has well established roles in spindle orientation and positioning (detailed in Section 1.3). Complete loss or inhibition of dynein during mitosis results in splayed spindle poles and failure to complete mitosis [60, 91]. As such, mechanisms to specifically target cortical localization of dynein during mitosis, while leaving dynein localized to spindle poles and kinetochores unaltered, has been challenging. Mathematical and computational modeling is an appealing approach to overcome this challenge, since protein activity and force generation can be directly modulated. We use this approach to make novel predictions about the impact of cortical dynein force generation on spindle dynamics. By directly comparing biological results from fixed and live-cell imaging approaches, we optimized model parameters and validated model behavior. Importantly, the model achieves a bipolar “steady-state" spindle length, characteristic of a mitotic cell in metaphase (Fig. 16). Altering motor-dependent forces provides further confidence in model outputs, as loss of Eg5 and HSET overexpression results in spindle collapse and loss of cortical dynein reduces bipolar spindle length, consistent with the well-established biological functions of these proteins (Fig. 17 A,B) [107, 115, 156, 162, 181, 219, 222, 277, 278].

While examining spindle length, defined as the distance between centrosomes, over time in simulations, we found that rather than maintaining a balanced “steady-state", spin-

dle length was instead dynamic over time (Fig. 18). We found that drastic peaks in spindle length corresponded with increases in force by cortical dynein. To test the impact of cortical dynein activity on spindle length, we reduced its activity within the model. We found that loss of cortical dynein not only reduces bipolar spindle length, but it also nearly removes dynamic fluctuations in spindle length (Fig. 19). These results suggest that cortical dynein is a primary regulator of both bipolar spindle length and spindle dynamics.

One strength of our model is the ability to selectively perturb motor protein populations. However, biological approaches have also succeeded in modulating cortical dynein localization and activity. Specifically, dynein activity can be perturbed by targeting proteins responsible for anchoring dynein to the actin cell cortex [53, 56, 122]. Proteins, such as Afadin and LGN, are required for cortical dynein localization and do not impact other mitotic functions [28, 53, 56]. As such, loss of either of these proteins disrupts cortical dynein localization while maintaining mitotic spindle structure and function. To test the model prediction that cortical dynein activity induces fluctuations in bipolar spindle length, we performed live-cell imaging of cells expressing fluorescently tagged centrosomes. By tracking cells progressing through mitosis, we assessed spindle length in cells with and without cortical dynein. Similar to our model prediction, we found that loss of cortical dynein reduces fluctuations in spindle length over time (Fig. 21,22). These results confirm our model prediction and validate the novel prediction that cortical dynein regulates bipolar spindle dynamics.

This finding extends the body of work implicating cortical dynein in mitotic spindle formation, orientation, positioning, length, and dynamics [25,78,122,190,191]. However, how dynein regulates changes in metaphase spindle length remains elusive. Dynein is known to localize dynamically to the cell cortex during mitosis, where its transient localization and activity is dependent on Plk1 phosphorylation of NuMA [122]. This phosphorylation activity is dependent on the proximity of the spindle pole to the cell cortex where dynein is located. Rather than being dynamic, our model considers dynein to be uniformly distributed

around the cell boundary, with all MTs having an equal probability of binding to dynein. To determine whether changes in spindle length are a consequence of uniformly distributed dynein localization in our model, we can instead make dynein localization dynamic in time or space to better capture its activity in cells. Additionally, dynein activity alters MT dynamics by inducing MT depolymerization through cargo adaptors [62, 64, 129, 133, 179], and astral MT dynamics are known to impact spindle orientation, positioning, and dynamics [16, 213, 245]. To determine if astral MT dynamics impact metaphase spindle length changes in mitosis, one could stabilize MT dynamics, either experimentally or within the model. This work would further elucidate the mechanism by which dynein regulates fluctuations in bipolar spindle length.

6.1.2 High Eg5 activity rescues spindle length and dynamics in the absence of cortical dynein

The mitotic spindle is formed and maintained through a dynamic balance of forces [59]. A combination of motor-dependent forces at the cell cortex and spindle midzone are responsible for spindle formation and maintenance. Disruption to this balance of forces can impact the ability for cells to form a spindle or divide [35, 115, 155, 162]. Eg5 overexpression is common in cancer and is associated with genomic instability, tumor progression, and poor patient prognosis [30, 111, 217]. Eg5 and cortical dynein activity are thought to act synergistically to initiate and maintain centrosome separation in mitosis and overexpression of Eg5 results in an imbalance of forces, disrupting spindle structure [30, 59]. Results from our model, however, suggest that high Eg5 activity may be important in regulating spindle length and dynamics in the absence of cortical dynein. Specifically, we find that high Eg5 activity can partially rescue both steady-state spindle length and spindle dynamics following loss of cortical dynein (Fig.23). These data suggest that high Eg5 activity may be beneficial to cells lacking cortical dynein. Experiments performed in cancer cells with Eg5 overexpression, or in cells with experimentally induced Eg5 overexpression, with

and without cortical dynein activity can further explore this hypothesis and determine the extent to which Eg5 activity regulates spindle length and dynamics.

6.1.3 High cortical dynein activity is required for spindle formation when HSET activity is high

Overexpression of HSET is common in cancer and is associated with poor patient prognosis [74, 126, 146, 192, 235]. High HSET activity is traditionally thought to aid cancer progression by clustering supernumerary centrosomes in cancer cells with CA, promoting bipolar spindle formation and continued cell proliferation [34, 79, 81, 123, 131, 183, 199]. However, clustering-independent mechanisms of HSET overexpression in cancer progression have more recently been found, making HSET a promising target for cancers independent of centrosome number [123, 192, 273]. By increasing HSET activity in our model, we can assess the force requirements for spindle formation in the presence of high HSET. We find that high cortical dynein activity is required for bipolar spindle formation in contexts with high HSET activity, whereas spindles collapse with moderate dynein activity under this condition (Fig. 17 A(ii),B(ii),D, Fig. 24). While it has been shown that a bipolar spindle can form in the presence of HSET overexpression in cells, dynein activity has not been implicated in this process [26]. From our results, we speculate that cancer cells having high levels of HSET, regardless of centrosome number, may be dependent on cortical dynein for bipolar spindle formation and accurate cell division. If true, therapeutic approaches to inhibit or reduce cortical dynein activity may be particularly effective at limiting mitotic progression in contexts of HSET overexpression, independent of centrosome number.

6.2 Cortical Dynein Drives Centrosome Clustering in Cancer Cells with CA

Centrosome amplification is a hallmark of cancer and is associated with drug resistance, tumor progression, and poor patient prognosis [51, 75, 175]. Targeting centrosome cluster-

ing to prevent cancer cell proliferation in cells with CA is a promising approach for tumors with a high frequency of CA [131, 183, 199, 207]. The primary motor-dependent force implicated in centrosome clustering is HSET [131, 207]. HSET is often overexpressed in cancers with CA, and HSET activity is required for centrosome clustering in this context. While the protein dynein has been implicated in centrosome clustering, this has exclusively been associated with its function at spindle poles [199]. Our findings that cortical dynein activity drives both fluctuations in spindle length and bipolar spindle formation when HSET activity is high led us to hypothesize that cortical dynein influences centrosome clustering in cells with supernumerary centrosomes.

6.2.1 Cortical Dynein Localizes Asymmetrically in Cells with CA

Cortical NuMA/dynein localizes asymmetrically in cells with two centrosomes [122, 216]. To determine the localization of cortical NuMA in cells with CA, we used fixed-cell imaging and found that NuMA localizes asymmetrically on the cell boundary in cells with CA, with most mitotic cells having increased localization behind 1 spindle pole (Fig. 26 C,D). This characteristic was independent of spindle morphology, where both clustered and unclustered spindles showed asymmetric cortical NuMA localization (Fig. 26 C,D). Using the model described in Section 2.2, extended to have 4 centrosomes, we simulate asymmetric dynein localization by allowing MTs to only bind to cortical dynein on one specific region of the boundary (Fig. 28 A,B). In doing this, we found that centrosomes cluster toward the region where MTs bind to dynein and a clustered bipolar spindle forms at a high frequency (Fig. 28 B,C,F). These data suggest that centrosome clustering is responsive to cortical dynein activity.

To biologically test the model prediction that centrosome movement and clustering is responsive to dynein activity, one could use optogenetic manipulation of cortical NuMA to specifically target NuMA/dynein to regions of the cell boundary in cells with CA. In 2018, Okumura, et al. used this technique in cells with two centrosomes following

loss of NuMA/dynein/dynactin complex through siRNA-mediated gene silencing of LGN [191]. The authors found that light-induced targeting of NuMA was sufficient to recruit dynein/dynactin to the cell cortex and generate force. Pairing this approach with our model would further inform the extent to which centrosome clustering relies of cortical dynein activity.

6.2.2 Dynamic dynein localization may assist centrosome clustering

Asymmetric dynein localization is dynamic in cells with two centrosomes [122]. To recapitulate this, we make asymmetric dynein localization dynamic in time, where oscillations in dynein localization occur at a set frequency T. We find that nearly all simulations with dynamic dynein, regardless of the value of the parameter T, cluster centrosomes (Fig. 30, Fig. 31). However, we find that while dynamic and asymmetric dynein is sufficient to cluster centrosomes, it is not sufficient to sustain clustering (Fig. 30, Fig. 31). This is in contrast to asymmetric and statically localized cortical dynein, where clustering is maintained (Fig. 28, Fig. 30 A). When dynein is dynamic, we find that dynein-dependent forces pull centrosomes together toward the region on the cell boundary where it is active, and the removal of dynein causes centrosomes to begin moving apart (Fig. 30, Fig. 31). These results suggest that other force-derived mechanisms likely contribute to the maintenance of centrosome clustering in cells with CA.

Importantly, motor-independent mechanisms, such as non-motor protein activity and k-fiber tension are implicated in centrosome clustering [69, 137]. Specifically, sufficient MT tension through interactions with kinetochores is required for centrosome clustering, such that loss of tension disrupts clustering [137]. Additionally, centrosomal proteins TACC3 and ch-TOG influence centrosome clustering, likely through their regulation of MT nucleation and dynamics [7,55,69]. Our results suggest that these motor-independent forces may specifically be involved in the maintenance of centrosome clustering. Exploring the relationship between kinetochore, non-motor, and cortical dynein-derived forces, both compu-

tationally and experimentally, would be valuable in elucidating the mechanism(s) required for sustained centrosome clustering in cells with CA.

It has been previously established in cells with two centrosomes that cortical dynein localization and activity is dependent on the phosphorylation of NuMA by Cdk1 and Plk1 localized at the spindle poles [122]. Kiyomitsu & Cheeseman (2012) found that as the spindle pole nears the cell cortex where dynein is localized, Plk1-dependent phosphorylation of NuMA induces the unbinding of dynein/dynactin from NuMA. Dynein localization then shifts to the opposing side of the cell, initiating pulling forces to shift the entire spindle structure within the cell. This spatially-dependent cortical dynein localization causes oscillations of the spindle structure within the cell during mitosis [122]. From our modeling results, we propose a similar mechanism in cells with CA. Specifically, we propose that asymmetric cortical dynein drives initial centrosome clustering and pulls centrosomes close to the cortex (Fig. 40). Once close to the cell boundary, kinase-dependent phosphorylation of cortical NuMA removes dynein from the cell boundary (Fig. 40). Once cortical dynein is moved, in the absence of chromosomes, centrosomes decluster (Fig. 40 A). Alternatively, in the presence of chromosomes and chromosome-derived forces, kinetochore-mediated tension aids the maintenance of clustered centrosomes once cortical dynein is re-localized (Fig. 40 B). We hypothesize that this dynamic localization of cortical dynein assists centrosome clustering and the continued proliferation of cancer cells with CA.

Extension of our model to include spatially-dependent dynein localization, rather than temporally-dependent, may make further predictions about the dynamics of dynein-dependent centrosome clustering.

6.2.3 Loss of cortical dynein disrupts centrosome clustering

To determine the extent to which cortical dynein contributes to centrosome clustering, we prevent MT binding to dynein anywhere on the cell boundary in our model. In doing this, we found that loss of cortical dynein activity disrupts centrosome clustering (Fig. 32). To

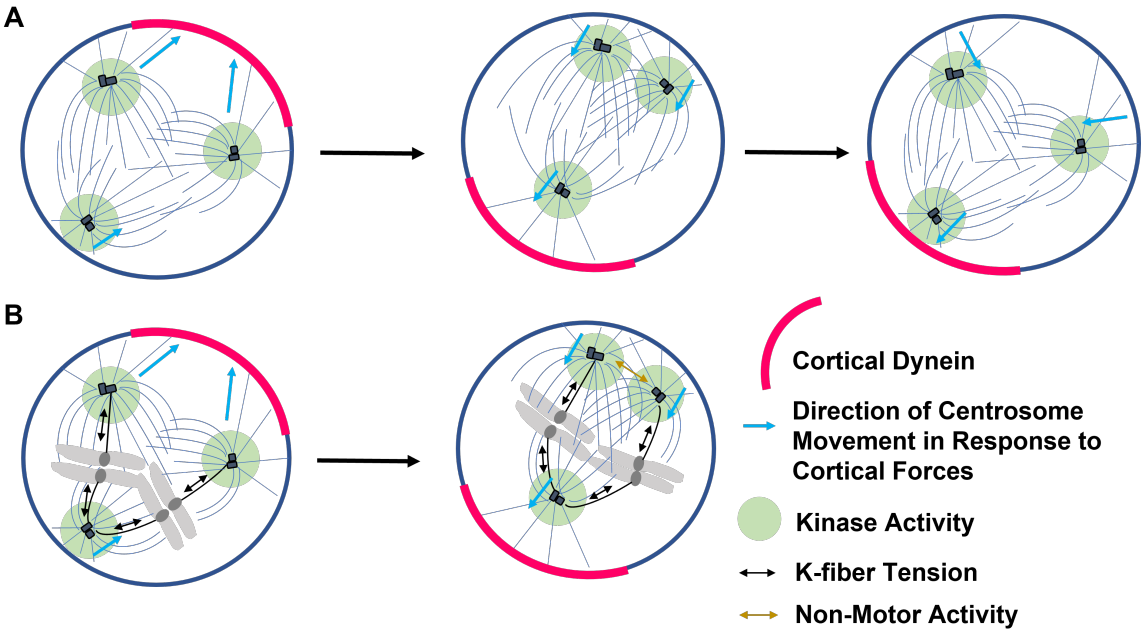

Figure 40: **Proposed model of dynein-dependent centrosome clustering.** (A) Schematic of a cell with three centrosomes with no chromosomes in mitosis. Cortical dynein localizes asymmetrically on the cell boundary (pink arc). Cortical dynein activity pulls centrosomes together towards the region of dynein localization until kinase-dependent phosphorylation of NuMA induces unbinding of dynein. Dynein localizaton oscillates to the opposing side of the cell while centrosomes that were clustered by cortical dynein activity decluster. (B) Schematic of cell with three centrosomes with chromosomes in mitosis. Asymmetric cortical dynein pulls centrosomes together toward the region of dynein localization until kinase-dependent phosphorylation of NuMA induces unbinding of dynein. Dynein localization oscillates to the opposing side of the cell while clustered centrosomes are reinforced by non-motor and/or k-fiber tension-dependent mechanisms.

validate this model prediction, we used using fixed and live-cell imaging approaches in cells with CA with and without cortical dynein. Biological results were consistent with model results, with a significant reduction in clustered spindles and an increase in multipolar divisions following loss of cortical dynein (Fig. 34, Fig. 35). Furthermore, this finding was consistent across cell lines, suggesting that dynein's role in centrosome clustering is independent of centrosome number (>2) and DNA content (Fig. 34). Together, these data suggest that cortical dynein contributes to centrosome clustering in cells with CA. Work from our lab previously showed that inhibition of the kinase Aurora A disrupts centrosome clustering [183]. NuMA is a target of Aurora A phosphorylation, and inhibition of Aurora

A induces an accumulation of NuMA at spindle poles while simultaneously reducing its localization at the cell cortex [80]. Based on our results suggesting that loss of cortical dynein disrupts clustering, it is tempting to speculate that Aurora A's phosphorylation of cortical NuMA is the mechanism by which it aids centrosome clustering. Future work further exploring this relationship in cells with CA could further elucidate mechanisms by which Aurora A and cortical dynein assists in centrosome clustering.

6.2.4 Actin and dynein act independently to cluster centrosomes

While cortical dynein has not been previously implicated in centrosome clustering, other proteins associated with the cell cortex have. These proteins include the actin cytoskeleton, E-cadherin, and the ERM complex [102, 131, 207]. All of these components are complexly linked to dynein localization and activity at the cell cortex. Dynein is directly linked to the actin cell cortex through astral MTs and a complex including NuMA, LGN, and Gαi [53]. Previous work has established that cortical dynein and the actin cell cortex act through independent mechanisms to orient the spindle in cells with two centrosomes [216]. Consistent with these previously published results, we find no disruption to cortical NuMA localization upon loss of actin-dependent cortical contractility via treatment the myosin II inhibitor Blebbistatin (Fig. 41 C,D) [232]. To determine if actin and dynein act through independent mechanisms to aid centrosome clustering, we assessed spindles in tetraploid RPE p53-/- cells with four centrosomes following Blebbistatin treatment with and without cortical dynein. We found that Blebbistatin treatment in cells with CA with normal cortical dynein activity (siCtl) impairs centrosome clustering, with a 20% decrease in cells with clustered spindles following Blebbistatin treatment (Fig. 41 A,B). These data suggest that cortical contractility contributes to clustering, consistent with the previous finding that actin is implicated in centrosome clustering [131]. In cells lacking cortical dynein (siLGN), however, we see no further disruption in centrosome clustering, with no significant difference in Blebbistatin treated cells with and without cortical dynein (Fig. 41 A,B). These

data suggest that the actin-dependent forces and cortical dynein-derived forces act through independent mechanisms to cluster centrosomes in cells with CA.

Loss of E-cadherin has been shown to disrupt centrosome clustering by reducing cortical contractility [207]. In epithelial tissues, however, E-cadherin binds to LGN to direct the localization of NuMA to cell-cell junctions [87]. Furthermore, in non-dividing cells, dynein co-localizes with E-cadherin and β-catenin at cell-cell junctions [145]. These findings, in combination with our results, suggest that loss of E-cadherin may also disrupt centrosome clustering through loss of cortical dynein localization and force-generation. Further exploration of the localization of dynein in cells with and without E-cadherin would be necessary to inform this hypothesis.

The cell cortex is not the only region of actin localization during mitosis. In addition to its well established role in cortical rigidity, actin filaments form an amorphous rotating cloud during mitotic progression [174]. The unconventional myosin motor, myosin X, which is able to bind to both MTs and actin filaments, has been shown to directly interact with this cloud of actin to orient the spindle [8, 132, 270]. Previous findings show that loss of LGN and myosin X have a synergistic disruption to spindle orientation, where loss of both have a more significant impact on orientation than loss of either one alone [132]. These findings suggest that the mechanism by which MT/myosin X/actin orients the spindle is independent of the MT/dynein/NuMA/LGN/actin mechanism. Additionally, a human myosin X ortholog has been implicated in centrosome clustering in *drosophila*, however this has not been explored in human cells [131]. Therefore, astral MT interactions with myosin X may additionally contribute to centrosome clustering in the absence of cortical dynein. Experiments exploring centrosome clustering efficiency with and without myosin X activity, in combination with loss of cortial dynein, would be necessary to explore this hypothesis.

6.2.5 Merlin/ERM-dependent centrosome clustering may be driven by dynein activity

ERM proteins have been implicated in spindle orientation and positioning through direct modulation of LGN/NuMA localization and astral MT dynamics [153, 228]. Loss of the tumor suppressor protein Merlin disrupts localization of ERM proteins to the cell cortex and impacts spindle positioning and orientation [102]. Furthermore, disruption of cortical Ezrin localization through loss of Merlin prevents centrosome clustering [102]. It is therefore tempting to speculate that the Merlin-dependent decrease in centrosome clustering is a result of loss of cortical dynein and force generation. Exploring the impact of loss of Merlin on centrosome clustering in the absence of cortical dynein could link the mechanisms by which loss of each of these proteins disrupts clustering.

6.3 Loss of Cortical Dynein Influences Chromosome Alignment and Segregation Following Loss of MT-Kinetochore Attachments

MT interactions with kinetochores are the major force-generating component driving chromosome movement and alignment during mitosis. In the absence of kinetochore attachments, via loss of MT binding to the Ndc80 complex, chromosomes become widely dispersed throughout the cell (Fig. 15 A,B). We found that following loss of cortical dynein activity chromosome alignment is partially rescued in the absence of Nuf2, a critical component of the Ndc80 complex (Fig. 36 B). These results suggest that either MT attachments to kinetochores are being rescued in the absence of Nuf2 when cortical dynein is lost, or mechanism(s), such as lateral MT attachments or polar ejection forces are compensating for disrupted forces within the spindle to align and segregate chromosomes. To determine if end-on MT attachments to kinetochores are being rescued following loss of cortical dynein in the absence of Nuf2, we assessed the localization of astrin, a protein that localizes along MTs, at spindle poles, and at kinetochores where it acts to stabilize kinetochore

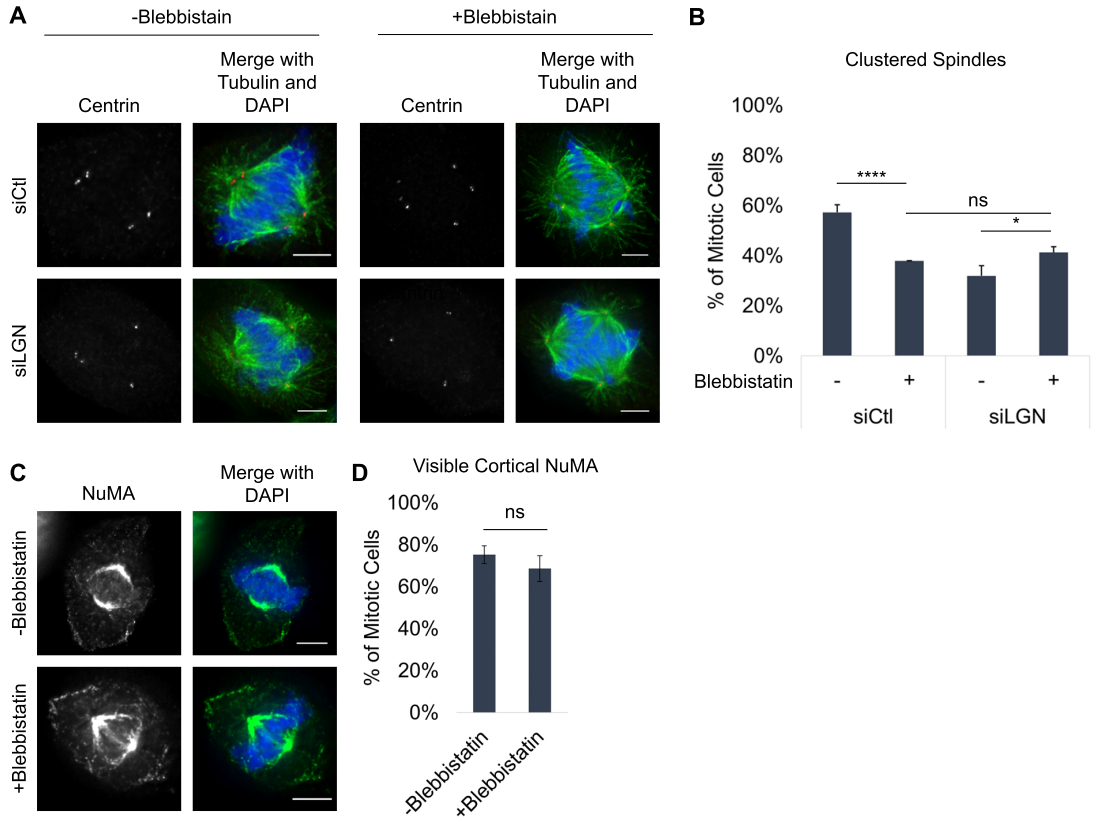

Figure 41: **Cortical contractility and dynein act independently to aid centrosome clustering.** (A) Fixed-cell images of tetraploid RPE p53-/- cells with or without Blebbistatin treatment. (B) Quantification of the percent of mitotic cells with clustered spindles in tetraploid RPE p53-/- cells with and without cortical dynein and Blebbistatin treatment. (C) Fixed RPE cells stained for NuMA with and without Blebbistatin treatment. (D) Quantification of the percent of mitotic RPE cells with visible cortical NuMA with and without Blebbistatin treatment. All scale bars are 5 μm. All quantification was performed on at least 50 cells per condition from 3 biological replicates. Error bars are SD.

MT attachments and promotes chromosome alignment [159]. Preliminary results from this analysis suggest that end-on attachments are not being rescued in the absence of cortical dynein (data not shown; incomplete replicates performed by Kylie Belanger). Therefore, a Ndc80-independent mechanism is aiding chromosome alignment in the absence of cortical dynein. Future work could explore key force regulators involved in this process, including chromoskinesin-derived forces and lateral attachments to the kinetochore by k-fibers.

Additionally, we found that more cells progress into anaphase when they lack both Nuf2

and cortical dynein compared to Nuf2 alone (Fig. 36 C,D). The ability of cells to progress through to anaphase following loss of Nuf2 and cortical dynein suggests that components of the SAC may be compromised. The SAC is required to prevent premature chromosome segregation prior to the establishment of stable bi-oriented kinetochores (attached to MTs from both spindle poles) and components of the SAC are regulated by the Ndc80 complex [65, 95, 164, 182, 262]. Our results suggest that disruption to SAC signaling following loss of Nuf2 may be rescued in the absence of cortical dynein. Future work should explore localization and activity of SAC components in cells lacking Nuf2 and/or cortical dynein.

6.3.1 Modeling chromosomes and kinetochores can inform force requirements for chromosome alignment and centrosome clustering

The purpose of the mitotic spindle is to separate the genetic material in the cell evenly to form two new daughter cells. Therefore, understanding how the mitotic spindle and chromosomes interact to allow this process to take place is essential. In this work, I describe a mathematical and computational model to simulate the formation and function of the mitotic spindle in the absence of chromosomes and chromosome-derived forces. We have additionally described an approach to model chromosomes and MT interactions with chromosome arms (see Section 5.3). We find that with chromokinesin and MT pushing forces on the chromosomes alone, chromosomes become positioned near the boundary of the cell (Fig. 39). This phenotype is similar to the chromatin dispersion seen following loss of end-on MT attachments to kinetochores following loss of Nuf2 (Fig. 15 A,B).

Both chromosomes and centrosomes move in response to forces generated by these MT interactions. While chromokinesin-derived forces are essential for chromosome alignment, they are not the major component of force generation on the chromosome [2]. Instead, MT interactions with kinetochores dominate chromosome movement, alignment, and segregation [203]. Consisting of over 100 proteins, the kinetochore is an incredibly complex region [38]. MT interactions with the kinetochore are equally complex, and there are many

components that should be carefully considered when modeling MT-kinetochore interactions and force generation. First, rather than individual MTs, 15-30 MTs bundle to form a k-fiber that interacts with the kinetochore region of the chromosome [243]. The number of MTs in the k-fiber bundle increases during mitotic progression, and the bundling activity is dependent on non-motor crosslinking activity by a protein complex of TACC3-ch-TOG-clathrin [15, 41]. While tools like Cytosim would be particularly useful in modeling crosslinking-dependent MT bundling and k-fiber binding and dynamics, using a minimalistic modeling approach to capture kinetochore dynamics can accurately capture biological phenomena while reducing computational complexity [5]. The model described in this work could be extended to allow MT bundling and k-fiber interactions with kinetochores. Alternatively, since the force generation at kinetochores is well characterized, an approach directly simulating force generation, rather than simulating individual MTs and MT interactions, could be used [203]. Upon successfully capturing kinetochore-dependent forces in our model, we can make novel predictions about the force requirements for proper chromosome alignment and centrosome clustering.

6.4 Non-Motor Proteins are Essential for Spindle Formation and Function

Throughout this work I have discussed the role of motor-dependent forces on mitotic spindle formation and function. However, equally important components of the spindle are non-motor proteins. Non-motor proteins have essential roles in MT dynamics, spindle pole integrity, chromosome alignment, and chromosome segregation [158]. Additionally, models in yeast have shown that a stable bipolar spindle can form in the presence of non-motor proteins alone through dynamic binding and unbinding activity [135]. Yeast undergo a closed mitosis, with spindle poles remaining embedded in the nuclear envelope, and have a simple spindle structure, with only 14 MTs per spindle pole. This makes yeast an appealing model organism to use for modeling the mitotic spindle [11, 61, 135, 208]. However, to understand

the implications of mitotic spindle function or disruption on human disease development and progression, modeling the mammalian mitotic spindle is essential. Experimentally testing whether non-motor-dependent activity is sufficient to form a spindle in mammalian cells is impossible due to the complexity of the cell. Through extending our model to either consider individual non-motor/crosslinking proteins or simulating crosslinking activity, we could explore the impact of non-motor activity on spindle formation, function, and centrosome clustering. Furthermore, by removing motor-dependent forces we could determine if crosslinking activity is sufficient to form a spindle in mammalian cells or maintain centrosome clustering in cells with CA.

7 Conclusions

Overall, this work described novel mechanisms by which cortical dynein-derived forces impact spindle dynamics and centrosome clustering. We defined a mathematical model that captures bipolar spindle formation and function by considering dynamic MT interactions with the motor proteins Eg5, HSET, and dynein. Using this model, we found that cortical dynein drives dynamic fluctuations in spindle length over time in cells with two centrosomes (described in Chapter 3). By extending the model to have extra centrosomes, we found that cortical dynein-dependent pulling forces drive centrosome clustering in cells with CA. This finding has important implications in cancer where CA results in cancer progression and poor patient prognosis. Together, this work highlights the strength of using mathematical modeling alongside biological experimentation to make novel predictions about dynamic biological processes and reveals new insight into potential mechanisms to suppress centrosome clustering in cancers with CA.

8 Methods

8.1 Biological Approaches

8.1.1 Cell Culture

All cell lines were maintained at 37°C with 5% CO_2. hTERT-immortalized Retinal Pigment Epithelial (RPE) cells expressing the tet-inducible Plk4 or GFP-centrin construct (provided by Neil Ganem, Boston University) and MDA-MB-231 (provided by Catherine Whittington, Worcester Polytechnic Institute) cells were maintained in Dulbecco's Modified Essential Medium (DMEM) while RPE p53 deficient cells (provided by Meng-Fu Bryan Tsou, Memorial Sloan Kettering Cancer Center) were maintained in DMEM F-12. All cell culture medium was supplemented with 10% Fetal Bovine Serum (FBS) and 1% Penicillin and Streptomycin.

8.1.2 Lentiviral Vectors

RPE cells stably expressing the tet-inducible Plk4 construct were previously described [89, 207] and generously provided by Neil Ganem. RPE cells stably expressing L304-EGFP-Tubulin (Addgene #64060) were generated by lentiviral transduction and placed under 10 μm/mL Puromycin selection for 5-7 days. Expression of the tagged constructs was confirmed by immunofluorescent imaging [166]. RPE cells stably expressing GFP-centrin were previously described [197] and generously provided by Neil Ganem.

8.1.3 siRNA and qPCR

Depletion of Nuf2, Afadin, and LGN was achieved by transient transfection of a pool of four siRNA constructs (Nuf2 target sequences: 5'-gaacgaguaaccacaauua-3', 5'-uagcugagauugugauuca-3', 5'-ggauugcaauaaaguucaa-3', 5'-aaacgauagugcugcaaga-3'; Afadin target sequences: 5'-ugagaaaccucua guugua-3', 5'-ccaaaugguuuacaagaau-3', 5'-guuaagggcccaagacaua-3', 5'-acuugagcggcaucgaaua-3', LGN target sequences: 5'-gaacuaacagcacgacuua-3', 5'-cuucagggaugcaguuaua-

3', 5'-acagugaaauucuugcuaa-3', 5'-ugaaggguucuuugacuua-3') at 50 nM using RNAiMAX transfection reagent according to manufacturer's instructions. Knockdwon conditions were performed alongside a scrambled control (siScr/siCtl) with a pool of four non-specific sequences (5'-ugguuuacaugucgacuaa-3', 5'-ugguuuacaugu
uguguga-3', 5'-ugguuuacauguuuucuga-3', 5'-gguuuacauguuuuccua-3').

Cells were collected in Trizol either 48 or 72 hours after transfection for gene expression analysis via qPCR. Phase separation and RNA isolation was performed according to manufacturer's instructions. cDNA was synthesized according to manufacturer's instructions. Depletion was confirmed by qPCR with primers for Nuf2 (F:5'-taccattcagcaatttagttact-3', R:5'-tagaatatcagcagtctcaaag-3'), Afadin (F:5'-gtgggacagcattaccgaca-3', R:5'tcatcggcttcaccattcc-3'), LGN (F:5'-gtgaccacccgtctgtcg-3', R:5'-ttcagcaacatttctcccgc-3'), and GAPDH (F:5'-ctagctggcccgatttctcc-3', R:5'-cgcccaatacgaccaaatc
aga-3') as a control. Media with transfection reagents was removed from cells at least 4 hours after transfection and replaced with fresh complete medium.

8.1.4 Chemicals

Table 4: Chemicals Used in Biological Experiments

Chemical	**Stock**	**Treatment Concentration**	**Treatment Concentration**	**Manufacturer Duration**
Blebbistatin	17 mM	50 μm	4 h	Sigma-Aldrich
Dihydrocytochalasin B	1.5mg/mL	1.5 μg/mL	24 h	Sigma-Aldrich
Doxycycline	2 mg/mL	2 μg/mL	48 h, 72 h	Acros Organics
MG132	20 mM	20 μM	30 min, 1 h	Fisher (Tocris)
RO-3306	10 mM	9 μm	5 min	Sigma-Aldrich

8.1.5 Immunofluorescence Imaging

Cells were captured with a Zyla sCMOS (Oxford Instruments, Belfast, UK) camera mounted on a Nikon Ti-E microscope (Nikon, Tokyo, Japan). A 60x Plan Apo oil immersion objective was used for fixed-cell imaging and live-cell imaging of RPE cells expressing GFP-

centrin to visualize centrosomes [81], and a 20x CFI Plan Fluor objective was used for live-cell imaging of RPE cells expressing GFP-tubulin [166]. Representative images of RPE cells expressing GFP-tubulin were captured with a 40x Plan Apo objective.

8.1.6 Fixed-Cell Imaging and Analysis

Cells seeded onto glass coverslips that were stained for NuMA were rinsed briefly in phosphate buffered saline (PBS) and placed in PHEM buffer with 0.3% Triton X-100 (TX-100) for 5 min. Cells were fixed in warmed 3.7% paraformaldehyde supplemented with 30 mM sucrose for 15 min and then permeabilized in 0.1% TX-100 in PBS for 5 min. Cells were blocked in 3% PBS-BSA with 0.05% Tween-20 for 15 min. Primary antibodies (anti-NuMA (1:100; Abcam ab109262, Cambridge, UK)) were diluted in blocking solution and cells were incubated in a humid chamber for 1 h. Cells were washed briefly in blocking solution. Secondary antibodies were diluted 1:1000 in blocking solution and cells were incubated in a humid chamber in the dark for 1 h. Cells were washed briefly in blocking solution. Cells were post-stained with TBS-BSA + 0.2 μg/mL DAPI for 20 min.

Cells stained for all other antibodies were rinsed briefly in phosphate buffered saline (PBS) and placed in ice cold methanol for 10 minutes at -20°C. Coverslips were washed briefly with PBS and blocked in TBS-BSA (10 mM Tris at pH 7.5, 150 mM NaCl, 1% bovine serum albumin (BSA)) for 10 minutes. Cells were incubated with primary antibodies diluted in TBS-BSA (anti-α-tubulin (1:1500; Abcam ab18251, Cambridge, UK), anti-Ndc80 (1:500; Novus Biologicals, Littleton, CO), anti-Centrin (1:1000; Millipore 04-1624, Burlington, MA), for 1 hour in a humid chamber. Cells were washed in TBS-BSA for 10 minutes then incubated with fluorophore-conjugated secondary antibodies (Invitrogen, Carlsbad, CA) diluted 1:1000 in TBS-BSA + 0.2 μg/mL DAPI for 45 minutes.

Fixed and live-cell image analysis was performed in NIS Elements. In Chapter 2.6, fixed cell analysis of DNA area was quantified by gating a region of interest by DAPI fluorescence intensity. In Chapter 3, spindle length was quantified by performing line

scans along the long axis of the mitotic spindle and considering the spindle poles to be the two highest peaks in fluorescence intensity. All analysis performed and all representative images are of a single focal plane. Background was subtracted by the rolling-ball algorithm [31] and contrast was adjusted in ImageJ to prepare fixed-cell images and GFP-centrin live-cell images for publication. Statistical analysis between two conditions was performed in Excel; two-tailed Student's *t*-test was used for comparisons between two groups. To assess multiple comparisons, a one-way ANOVA was performed with Dunnett's test post-hoc for simultaneous comparison between each test condition and a control.

In Chapter 4, spindle morphology was characterized as clustered or unclustered. Clustered spindles were those with < 4 μm between adjacent centrosomes. NuMA localization was determined to be present or not present, as described previously [216]. Cells with NuMA present were further characterized by location with respect to spindle poles, with NuMA localized behind 1, behind >1, or between spindle poles, as determined by increased cortical localization in those regions.

8.1.7 Live-Cell Imaging and Analysis

RPE cells stably expressing α-tubulin-EGFP were seeded onto a 6-well plate. NIS elements HCA jobs software was used to enable multi-coordinate, multi-well imaging in a single z-stack (0.67 μm per pixel) [166]. Images were captured every 5 minutes for 16 hours in Chapter 2.7 or every 2.5 min for 12 hours in Chapter 4. Analysis was performed on at least 50 mitotic cells. Mitotic duration was quantified as the time between nuclear envelope breakdown, determined by loss of GFP exclusion from the nucleus, to anaphase B, determined by rapid elongation of the spindle. Mitotic fate was determined by the number of cytokinetic furrows (bipolar: 2 cytokinetic furrows, multipolar: >2 cytokinetic furrows).

RPE cells stably expressing GFP-centrin were seeded onto glass coverslips and placed in a sealed chamber slide with 100 μl of media. Single cells entering mitosis were captured at 60x in a single z-stack (0.11 μm per pixel) every fifteen seconds for the duration of

mitosis or until centrosomes were no longer in the same plane. Spindle length fluctuations were quantified as the average number of peaks per minute, rather than the total number of peaks per trace to account for changes in movie duration.

8.2 Modeling Approaches

8.2.1 Model and Data Generation

All computational modeling and model analysis was performed in MATLAB. Due to the benefit of running many parallel operations simultaneously, the code was written to run on a graphics processing unit (GPU). We leveraged the parallelism of GPUs to perform every calculation on every MT at each time step. While it seems counterintuitive to perform thousands of unnecessary computations, this structure runs 93% faster than an iterative method on a CPU (simulations completed in 24h on a CPU take 1.5h on GPU).

We create a file that defines the parameters within the model and one that initializes the components that define the physical structures within the model (centrosome position, MT characteristics, etc.) and force vectors. These files are called into the main file, after which the time loop is defined. To define our MTs, we establish a parameter U that is equal to the maximum number of MTs allowed in the system. We then create vectors for each characteristic that defines MTs (MT length, MT angle, MT coordinates, the centrosome it is attached to, etc.). Each of these vectors has length U, where the entries are non-zero if the MT exists. At time $t = 0$, 300 entries are non-zero. As MTs are nucleated over time, more entries become non-zero.

Similarly, each force is initialized as a vector of zeros with length U. If the probability and distance requirements for force generation are not satisfied (Fig. 8), entries remain non-zero. Alternatively, forces will be calculated by equations described in Chapter 2.2. Forces are calculated in individual function files to which the necessary information to calculate the force is passed in. Within each force function file, we use the MATLAB function "arrayfun", which applies a function to each element of an array. This allows us to loop on

MTs while maintaining the speed of GPU computation. Within each “arrayfun", the force on *individual* MTs is calculated. This force vector is updated based on these calculations then called back out to the function file for the respective force. The total force is then calculated based on Eqs. (4),(6),(11),(12),(13). Updated forces within the function files are called back out into the main file. These forces are then summed by Eq. (2) to calculate the net force on each centrosome, then the position of the centrosome is updated based on these forces.

Data was generated using a high-performance computing system acquired through NSF MRI grant DMS-1227943 to WPI. Data was averaged over at least 10 simulations for each condition. Additional model details and analysis in the Appendix.

9 Appendix

9.1 Existing Models of Mitosis

Mathematical modeling of mitotic progression has been a valuable tool in making novel predictions and better understanding the dynamic process. Below I summarize existing models of early spindle elongation (Table 5), spindle assembly (Table 6), spindle pole organization (Table 7), the regulation of interpolar MT overlap regions (Table 8), spindle movement and positioning (Table 9), the regulation of spindle length and structure (Table 10), and centrosome clustering (Table 11).

Table 5: Early Spindle Elongation

Species	**Model Outcome**	**Limitations**
Drosophila	Cortical dynein balances Ncd (HSET in humans) to regulate centrosome separation in prophase.	Omits MT dynamics and MT-dependent forces, such as polymerization against the cell cortex. [49]
Drosophila	Force produced by nuclear elasticity is synergistic to Ncd-derived forces during centrosome separation during prophase.	Omits MAPs and other regulators of MT dynamics. [50]

Table 6: Spindle Assembly

Species	**Model Outcome**	**Limitations**
Xenopus	Proposes the existence of motor proteins with plus and minus-end-directed activity at the interpolar region of the spindle.	Omits motor-independent forces and protein-dependent regulation of MT stability. Does not include chromosomes. [185]
Xenopus	Characterize optimal parameters for spindle formation via Eg5 and chromokinesin-derived forces.	Omits inward forces by kinesin-14 and MT dynamics. [215]

Xenopus	Propose a model for anastral (lacking asters) spindle assembly where MTs nucleated near chromosomes slide outward and cluster to form functional spindle poles, which depends on two distinct classes of molecular motors.	Considers general plus and minus-end-directed motors rather than specific motor proteins (dynein versus kinesin-14), and non-dynamic MT plus ends. [24]
General	Spatial regulation of MT catastrophe parameters can lead to better spindle morphology and longer antiparallel MT overlap.	Considers only motor proteins with heterocomplexes, those with motor heads that move in opposite directions. [36]
Xenopus	NuMA/dynein-dependent transport of the MT depolymerizing agents kinesin-13 and MCAK are required for spindle formation.	Omits kinesin-14 derived forces. [149]
Human	Spindle assembly is sensitive to kinetochore size and architecture.	Does not consider motor proteins. [154]
S. pombe	MT bundling by crosslinking proteins and sliding by kinesin-14 is sufficient to generate a bipolar spindle.	Only considers a static crosslinker and kinesin-14, omits activity by other motor proteins including kinesin-5. [109]
S. pombe	A bipolar spindle can form in the presence of passive crosslinkers alone.	Omits chromosomes and chromosome-derived forces. [11]
S. pombe	Define the required characteristics of passive crosslinkers to form and maintain a bipolar mitotic spindle.	No motor protein-derived forces included or tested. [135]
S. pombe	Define the requirements of chromosome biorientation and bipolar spindle formation and maintenance.	*S. pombe* have simplified spindles with a set number of MTs, and spindle pole bodies embedded in the nuclear envelope. Relevant applications to metazoans is unclear. [61]

Table 7: Spindle Pole Organization

Species	**Model Outcome**	**Limitations**

Human (cell-free)	MT organization at the spindle poles requires both motor and non-motor forces.	No MT-cortex interactions or forces considered; HSET and dynein only bound to parallel MTs. [33]
Human (cell-free)	Dynein activity promotes MT organization and aster formation.	Prevent continuous motor-dependent transport and does not reproduce experimentally established results of aster centering. [48]

Table 8: Regulation of Interpolar MT Overlaps

Species	**Model Outcome**	**Limitations**
General	Passive cross-linkers have a dynamic role in regulating interpolar MT overlap length in the spindle.	Omits MT dynamics. [112]
S. cerevisiae	Minus-end-directed motility by kinesin-14 aligns MTs along the spindle axis, allowing kinesin-5 to modulate spindle length at antiparallel MT overlaps.	Omits MT dynamics and considers only the simple spindle structure of budding yeast. [104]

Table 9: Spindle Movement and Positioning

Species	**Model Outcome**	**Limitations**
C. elegans	Cooperative cortical force generation contributes to spindle oscillations during asymmetric cell division.	One-dimensional model. [94]
C. elegans	MT dynamics impact spindle positioning and oscillations.	Considers only cortical force generators. [129]
C. elegans	The asymmetric distribution of cortical dynein contributes to asymmetric spindle positioning within the cell.	Only a single MT aster is considered. [152]
General	Spindle positioning and orientation is dependent on cell shape and size.	Assume both dynein and kinesin generate force at the cell cortex; considers kinesin to always be plus-end-directed (omits kinesin-14). [142]

General	Interpolar and astral MT length differences, inducing geometric asymmetry within the spindle, induce an upper limit of spindle length.	Assume both dynein and kinesin generate force at the cell cortex; considers kinesin to always be plus-end-directed (omits kinesin-14). [143]
General	Tricellular junctions competes with cell size to be the dominant factor regulating spindle orientation in tissues.	Omits cell rounding when testing the impact of tricellular junctions on spindle orientation; omits kinesin-5-derived forces. [141]

Table 10: Regulation of Spindle Length and Structure

Species	**Model Outcome**	**Limitations**
Xenopus	Katanin-dependent MT stabilization impacts spindle length.	Omits kinesin-14 derived forces. Simulated with Cytosim, limiting the available components for testing and validation. [150]
Drosophila	Reverse engineering of experimental data reveals essential biophysical properties of the mitotic spindle, and implicate opposing forces by Eg5 and k-fibers in the maintenance of the spindle.	Composes a simplistic one-dimensional, symmetric spindle with a homogeneous distribution of motor proteins. [267]
Drosophila	A balance between MT depolymerization and MT sliding regulates metaphase spindle length.	Omits astral MT interactions with the cell cortex and chromokinesins. [91]
Drosophila	The lamin-B spindle envelope supplements kinesin-5 and kinesin-14 forces balance at the spindle midzone in prometaphase.	Omits chromosomes and chromosome-associated forces and cortex-associated forces. [44]
Human	Torque within the spindle contributes to its chirality.	Omits motor-dependent forces and considers only established, static MT bundles. [189]

Table 11: Centrosome Clustering

Species	**Model Outcome**	**Limitations**

Drosophila	Chromosomes are a barrier that prevents centrosome clustering in polyploid cells.	Omits cortex and kinesin-5-derived forces. [92]
General	Define attractive and repulsive forces required for centrosome clustering; centrosome attraction to the cell cortex (cortical dynein force) offsets centrosome-centrosome attraction (kinesin-14 force).	Does not explicitly model MTs (MT dynamics and forces omitted). [37]
General	MT-derived torque on chromosome arms, in combination with centrosome-centrosome attraction promotes centrosome clustering.	Omits cortex-derived forces. [170]

9.2 Model Analysis

Two Centrosomes

While many parameters in our model have been well established by biological, biophysical, or mathematical studies, we define novel parameters in our model that we have optimized to reflect accurate spindle formation and maintenance. We explore the sensitivity of our model, as a readout of bipolar spindle length at $t = 10$ min, with values above and below our selected parameters. While manipulating a parameter, all other parameters remain unchanged from the base case.

The parameter C accounts for crosslinking proteins within the spindle, and dampen Eg5 and HSET-derived forces at the interpolar region. We find that decreasing C reduces spindle length, while increasing C increases spindle length (Table 12). We find similar results when we manipulate the parameter K, which scales forces in a MT length-dependent manner (Table 12).

The parameter s scales MT catastrophe frequency. We find that if we decrease s, allowing MTs to become longer, the average spindle length increases (Table 13). Alternatively, if we increase s such that MTs have a shorter average length, spindle length decreases (Table

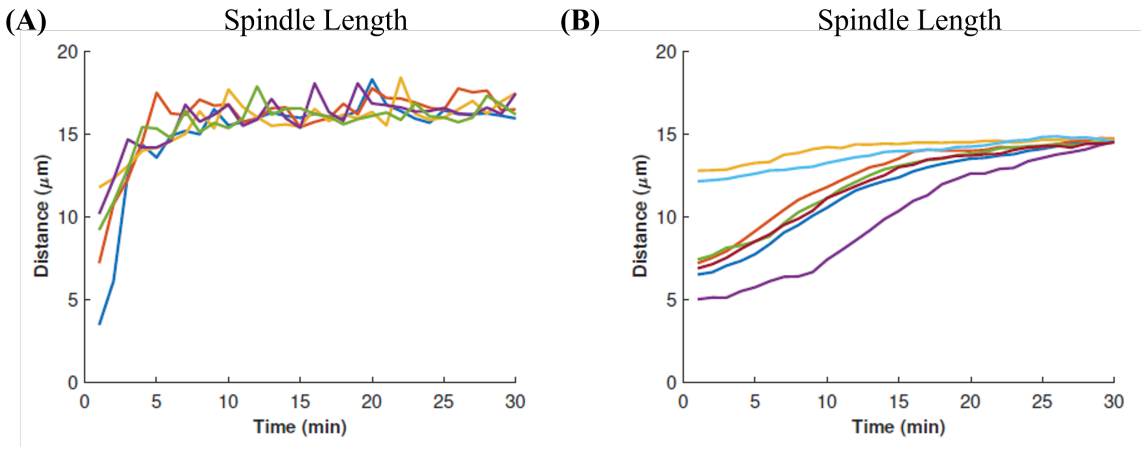

Figure 42: **Increasing the constant drag coefficient alters the length and dynamics of the bipolar spindle**. Curves of spindle length over time with the base parameter (A, $\xi = 20.6$) and the high drag parameter (B, $\xi = 103$).

13). This is likely due to the fact that MTs are not long enough to reach the cell boundary or interact with each other to generate force.

The parameter ξ is the constant drag parameter that dampens centrosome movement. This parameter accounts for the viscous cytoplasm within the cell. We find that if we increase ξ, spindle length decreases and spindle dynamics are significantly impacted (Table 13, Fig.42).

To understand how model outcomes such as spindle length vary due to stochasticity by MT dynamics and MT-motor protein binding and unbinding, we performed an increasing number of simulations with the same initial centrosome positioning. Traces of centrosome movement over time show different trajectories (Fig.43 A), but the distance between centrosomes at $t = 25$ min (spindle length) are similar (Fig.43 B).

Table 12: Sensitivity analysis to crossklinking parameter C and force/drag scaling parameter K. Base case corresponds to $C = 0.1$ and $K = 0.25$. Results are averaged over 10 simulations at $t = 10$ min.

C	0.025	0.05	**0.1**	0.15	0.2
Spindle Length (μm)	5.09	14.8	**16.5**	17.31	17.67
K	0.1	0.2	**0.25**	0.3	0.4
Spindle Length (μm)	11.43	14.88	**16.5**	18.42	20.35

Table 13: Sensitivity analysis to MT catastrophe rate scaling s and constant drag parameter ξ. Base case corresponds to $s = 0.15$ and $\xi = 20.6$. Results are averaged over 10 simulations at $t = 10$ min.

s	0.05	**0.15**	0.3
Spindle Length (μm)	18.93	**16.5**	12.9
ξ		**20.6**	5ξ
Spindle Length (μm)		**16.5**	13.33

(A) Centrosome Movement **(B)**

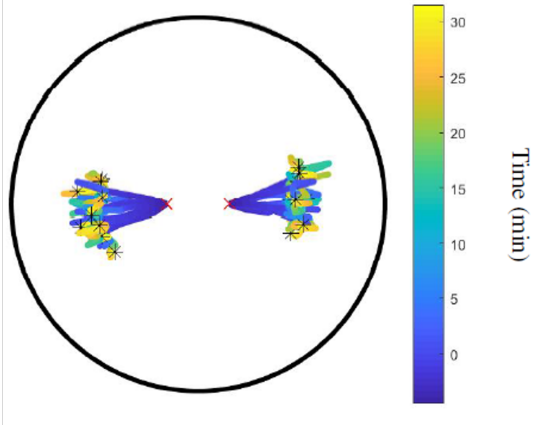

# of sims	Avg length (μm)
5	17.79
10	17.53
15	17.56
20	17.65

Figure 43: **Multiple simulations with the same initial centrosome positioning reveal variations due to model stochasticity**. (A) Traces of centrosome movement over time for 10 simulations with the same initial centrosome positions. Red 'x' is initial position, black asterisk is final position. (B) Table of the average spindle length at $t = 25$ min for 5, 10, 15, and 20 simulations with the same initial centrosome positions.

References

[1] S.J. Anderhub, A. Kramer, and B. Maier. Centrosome amplification in tumorigenesis. *Cancer Lett.*, 322:8–17, 2012.

[2] C. Antonio, I. Ferby, H. Wilhelm, M. Jones, E. Karsenti, A.R. Nebreda, and I Vernos. Xkid, a chromokinesin required for chromosome alignment on the metaphase plate. *Cell*, 102:425–435, 2000.

[3] C. Aponte-Rivera and R.N. Zia. Simulation of hydrodynamically interacting particles confined by a spherical cavity. *Phys. Rev. Fluids*, 1:023301, 2016.

[4] JR Bader and KT Vaughan. Dynein at the kinetochore: timing, interactions, and functions. *Semin Cell Dev Biol*, 21:269–275, 2010.

[5] E.J. Banigan, K.K. Chiou, E.R. Ballister, A.M. Mayo, M.A. Lampson, and A.J. Liu. Minimal model for collective kinetochore-microtubule dynamics. *Proc. Natl. Acad. Sci. U.S.A.*, 112:12699–12704, 2015.

[6] M. Barisic, P. Aguiar, S. Geley, and H. Maiato. Kinetochore motors drive congression of peripheral polar chromosomes by overcoming random arm-ejection forces. *Nat. Cell Biol.*, 16:1249–1257, 2014.

[7] A.R. Barr and F. Gergely. Mcak-independent functions of ch-tog/xmap15 in microtubule plus-end dynamics. *Mol. Cell Biol.*, 28:7199–7211, 2008.

[8] J.S. Berg, B.H. Derfler, C.M. Pennisi, D.P. Corey, and R.E. Cheney. Myosin-x, a novel myosin with pleckstrin homology domains, associates with regions of dynamic actin. *J. Cell Sci.*, 113:3439–3451, 2000.

[9] M. Bettencourt-Dias and D.M. Glover. Centrosome biogenesis and function: centrosomics brings new understanding. *Nat. Rev. Mol. Cell Biol.*, 8:451–463, 2007.

[10] M. Biro, Y. Romeo, S. Kroschwald, M. Bovellan, A. Boden, J. Tcherkezian, P.P. Roux, G. Charras, and E.K. Paluch. Cell cortex composition and homeostasis resolved by integrating proteomics and quantitative imaging. *Cytoskeleton*, 70:741–754, 2013.

[11] R. Blackwell, C. Edelmaier, O. Sweez-Schindler, A. Lamson, Z.R. Gergely, E. O'Toole, A. Crapo, L.E. Hough, J.R. McIntosh, M.A. Glaser, and M.D. Betterton. Physical determinants of bipolar mitotic spindle assembly and stability in fission yeast. *Cell Biol*, 3:e1601603, 2017.

[12] T. Bodrug, E.M. Wilson-Kubalek, S. Nithianantham, A.F. Thompson, A. Alfieri, I. Gaska, J. Major, G. Debs, S. Inagaki, P. Gutierrez, L. Gheber, R.J. McKenny, C.V. Sindler, R. Milligan, J. Stumpff, S.S. Rosenfeld, S.T. Forth, and J. Al-Bassam. The kinesin-5 tail domain directly modulates the machanochemical cycle of the motor domain for anti-parallel microtubule sliding. *eLife*, 9:e51131, 2020.

[13] H. Boleti, E. Karsenti, and I. Vernos. Xklp2, a novel xenopus centrosomal kinesin-like protein required for centrosome positioning during mitosis. *Cell*, 84:49–59, 1996.

[14] A.J.R. Booth, Z. Yue, J.K. Eykelenboom, T. Stiff, G.W.G. Luxton, H. Hochegger, and T.U. Tanaka. Contractile acto-myosin network on nuclear envelope remnants positions human chromosomes for mitosis. *eLife*, 8:e46902, 2019.

[15] D.G. Booth, F.E. Hood, and S.J. Prior, I.A. Royle. A tacc3/ch-tog/clathrin complex stabilises kinetochore fibers by inter-microtubule bridging. *EMBO J.*, 30:906–919, 2011.

[16] A. Bouissou, C. Verollet, H. de Forges, L. Haren, Y. Bellaiche, F. Perez, A. Merdes, and B. Raynaud-Messina. gamma-tubulin ring complexes and eb1 play antagonistic roles in microtubule dynamics and spindle positioning. *EMBO J.*, 33:114–128, 2014.

[17] M. Braun, D.R. Drummond, R.A. Cross, and A.D. McAnish. The kinesin-14 klp2 organizes microtubules into parallel bundles by an atp-dependent sorting mechanism. *Nat. Cell Biol.*, 11:724–730, 2009.

[18] M. Breuer, A. Kolano, M. Kwon, C.C. Li, T.F. Tsai, D. Pellman, S. Brunet, and M-H. Verlhac. Hurp permits mtoc sorting for robust meiotic spindle bipolarity, similar to extra centrosome clustering in cancer cells. *J. Cell Biol.*, 191:1251–1260, 2010.

[19] G. Brouhard and A.J. Hunt. Microtubule movements on the arms of mitotic chromosomes: Polar ejection forces quantified in vitro. *Proc. Natl. Acad. Sci. U.S.A.*, 102:13903–13908, 2005.

[20] C.W. Brownlee and G.C. Rogers. Show me your license, please: deregulation of centriole duplication mechanisms that promote amplification. *Cell. Mol. Life Sci.*, 70:1021–1034, 2013.

[21] I. Brust-Mascher, G. Civelekoglu-Scholey, M. Kwon, A. Mogilner, and J.M. Scholey. Model for anaphase B: role of three mitotic motors in a switch from poleward flux to spindle elongation. *Proc. Natl. Acad. Sci. U.S.A.*, 101:15938–15943, 2004.

[22] I. Brust-Mascher and J.M. Scholey. Mitotic spindle dynamics in Drosophila. *Int. Rev. Cytol.*, 259:139–172, 2007.

[23] A. Burakov, E. Nadezhdina, B. Slepchenko, and V. Rodinov. Centrosome positioning in interphase cells. *J. Cell Biol.*, 162:963–969, 2003.

[24] K.S. Burbank, T.J. Mitchison, and D.S. Fisher. Slide-and-cluster models for spindle assembly. *Curr. Biol.*, 17:1373–1383, 2007.

[25] S. Busson, D. Dujardin, A. Moreau, J. Dompierrre, and J.R. De Mey. Dynein and dynactin are localized to astral microtubules and at cortical sites in mitotic epithelial cells. *Curr. Biol.*, 8:541–544, 1998.

[26] S. Cai, L.N. Weaver, S.C. Ems-McClung, and C.E. Walczak. Kinesin-14 family proteins hset/xtck2 control spindle length by cross-linking and sliding microtubules. *Mol Biol Cell*, 20:1348–1359, 2009.

[27] O. Campas and P. Sens. Chromosome oscillation in mitosis. *Phys. Rev. Lett.*, 97:128102, 2006.

[28] M. Carminati, S. Gallini, L. Pirovano, A. Alfieri, S. Bisi, and M. Mapelli. Concomitant binding of afadin to lgn and f-actin directs planar spindle orientation. *Nat. Struct. Mol. Biol.*, 23:155–163, 2016.

[29] S. Carreno, I. Kouranti, E.S. Glusman, M.T. Fuller, A. Echard, and F. Payre. Moesin and its activating kinase slik are required for cortical stability and microtubule organization in mitotic cells. *J. Cell Biol.*, 180:739–746, 2008.

[30] A. Castillo, H.C. Morse, V.L. Godfrey, R. Naeem, and M.J. Justice. Overexpression of eg5 causes genomic instability and tumor formation in mice. *Cancer Res.*, 67:10138–10147, 2007.

[31] M. Castle and J. Keller. *Rolling Ball Background Subtraction*, 2007.

[32] J.M. Cesario, J.K. Jang, B. Redding, N. Hah, T. Rahman, and K.S. McKim. Kinesin 6 family member subito participates in mitotic spindle assembly and interacts with mitotic regulators. *J. Cell Sci.*, 119:4770–4780, 2006.

[33] A. Chakravarty, L. Howard, and D.A. Compton. A mechanistic model for the organization of microtubule asters by motor and non-motor proteins in a mammalian mitotic extract. *Mol Biol Cellol. Cell*, 15:2116–2132, 2004.

[34] J.Y. Chan. A clinical overview of centrosome amplification in human cancers. *Int. J. Biol. Sci.*, 7:1122–1144, 2011.

[35] G. Chandrasekaran, P. Tatrai, and F. Gergley. Hittin the brakes: targeting microtubule motors in cancer. *Br. J. Cancer*, 113:693–698, 2015.

[36] W.E. Channels, F.J. Nedelec, Y. Zheng, and PA. Iglesias. Spatial regulation improves antiparallel microtubule overlap during mitotic spindle assembly. *Biophys. J.*, 94:2598–2609, 2008.

[37] S. Chatterjee, A. Sarker, A. Khodjakov, A. Mogilner, and R. Paul. Mechanics of multi-centrosomal clustering in bipolar mitotic spindles. In Press, preprint at bioRxiv 0.1101/2019.12.17.879817, 2020.

[38] I.M. Cheeseman. The kinetochore. *Cold Spring Harb. Perspect. Biol.*, 6:a015826, 2014.

[39] I.M. Cheeseman, J.S. Chappie, E.M. Wilson-Kubalek, and A. Desai. The conserved kmn network consistutes the core microtubule-binding site of the kinetochore. *Cell*, 127:983–997, 2006.

[40] I.M. Cheeseman and A. Desai. Molecular architecture of the kinetochore-microtubule interface. *Nat. Rev. Mol. Cell Biol.*, 9:33–46, 2008.

[41] L.P. Cheeseman, E.F. Harry, A.D. McAnish, I.A. Prior, and S.J. Royle. Specific removal of tacc3-ch-tog-clathrin at metaphase deregulates kinetochore fiber tension. *J. Cell Sci.*, 126:2102–2113, 2013.

[42] C. Chen, H. Hehnly, Q. Yu, D. Farkas, G. Zheng, S.D. Redick, H. Hung, R. Samtani, A. Jurczyk, S. Akbarian, C. Wise, A. Jackson, M. Bober, Y. Guo, C. Lo, and S. Doxsey. A unique set of centrosome proteins requires pericentrin for spindle-pole localization and spindle orientation. *Curr. Biol.*, 24:2327–2334, 2014.

[43] G. Civelekoglu-Scholey, D.J. Sharp, A. Mogilner, and J.M. Scholey. Model of chromosome motility in Drosophila embryos: adaptation of a general mechanism for rapid mitosis. *Biophys. J.*, 90:3966–3982, 2006.

[44] G. Civelekoglu-Scholey, L. Tao, I. Brust-Mascher, R. Wollman, and J.M. Scholey. Prometaphase spindle maintenance by an antagonistic motor-dependent force balance made robust by a disassembling lamin-b envelope. *J. Cell Biol.*, 188:49–68, 2010.

[45] A.G. Clark, K. Dierkes, and E.K. Paluch. Monitoring actin cortex thickness in live cells. *Biophys. J.*, 105:570–580, 2013.

[46] G.M. Cooper. *The Cell: A Molecular Approach*. Sinauer Associates, 2000.

[47] I. Cunha-Ferriera, A. Rodrigues-Martins, I. Bento, M. Riparbelli, W. Zhang, E. Laue, G. Callaini, D.M. Glover, and M. Bettencourt-Dias. The scf/slimb ubiq-

uitin ligase limits centrosome amplification through deregulation of sak/plk4. *Curr. Biol.*, 19:43–49, 2009.

[48] E.N. Cytrynbaum, V. Rodionov, and A. Mogilner. Computational model of dynein-dependent self-organization of microtubule asters. *J. Cell Sci.*, 114:1381–1397, 2004.

[49] E.N. Cytrynbaum, J.M. Scholey, and A.M. Mogilner. A force balance model of early spindle pole separation in drosophila embryos. *Biophys. J.*, 84:757–769, 2003.

[50] E.N. Cytrynbaum, P. Sommi, I. Brust-Mascher, J.M. Scholey, and A. Mogilner. Early spindle assembly in Drosophila embryos: role of a force balance involving cytoskeletal dynamics and nuclear mechanics. *Mol Biol Cellol. Cell*, 16:4967–4981, 2005.

[51] A.B. D'Assoro, W.L. Lingle, and J.L. Salisbury. Centrosome amplification and the development of cancer. *Oncogene*, 21:6146–6153, 2002.

[52] J.G. DeLuca, B. Moree, J.M. Hickey, J.V. Kilmartin, and E.D. Salmon. hnuf2 inhibition blocks stable kinetochore-microtubule attachment and induces mitotic cell death in HeLa cells. *J. Cell Biol.*, 159:549–555, 2002.

[53] F. di Pietro, A. Echard, and X. Morin. Regulation of mitotic spindle orientation: an integrated view. *EMBO Rep*, 17:1106–1130, 2016.

[54] A. Dinarina, C. Pugieux, M.M. Corral, M. Loose, J. Spatz, E. Karsenti, and F. Nedelec. Chromatin shapes the mitotic spindle. *Cell*, 138:502–513, 2009.

[55] Z. Ding, C. Huang, X. Jiao, D. Wu, and L. Huo. The role of tacc3 in mitotic spindle organization. *Cytoskeleton (Hoboken)*, 74:369–378, 2017.

[56] Q. Du and I.G. Macara. Mammalian pins is a conformational switch that links numa to heterotrimeric g proteins. *Cell*, 119:503–516, 2004.

[57] T. Duke and S. Leibler. Motor protein mechanics: A stochastic model with minimal mechanochemical coupling. *Biophys. J.*, 71:1235–1247, 1996.

[58] J. Dumont. Acentrosomal spindle assembly and chromosome segregation during oocyte meiosis. *Trends Cell Biol.*, 22:241–249, 2012.

[59] S. Dumont and T.J. Mitchison. Force and length in the mitotic spindle. *Curr. Biol.*, 19:R749–R761, 2009.

[60] C.J. Echeverri, B.M. Paschal, K.T. Vaughan, and R.B. Vallee. Molecular characterization of the 50-kd subunit of dynactin reveals function for the complex is chromosome alignment and spindle organization during mitosis. *J. Cell Biol.*, 132:617–633, 1996.

[61] C. Edelmaier, A.R. Lamson, Z.R. Gergley, S. Ansari, R. Blackwell, J.R. McIntosh, M.A. Glaser, and M.D. Betterton. Mechanisms of chromosome biorientation and bipolar spindle assembly analyzed by computational modeling. *eLife*, 9:e48787, 2020.

[62] M.M. Elshenawy, J.T. Canty, L. Oster, L.S. Ferro, Z. Zhou, S.C. Blanchard, and A. Yildiz. Cargo adaptors regulate stepping and force generation of mammalian dynein-dynactin. *Nat Chem Biol*, 15:1093–1101, 2019.

[63] S.A. Endow, R. Chandra, D.J. Komma, A.H. Yamamoto, and E.D. Salmon. Mutants of the drosophila ncd microtubule motor protein cause centrosomal and spindle pole defects in mitosis. *J. Cell Sci.*, 107:859–867, 1994.

[64] C. Estrem, C.P. Fees, and J.K. Moore. Dynein is regulated by the stability of its microtubule track. *J. Cell Biol.*, 216:2047–2058, 2017.

[65] B. Etemad, T.E.F. Kuijt, and G.J.P.L. Kops. Kinetochore-microtubule attachment is sufficient to satisfy the human spindle assembly checkpoint. *Nat. Comm.*, 6:8987, 2015.

[66] R.G. Fehon, A.I. McClatchey, and A. Bretscher. Organizing the cell cortex: the role of erm proteins. *Nat. Rev. Mol. Cell Biol.*, 11:276–287, 2010.

[67] N.P. Ferenz, A. Gable, and P. Wadsworth. Mitotic functions of kinesin-5. *Semin Cell Dev Biol*, 21:255–259, 2010.

[68] N.P. Ferenz, R. Paul, C. Fagerstrom, A. Mogilner, and P. Wadsworth. Dynein antagonizes Eg5 by crosslinking and sliding antiparallel microtubules. *Curr. Biol.*, 19:1833–1838, 2009.

[69] A.B. Fielding, S. Lim, K. Montgomery, I. Dobreva, and S. Dedhar. A critical role of integrin-linked kinase, ch-tog and tacc3 in centrosome clustering in cancer cells. *Oncogene*, 30:521–534, 2010.

[70] G. Fink, L. Hajdo, K.J. Skowronek, C. Reuther, A.A. Kasprzak, and S. Diez. The mitotic kinesin-14 ncd drives directional microtubule-microtubule sliding. *Nat. Cell Biol.*, 11:717–723, 2009.

[71] S. Forth and T.M. Kapoor. The mechanics of microtubule networks in cell division. *J. Cell Biol.*, 216:1525–1531, 2017.

[72] K.F. Freed. Analytical solution for steady-state populations in the self-assembly of microtubules from nucleating sites. *Phys. Rev. E*, 66:061916, 2002.

[73] C. Fu, J.J. Ward, I. Loiodice, G. Velve-Casquillas, F.J. Nedelec, and P.T. Tran. Phospho-regulated interaction between kinesin-6 klp9p and microtubule bundler ase1p promotes spindle elongation. *Dev. Cell*, 17:257–267, 2009.

[74] X. Fu, Y. Zhu, B. Zheng, Y. Zou, C. Wang, P. Wu, J. Wang, H. Chen, P. Du, and B. Liang. Kifc1, a novel potential prognostic factor and therapeutic target in hepatocellular carcinoma. *Int. J. Oncol.*, 52:1912–1922, 2018.

[75] K. Fukasawa. Centrosome amplification, chromosome instability, and cancer development. *Cancer Lett.*, 8:6–19, 2005.

[76] H. Funabiki and A.W. Murray. The xenopus chromokinesin xkid is essential for metaphase chromosome alignment and must be degraded to allow anaphase chromosome movement. *Cell*, 102:411–424, 2000.

[77] S. Gadde and R. Heald. Mechanisms and molecules of the mitotic spindle. *Curr. Biol.*, 14:797–805, 2004.

[78] J. Gaetz and T.M. Kapoor. Dynein/dynactin regulate metaphase spindle length by targeting depolymerizing activities to spindle poles. *J. Cell Biol.*, 166:465–471, 2004.

[79] F. Galimberti, S.L. Thompson, S. Ravi, D.A. Compton, and E. Dmitrovsky. Anaphase catastrophe is a target for cancer therapy. *Clin. Cancer Res.*, 17:1218–1211, 2011.

[80] S. Gallini, M. Carminati, F. De Mattia, L. Pirovano, E. Martini, A. Oldani, G. Asteriti, I.A. Guarguaglini, and M. Mapelli. Numa phosphorylation by aurora-a orchestrates spindle orientation. *Curr. Biol.*, 26:458–469, 2016.

[81] N.J. Ganem, S.A. Godinho, and D. Pellman. A mechanism linking extra centrosomes to chromosomal instability. *Nature*, 460:278–282, 2009.

[82] NJ Ganem, Z Storchova, and D Pellman. Tetraploidy, aneuploidy and cancer. *Curr. Opin. Genet. Dev.*, pages 157–162, 2007.

[83] M.K. Gardner, D.C. Bouck, L.V. Paliulis, J.B. Meehl, E.T. O'Toole, J. Haase, A. Soubry, A.P. Joglekar, M. Winey, E.D. Salmon, K. Bloom, and D.J. Odde. Chromosome congression by kinesin-5 motor-mediated disassembly of longer kinetochore microtubules. *Cell*, 135:894–906, 2008.

[84] M.K. Gardner, M. Zanic, C. Gell, V. Bormuth, and J. Howard. Depolymerizing kinesins Kip3 and MCAK shape cellular microtubule architecture by differential control of catastrophe. *Cell*, 147:1092–1103, 2011.

[85] M.K. Gardner, M. Zanic, and J. Howard. Microtubule catastrophe and rescue. *Curr. Opinion Cell Biol.*, 25:14–22, 2013.

[86] S. Garrett, K. Auer, D.A. Compton, and T.M. Kapoor. htpx2 is required for normal spindle morphology and centrosome integrity during vertebrate cell division. *Curr. Biol.*, 12:731–742, 2002.

[87] M. Gloerich, J.M. Bianchini, K.A. Siemers, D.J. Cohen, and W.J. Nelson. Cell division orientation is coupled to cell-cell adhesion by the e-cadherin/lgn complex. *Nat. Comm.*, 8:13996, 2017.

[88] S.A. Godinho, M. Kwon, and D. Pellman. Centrosomes and cancer: how cancer cells divide with too many centrosomes. *Cancer Metastasis Rev.*, 28:85–98, 2009.

[89] S.A. Godinho and D. Pellman. Causes and consequences of centrosome abnormalities in cancer. *Philos. Trans. R. Soc. B Bio. Sci.*, 369:20130467, 2014.

[90] D.J. Gordon, B. Resio, and D. Pellman. Causes and consequences of aneuploidy in cancer. *Nat. Rev. Genet.*, 13:289–203, 2012.

[91] G. Goshima, F. Nedelec, and R.D. Vale. Mechanisms for focusing mitotic spindle poles by minus end-directed motor proteins. *J. Cell Biol.*, 171:220, 2005.

[92] A. Goupil, M. Nano, G. Letort, S. Gemble, F. Edwards, O. Goundiam, D. Gogendeau, C. Pennetier, and R. Basto. Chromsomes function as a barrier to mitotic spindle bipolarity in polyploid cells. *J. Cell Biol.*, 219:e201908006, 2020.

[93] J. Gregan, S. Polakova, L. Zhang, I.M. Tolic-Norrelykke, and D. Cimini. Merotelic kinetochore attachment: causes and effects. *Trends Cell Biol.*, 21:374–381, 2011.

[94] S.W. Grill, K. Kruse, and F. Julicher. Theory of mitotic spindle oscillations. *Phys. Rev. Lett.*, 94:108104, 2005.

[95] P. Gui, D.M. Sedzro, X. Yuan, S. Liu, M. Hei, W. Tian, N. Zohbi, F. Wang, Y. Yao, F.O. Aikhionbare, X. Gao, D. Wang, X. Yao, and Z. Dou. Mps1 dimerization and multiscale interactions with ndc80 complex enable responsive spindle assembly checkpoint signaling. *J. Mol. Cell Biol.*, 12:486–498, 2020.

[96] S. Guo, P. Wang, and P. Xie. A model of processive movement of dimeric kinesin. *J. Theor. Biol.*, 414:62–75, 2017.

[97] S. Guo, W. Wang, P. Wang, and P. Xie. Force dependence of velocity and run length on kinesin-1, kinesin-2, and kinesin-5 family molecular motors. *Molecules*, 24:287, 2019.

[98] R. Habedanck, Y.D. Stierhod, C.J. Wilkinson, and E.A. Nigg. The polo kinase plk4 functions in centriole duplication. *Nat. Cell Biol.*, 7:140–1146, 2005.

[99] J. Happel and H. Brenner. *Low Reynolds Number Hydrodynamics*. Matrinus Nijhoff Publishers, 1965.

[100] R. Heald, R. Tournebize, T. Blank, R. Sandaltzopoulos, P. Becker, A. Hyman, and E. Karsenti. Self-organization of microtubules into bipolar spindles around artificial chromosomes in xenopus egg extracts. *Nature*, 382:420–425, 1996.

[101] R. Heald, R. Tournebize, A. Habermann, E. Karsenti, and A. Hyman. Spindle assembly in xenopus egg extracts: Respective roles of centrosomes and microtubule self-organization. *J. Cell Biol.*, 138:615–628, 1997.

[102] A.M. Hebert, B. DuBoff, J.B. Casaletto, A.B. Gladden, and A.I. McClatchey. Merlin/erm proteins establish cortical asymmetry and centrosome position. *Genes Dev.*, 26:2709–2723, 2012.

[103] K.J. Helmke and R. Heald. Tpx2 levels modulate meiotic spindle size and architecture in xenopus egg extracts. *J. Cell Biol.*, 3:385–393, 2014.

[104] A.J. Hepperla, P.T. Willey, C.E. Coombes, B.M. Schuster, M. Gerami-Nejad, M. McClellan, S. Mukherjee, J. Fox, M. Winey, D.J. Odde, E. O'Toole, and M.K. Gardner. Minus-end-directed kinesin-14 motors align antiparallel microtubules to control metaphase spindle length. *Dev. Cell*, 31:61–72, 2014.

[105] T.L. Hill. Introductory analysis of the gtp-cap phase-change kinetics at the end of a microtubule. *Proc. Natl. Acad. Sci. U.S.A.*, 81:6728–6732, 1984.

[106] E.H. Hinchliffe. The centrosome and bipolar spindle assembly. *Cell Cycle*, 10:3841–3848, 2011.

[107] S. Hoing, T.Y. Yeh, M. Baumann, N.E. Martinex, P. Habenberger, L. Kremer, H.C. Drexler, P. Kuchler, P. Reinhardt, A. Choidas, M.L Zischinsky, G. Zischinsky, S. Nandini, A.P. Ledray, S.A. Ketcham, L. Reinhardt, M. Abo-Rady, M. Glatza, P. King, S.J. Nussbaumer, S. Ziegler, B. Klebl, T.A. Schroer, H.R. Scholer, H. Waldmann, and J. Sterneckert. Dynarrestin, a novel inhibitor of cytoplsmic dynein. *Cell Chem. Biol.*, 25:357–369.e6, 2018.

[108] A.J. Holland, W. Lan, and D.W. Cleveland. Centriole duplication: a lesson in self-control. *Cell Cycle*, 9:2731–2736, 2010.

[109] M.E. Janson, R. Loughlin, I. Loiodice, C. Fu, D. Brunner, and F. Nedelec. Crosslinkers and motors organize dynamic microtubules to form stable bipolar arrays in fission yeast. *Cell*, 128:357–368, 2007.

[110] H. Jiang. Cell size modulates oscillation, positioning, and length of mitotic spindles. *Sci. Rep.*, 5:1–10, 2015.

[111] Q. Jin, F. Huang, X. Wang, H. Zhu, Y. Xian, J. Li, S. Zhang, and Q. Ni. High eg5 expression predicts poor patient prognosis in breast cancer. *Oncotarget*, 8:62208–62216, 2017.

[112] D. Johann, D. Goswami, and K. Kruse. Generation of stable overlaps between antiparallel filaments. *Phys. Rev. Lett.*, 115:118103, 2015.

[113] L.C. Kapitein, E.J. Peterman, B.H. Kwok, J.H. Kim, T.M. Kapoor, and C.F. Schmidt. A bipolar mitotic kinesin moves on both microtubules that it crosslinks. *Nature*, 435:114–118, 2005.

[114] T.M. Kapoor, M.A. Lampson, P. Hergert, A. Cameron, D. Cimini, E.D. Salmon, B.F. McEwen, and A. Khodjakov. Chromosomes can congress to the metaphase plate before biorientation. *Science*, 311:388–391, 2006.

[115] T.M. Kapoor, T.U. Mayer, M.L. Coughlin, and T.J. Mitchison. Probing spindle assembly mechanisms with monastrol, a small molecule inhibitor of the mitotic kinesin, Eg5. *J. Cell Biol.*, 150:975–988, 2000.

[116] J.R. Kardon and R.D. Vale. Regulators of the cytoplasmic dynein motor. *Nat. Rev. Mol. Cell Biol.*, 10:854–865, 2009.

[117] A.S. Kashina, R.J. Baskin, D.G. Cole, K.P. Wedaman, W.M. Saxton, and J.M. Scholey. A bipolar kinesin. *Nature*, 379:270–272, 2009.

[118] H. Khataee and A.W. Liew. Computational modeling of kinesin stepping. *J. Chem. Inf. Model.*, 54:3439–3445, 2014.

[119] A. Khodjakov, R.W. Cole, B.R. Oakley, and C.L. Rieder. Centrosome-independent mitotic spindle formation in vertebrates. *Curr. Biol.*, 10:59–67, 2000.

[120] M. Kikumotot, M. Kurachi, V. Tosa, and H. Tashiro. Flexural rigidity of individual microtubules measured by a buckling force with optical traps. *Biophys. J.*, 90:1687–1696, 2006.

[121] M.W. Kirschner and T. Mitchison. Microtubule dynamics. *Nature*, 324:621, 1986.

[122] T. Kiyomitsu and I.M. Cheeseman. Chromosome-and spindle-pole derived signals generate an intrinsic code for spindle position and orientation. *Nat. Cell Biol.*, 14:311–317, 2012.

[123] J. Klaylein-Sohn, B. Pollinger, M. Ohmer, F. Hofmann, E. Nigg, B. Hemmings, and M. Wartmann. Acentrosomal spindle organization renders cancer cells dependent on the kinesin hset. *J. Cell Sci.*, 125:5391–5402, 2012.

[124] J. Kleylein-Sohn, J. Westendorf, M. Le Clech, R. Habedanck, Y.D. Stierhof, and E.A. Nigg. Plk4-induced centriole biogenesis in human cells. *Dev. Cell*, 13:190–202, 2007.

[125] Y.A. Komarova, A.S. Akhmanova, S. Kojima, N. Galjart, and G.G. Borisy. Cytoplasmic linker proteins promote microtubule rescue in vivo. *J. Cell Biol.*, 159:589–599, 2002.

[126] L.G. Kostecka, A. Olseen, K. Kang, G. Torga, K.J. Pienta, and S.R. Amend. High kifc1 expression is associated with poor prognosis in prostate cancer. *Med. Oncol.*, 38:47, 2021.

[127] S. Kotak, C. Busso, and P. Gonczy. NuMA phosphorylation by CDK1 couples mitotic progression with cortical dynein function. *EMBO J.*, 32:2517–2520, 2013.

[128] S. Kotak, C. Busso, and P.J. Gonczy. Cortical dynein is critical for proper spindle positioning in human cells. *Cell Biol.*, 199:97–110, 2012.

[129] C. Kozlowski, M. Srayko, and F. Nedelec. Cortical microtubule contacts position the spindle in c. elegans embryo. *Cell*, 129:499–510, 2007.

[130] P. Kunda, A.E. Pelling, T. Liu, and B. Baum. Moesin controls cortical rigidity, cell rounding, and spindle morphogensis during mitosis. *Curr. Biol.*, 18:91–101, 2008.

[131] J. Kwon, S. Godinho, N.S. Chandhok, N.J. Ganem, A. Azioune, M. Thery, and D. Pellman. Mechanisms to suppress multipolar divisions in cancer cells with extra centrosomes. *Genes Dev.*, 22:2189–2203, 2008.

[132] M. Kwon, M. Bagonis, G. Danuser, and D. Pellman. Direct microtubule-binding by myosin-10 orients centrosomes toward retraction fibers and subcortical actin clouds. *Dev. Cell*, 34:323–337, 2015.

[133] L. Laan, N. Pavin, J. Husson, G. Romeg-Lemonne, M. van Duijn, M.P. Lopez, R.D. Vale, F. Julicher, S.L. Reck-Peterson, and M. Dogterom. Cortical dynein controls microtubule dynamics to generate pulling forces that reliably position microtubule asters. *Cell*, 148:502–514, 2012.

[134] L. Laan, S. Roth, and M. Dogterom. End-on microtubule-dynein interactions and pulling-based positioning of microtubule organizing centers. *Cell Cycle*, 11:3750–3757, 2012.

[135] A.R. Lamson, C.J. Edelmaier, M.A. Glaser, and M.D. Betterton. Theory of cytoskeletal reorganization during cross-linker-mediated mitotic spindle assembly. *Biophys. J.*, 116:1719–1731, 2019.

[136] O.M. Lancaster, M. Le Berre, A. Dimitracopoulos, D. Bonazzi, E. Zlotek-Zlotkiewicz, R. Picone, T. Duke, M. Piel, and B. Baum. Mitotic rounding alters cell geometry to ensure efficient bipolar spindle formation. *Dev. Cell*, 25:270–283, 2013.

[137] B. Leber, B. Maier, Fl. Fuchs, J. Chi, P. Riffel, S. Anderhub, L. Wagner, A.D. Ho, J.L. Salisbury, M. Boutros, and A. Kramer. Proteins required for centrosome clustering in cancer cells. *Cancer*, 2:33ra38, 2010.

[138] N. Lecland and J. Luders. The dynamics of microtubule minus ends in the human mitotic spindle. *Nat. Cell Biol.*, 16:770–778, 2014.

[139] G. Letort, F. Nedelec, L. Blanchoin, and M. Thery. Centrosome centering and decentering by microtubule network rearrangement. *Mol Biol Cellol. Cell*, 27:2833–2843, 2016.

[140] A.A. Levesque, L. Howard, M.B. Gordon, and D.A. Compton. A functional relationship between numa and kid is involved in both spindle organization and chromosome alignment in vertebrate cells. *Mol. Bio. Cell*, 14:3541–3552, 2003.

[141] J. Li, L. Cheng, and H. Jiang. Cell shape and intercellular adhesion regulate mitotic spindle orientation. *Mol Biol Cell*, 30, 2019.

[142] J. Li and H. Jiang. Geometric asymmetry induces upper limit of mitotic spindle size. *Biophys. J.*, 112:1503–1516, 2017.

[143] J. Li and H. Jiang. Regulating positioning and orientation of mitotic spindles via cell size and shape. *Phys. Rev. E*, 97:012407, 2018.

[144] Y. Li, W. Yu, Y. Liang, and X. Zhu. Kinetochore dynein generates a poleward pulling force to facilitate congression and full chromosome alignment. *Cell Res.*, 17:701–712, 2007.

[145] L.A. Ligon, S. Karki, M. Tokito, and E.L.F. Holzbaur. Dynein binds to beta-catenin and may tether microtubules at adherens junctions. *Nat. Cell Biol.*, 3:913–917, 2001.

[146] Y. Liu, P. Zhan, Z. Zhou, Z. Xing, S. Zhu, C. Ma, Q. Li, Q. Zhu, Y. Miao, J. Zhang, T. Lv, and Y. Song. The overexpression of kifc1 was associated with the proliferation and progression of non-small cell lung cancer. *J. Thorac. Dis.*, 8:2911–2923, 2016.

[147] A. Loncar, S.A. Rincon, M.L. Ramirez, A. Paoletti, and P.T. Tran. Kinesin-14 family proteins and microtubule dynamics define *S. pombe* mitotic and meiotic spindle assembly, and elongation. *J. Cell Sci.*, 133:jcs240234, 2020.

[148] J. Loncarek, P. Hergert, V. Magidson, and A. Khodjakov. Control of daughter centriole formation by the pericentriolar material. *Cell Biol.*, 10:322–328, 2008.

[149] R. Loughlin, R. Heald, and F. Nedelec. A computational model predicts xenopus meiotic spindle organization. *J. Cell Biol.*, 191:1239–1249, 2010.

[150] R. Loughlin, J.D. Wilbur, F.J. McNally, F.J. Nedelec, and R. Heald. Katanin contributes to interspecies spindle length scaling in Xenopus. *Cell*, 147:1397–1407, 2011.

[151] K. Luby-Phelps, S. Mujumdar, R.B. Mujumdar, L.A Ernst, W. Galbraith, and A.S. Waggoner. A novel fluorescence ratiometric method confirms the low solvent viscosity of the cytoplasm. *Biophys. J.*, 65:236–242, 1993.

[152] R. Ma, L. Laan, M. Dogterom, N. Pavin, and F. Julicher. General theory for the mechanics of confined microtubule asters. *New J. Phys.*, 16:013018, 2013.

[153] M. Machicoane and et al. Slk-dependent activation of erms controls lgn-numa localization and spindle orientation. *J. Cell Biol.*, 205:791–799, 2014.

[154] V. Magidson, R. Paul, N. Yang, J.G. Ault, C.B. O'Connell, I. Tikhonenko, B.F. McEwen, A. Mogilner, and A. Khodjakov. Adaptive changes in the kinetochore architecture facilitate proper spindle assembly. *Nat. Cell Biol.*, 17:1134–1144, 2015.

[155] Z. Maliga, T.M. Kapoor, and T.J. Mitchison. Evidence that monastrol is an allosteric inhibitor of the mitotic kinesin eg5. *Chem. Biol.*, 9:989–996, 2002.

[156] B.J. Mann and P. Wadsworth. Kinesin-5 regulation and function in mitosis. *Trends Cell Biol.*, 29:66–79, 2019.

[157] A.L. Manning and D.A. Compton. Mechanisms of spindle-pole organization are influenced by kinetochore activity in mammalian cells. *Curr. Biol.*, 17:260–265, 2007.

[158] A.L. Manning and D.A. Compton. Structural and regulatory roles of non-motor spindle proteins. *Curr. Opin. Cell Biol.*, 20:101–106, 2008.

[159] A.L. Manning, M.S. Longworth, and N.J. Dyson. Loss of pRB causes centromere dysfunction and chromosomal instability. *Genes Dev.*, 24:1364–1376, 2010.

[160] G. Martail, A. Guerrero, A.F. Vieira, B.P. de Almeida, P. Machado, S. Mendonca, M. Mesquita, B. Villarreal, I. Fonseca, M.E. Francia, K. Dores, N.P. Martins, S.C. Jana, E.M. Tranfield, N.L. Barbosa-Morais, J. Paredes, D. Pellman, S.A. Godinho, and M. Bettencourt-Dias. Over-elongation of centrioles in cancer promotes centriole amplification and chromosome missegregation. *Nat. Commun.*, 9, 2018.

[161] MathWorks. *findpeaks*, 2007.

[162] T.U. Mayer, T.M. Kapoor, S.J. Haggarty, R.W. King, S.L. Schreiber, and T.J. Mitchison. Small molecule inhibitor of mitotic spindle bipolarity identified in a phenotype-based screen. *Science*, 286:971–974, 1999.

[163] M.I. Mayr, S. Hummer, J. Bormann, T. Gruner, S. Adio, W. Guenther, and T.U. Mayer. The human kinesin kif18a is a motile microtubule depolymerase essential for chromosome congression. *Curr. Biol.*, 17:488–498, 2007.

[164] M.L. McCleland, R.D. Gardner, M.J. Kallio, J.R. Daum, G.J. Gorbsky, D.J. Burke, and P.T. Stukenberg. The highly conserved ndc80 complex is required for kinetochore assembly, chromosome congression, and spindle checkpoint activity. *Genes Dev.*, 17:101–114, 2003.

[165] R.J. McIntosh. Mitosis. *Cold Spring Harb Perpect Biol.*, 8:a023218, 2016.

[166] D.L. Mercadante, E.A. Crowley, and A.L. Manning. Live cell imaging to assess the dynamics of metaphase timing and cell fate following mitotic spindle perturbations. *J. Vis. Exp*, 151, 2019.

[167] D.L. Mercadante, A.L. Manning, and S.D. Olson. Modeling reveals cortical dynein-dependent fluctuations in bipolar spindle length. *Biophys. J.*, 120:3192–3210, 2021.

[168] A. Merdes, R. Heald, K. Samejima, W.C. Earnshaw, and D.W. Cleveland. Formation of spindle poles by dynein/dynactin-dependent transport of numa. *J. Cell Biol.*, 149:851–862, 2000.

[169] S. Meunier and I. Vernos. Microtubule assembly during mitosis - from distinct origins to distinct functions? *J. Cell Sci.*, 125:2805–2814, 2012.

[170] C.E. Miles, J. Zhu, and A. Mogilner. Mechanical torque promotes bipolarity of the mitotic spindle through multi-centrosomal clustering. *Bull. Math. Biol.*, 84:29, 2022.

[171] Z. Mirzoyan, M. Sallozza, M. Allocca, A.M. Valenza, D. Grifoni, and P. Bellosta. Drosophila melanogaster: A model organism to study cancer. *Front. Genet.*, 10, 2019.

[172] T. Mitchison and M. Kirschner. Dynamic instability of microtubule growth. *Nature*, 312:237–242, 1984.

[173] T.J. Mitchison. Polewards microtubule flux in the mitotic spindle: evidence from photoactivation of fluorescence. *J. Cell Biol.*, 109:637–642, 1989.

[174] M. Mitsushima, K. Aoki, M. Ebisuya, S. Matsumura, T. Yamamoto, M. Matsuda, F. Toyoshima, and E. Nishida. Revolving movements of a dynamic cluster of actin filaments during mitosis. *J. Cell Biol.*, 191:453–462, 2010.

[175] K. Mittal, J. Kaur, M. Jaczko, G. Wei, M.S. Toss, E.A. Rakha, E.A.M. Janssen, H. Soiland, O. Kucuk, M.D. Reid, M.V. Gupta, and R. Aneja. Centrosome amplification: a quantifiable cancer cell trait with prognostic value in solid malignancies. *Cancer Metastasis Rev.*, 40:319–339, 2020.

[176] M.M. Mogensen, A. Malik, M. Piel, V. Bouckson-Castaing, and M. Bornens. Microtubule minus-end anchorage at centrosomal and non-centrosomal sites: the role of ninein. *J. Cell Sci.*, 113:3013–3023, 2000.

[177] A. Mogilner, R. Wollman, G. Civelekoglu-Scholey, and J. Scholey. Modeling mitosis. *TRENDS in Cell Biol.*, 16:88–96, 2006.

[178] C. Mollinari, J. Kleman, W. Jiang, G. Schoehn, T. Hunter, and R.L. Margolis. Prc1 is a microtubule binding and bundling protein essential to maintain the mitotic spindle midzone. *J. Cell Biol.*, 157:1175–1186,, 2002.

[179] H.M. Moon, Y.H. Youn, H. Pemble, J. Yingling, T. Wittmann, and A. Wynshaw-Boris. Lis1 control mitosis and mitotic spindle organization via the lis1-ndel1-dynein complex. *Hum. Mol. Genet.*, 23:449–466, 2014.

[180] V Mountain and D.A. Compton. Dissecting the role of molecular motors in the mitotic spindle. *New ANAT.*, 261:14–24, 2000.

[181] V. Mountain, C. Simerly, L. Howard, A. Ando, G. Schatten, and D. A. Compton. The kinesin-related protein, Hset, opposes the activity of Eg5 and cross-links microtubules in the mammalian mitotic spindle. *J. Cell Biol.*, 147:351, 1999.

[182] A. Musacchio and E.D. Salmon. The spindle-assembly checkpoint in space and time. *Nat. Rev. Mol. Cell Biol.*, 8:379–393, 2007.

[183] B. Navarro-Serer, E.P. Childers, N.M. Hermance, D. Mercadante, and A.L. Manning. Aurora A inhibition limits centrosome clustering and promotes mitotic catastrophe in cells with supernumerary centrosomes. *Oncotarget*, 10:1649–1659, 2019.

[184] E. Nazockdast, A. Rahimian, D. Zorin, and M. Shelley. A fast platform for simulating semi-flexible fiber suspensions applied to cell mechanics. *J. Comp. Phys.*, 329:173–209, 2017.

[185] F. Nedelec. Computer simulations reveal motor properties generating stable antiparallel microtubule interactions. *J. Cell Biol.*, 158:1005–1015, 2002.

[186] F. Nedelec and D. Foethke. Collective langevin dynamics of flexible cytoskeletal fibers. *New J. Phys.*, 9:427, 2007.

[187] D. Needleman and M. Shelley. The stormy fluid dymanics of the living cell. *Phys. Today*, 72:33–38, 2019.

[188] S.R. Norris, S. Jung, P. Singh, C.E. Strothman, A.L. Erwin, M.D. Ohi, M. Zanic, and R. Ohi. Microtubule minus-end aster organization is driven by processive hset-tubulin clusters. *Nat. Comm.*, 9:2659, 2018.

[189] M. Novak, B. Polak, J. Simunic, Z. Boban, B. Kuzmic, A.W. Thomae, I.M. Tolic, and N. Pavin. The mitotic spindle is chiral due to torques within microtubule bundles. *Nat. Comm.*, 9:3571, 2018.

[190] C.B. OConnell and Y. Wang. Mammalian spindle orientation and position respond to changes in cell shape in a dynein-dependent fashion. *Mol. Biol. Cell*, 11:1765–1774, 2000.

[191] M. Okumura, T. Natsume, M.T. Kanemaki, and T. Kiyomitsu. Dynein-dynactin-NuMA clusters generate cortical spindle-pulling forces as a multi-arm ensemble. *eLife*, 7:e36559, 2018.

[192] V. Pannu, P. Rida, A. Ogden, R. Turaga, S. Donthamsetty, N. Bowen, K. Rudd, M. Gupta, M. Reid, G. Cantauria, C. Walczak, and R. Aneja. Hset overexpression fuels tumor progression via centrosome clustering-independent mechanisms in breast cancer patients. *Oncotarget*, 6:6079–6091, 2015.

[193] E.J.G. Peterman and J.M. Scholey. Mitotic microtubule crosslinkers: insights from mechanistic studies. *Curr. Biol.*, 19:R1089–R1094, 2009.

[194] S. Petry. Mechanisms of mitotic spindle assembly. *Ann. Rev. Biochem,*, 85:659–683, 2016.

[195] M. Piehl and L. Cassimeris. Organization and dynamics of growing microtubule plus ends during early mitosis. *Mol. Biol. Cell*, 14:916–925, 2003.

[196] M. Piehl, U.S. Tulu, P. Wadsworth, and L. Cassimeris. Centrosome maturation: measurement of microtubule nucleation throughout the cell cycle by using GFP-tagged EB1. *Proc. Natl. Acad. Sci. U.S.A.*, 101:1584–1588, 2004.

[197] M. Piel, P. Meyer, A. Khodjakov, C.L. Rieder, and M. Bornens. The respective contributions of mother and daughter centrioles to centrosome activity and behavior in vertebrate cells. *J. Cell Biol.*, 149:317–330, 2000.

[198] E.M. Purcell. Life at low reynolds number. *Am. J. Phys.*, 45:3–11, 1977.

[199] N.J. Quintyne, J.E. Reing, D.R. Hoffelder, S.M. Gollin, and W.S. Saunders. Spindle multipolarity is prevented by centrosomal clustering. *Science*, 307:127–129, 2005.

[200] J.A. Raaijmakers and R.H. Medema. Function and regulation of dynein in mitotic chromosome segregation. *Chromosoma*, 123:407–422, 2014.

[201] J.A. Raaijmakers, M.E. Tanenbaum, and R.H. Medema. Systematic dissection of dynein regulators in mitosis. *J. Cell Biol.*, 201:201–215, 2013.

[202] J.A. Raaijmakers, R.G.H.P. van Heesbeen, J.L. Meaders, E.F. Geers, B. Fernandez-Garcia, R.H. Medema, and M.E. Tanenbaum. Nuclear envelope-associated dynein drives prophase centrosome separation and enables eg5-independent bipolar spindle formation. *EMBO J.*, 31:4179–4190, 2012.

[203] F. Rago and I.M. Cheeseman. The functions and consequences of force at the kinetochores. *J. Cell Biol.*, 200:557–565, 2013.

[204] S. Redemann, J. Pecreaux, N.W. Goehring, K. Khairy, E.H. Seltzer, A.A. Hyman, and J. Howard. Membrane invaginations reveal cortical sites that pull on mitotic spindles in one-cell c. elegans embryos. *PLoS ONE*, 5:e12301, 2010.

[205] D.N. Reinemann, S.R. Norris, R. Ohi, and M.J. Lang. Processive kinesin-14 hset exhibits directional flexibility depending on motor traffic. *Curr. Biol.*, 28:2356–2632, 2018.

[206] C. Renna, F. Rizzelli, M. Carminati, C. Gaddoni, L. Pirovano, S. Cecatiello, V. Pasqualato, and M. Mapelli. Organizational principles of the numa-dynein interaction interface and implications for mitotic spindle functions. *Structure*, 28:820–829, 2020.

[207] A.D. Rhys, P. Monteiro, C. Smith, M. Vaghela, T. Arnandis, T. Kato, B. Leitinger, E. Sahai, A. McAinsh, G. Charras, and S.A. Godinho. Loss of E-cadherin pro-

vides tolerance to centrosome amplification in epithelial cancer cells. *J. Cell Biol.*, 217(1):195–209, 2018.

[208] S.A. Rincon, A. Lamson, R. Blackwell, V. Syrovatkina, V. Fraisier, A. Paoletti, M.D. Betterton, and P.T. Tran. Kinesin-5-independent mitotic spindle assembly requires the antiparallel microtubule crosslinker ase1 in fission yeast. *Nat. Comm.*, 8:15286, 2017.

[209] G.C. Rogers, N.M. Rusan, D.M. Roberts, M. Peifer, and S.L. Rogers. The scf slimb ubiquitin ligase regulates plk4/sak levels to block centriole reduplication. *J. Cell Biol.*, 184:225–239, 2009.

[210] J. Roostalu, J. Rickman, C. Thomas, F. Nedelec, and T. Surrey. Determinants of polar versus nematic organization in networks of dynamic microtubules and mitotic motors. *Cell*, 175:796–808, 2018.

[211] N.M. Rusan, C.J. Fagerstrom, A.M. Yvon, and P. Wadsworth. Cell cycle-dependent changes in microtubule dynamics in living cells expressing green fluorescent protein-alpha tubulin. *Mol. Biol. Cell*, 12:971–980, 2001.

[212] D. Sabat-Pospiech, K. Fabian-Kolpanowicz, I.A. Prior, J.M. Coulson, and A.B. Fielding. Targeting centrsome amplification, and achilles' heel of cancer. *Biochem. Soc. Trans.*, 47, 2019.

[213] C.P. Samora, B. Mogessie, L. Conway, J.L. Ross, A. Straube, and A.D. McAnish. Map4 and clasp1 operate as a safety mechanism to maintain a stable spindle position in mitosis. *Nat. Cell Biol.*, 13:1040–1050, 2011.

[214] S. Sana, R. Keshri, A. Rajeevan, S. Kapoor, and S. Kotak. Plk1 regulates spindle orientation by phosphorylating numa in human cells. *Life Sci. Alliance*, 1:e201800223, 2018.

[215] S.C. Schaffner and J.V. Jose. Biophysical model of self-organized spindle formation patterns without centrosomes and kinetochores. *Proc. Natl. Acad. Sci. U.S.A.*, 103:11166–11171, 2006.

[216] L. Seldin, N.D. Poulson, H.P. Foote, and T. Lechler. Numa localization, stability, and function in spindle orientation invovle 4.1 and cdk1 interactions. *Mol. Biol. Cell*, 24:3651–3662, 2013.

[217] Y. Shao, N. Sun, Y. Jeng, Y. Wu, C. Hsu, C. Hsu, H. Hsu, A. Cheng, and Z. Lin. Eg5 as a prognostic biomarker and potential therapeutic target for hepatocellular carcinoma. *Cells*, 10:10071698, 2021.

[218] D.J. Sharp, G.C. Rogers, and J.M. Scholey. Cytoplasmic dynein is required for poleward chromosome movement during mitosis in drosophila embryos. *Nat. Cell Biol.*, 2:922–930, 2000.

[219] D.J. Sharp, G.C. Rogers, and J.M. Scholey. Microtubule motors in mitosis. *Nature*, 407:41–47, 2000.

[220] Z.Y. She and W.X. Yang. Molecular mechanisms of kinesin-14 motors in spindle assembly and chromosome segregation. *J. Cell Sci.*, 130:2097–2110, 2017.

[221] Y. Shimamoto, S. Forth, and T.M. Kapoor. Measuring pushing and braking forces generated by ensembles of kinesin-5 crosslinking two microtubules. *Dev. Cell*, 34:669–681, 2015.

[222] S. Shu, M. Iimori, T. Wakasa, K. Ando, H. Saeki, Y. Oda, E. Oki, and Y. Maehara. The balance of forces generated by kinesins controls spindle polarity and chromosomal heterogeneity in tetraploid cells. *J. Cell Sci.*, 132:jcs231530, 2019.

[223] A.D. Silk, A.J. Holland, and D.W. Cleveland. Requirements for numa in maintenance and establishment of mammalian spindle poles. *J. Cell Biol.*, 184:677–690, 2009.

[224] W.T. Silkworth and D. Cimini. Transient defects of mitotic spindle geometry and chromosome segregation errors. *Cell Div.*, 7, 2012.

[225] W.T. Silkworth, I.K. Nardi, L.M. Scholl, and D. Cimini. Multipolar spindle pole coalescence is a major source of kinetochore mis-attachment and chromosome mis-segregation in cancer cells. *PLoS ONE*, 4:e6564, 2009.

[226] P.M.A. Silva, R.M. Reis, V.M. Bolanos-Garcia, C. Florindo, A.A. Tavares, and H. Bousbaa. Dynein-dependent transport of spindle assembly checkpoint proteins off kinetochores toward spindle poles. *FEBS Lett.*, 588:3265–3273, 2014.

[227] M.P. Singh, R. Mallik, S.P. Gross, and C.C. Yu. Monte carlo modeling of single-molecule cytoplasmic dynein. *Proc. Natl. Acad. Sci. U.S.A.*, 102:12059–12064, 2005.

[228] S. Solinet, K. Muhmad, S.F. Stewman, K.B. El Kadhi, B. Decelle, L. Talje, A. Ma, B.H. Kwok, and S. Carreno. The actin-binding erm protein meosin binds to and stabilizes microtubules at the cell cortex. *J. Cell Biol.*, 202:251–260, 2013.

[229] D. Splinter, M.E. Tanenbaum, A. Lindqvist, D. Jaarsma, A. Flotho, Yu K.L., I. Grigoriev, D. Engelsma, E.D. Haasdijk, N. Keijzer, J. Demmers, M. Fornerod, F. Melchoir, C.C. Hoogenraad, R.H. Medema, and A. Akhmanova. Bicaudal d2, dynein, and kinesin-1 associate with nuclear pore complexes and regulate centrosome and nuclear positioning during mitotic entry. *PLoS Biol.*, 8:e1000350, 2010.

[230] J. Splinter, D.S. Razafsky, A. Schlager, M.A. Serra-Marques, I. Grigoriev, J. Demmers, N. Keijzer, K. Jiang, I. Poser, A.A. Hyman, C.C. Hoogenraad, S.J. King, and

A. Akhmanova. Bicd2, dynactin, and lis1 cooperate in regulating dynein recruitment to the cellular structures. *Mol. Biol. Cell*, 23:4226–4241, 2012.

[231] L.M. Starita, Y. Machida, S. Sankaran, J.E. Elias, K. Griffin, S.P. Schlegel, B.P. Gygi, and J.D. Parvin. Brca1-dependent ubiquination of gamma-tubulin regulates centrosome number. *Mol. Cell Biol.*, 24:8457–8466, 2004.

[232] A.F. Straight, A. Cheung, J. Limouze, I. Chen, N.J. Westwood, J.R. Sellers, and T.J. Mitchison. Dissecting temporal and spatial control of cytokinesis with a myosin ii inhibitor. *Science*, 299:1743–1747, 2002.

[233] J. Stumpff, G. Von Dassow, M. Wagenbach, C. Asbury, and L. Wordeman. The kinesin-8 motor, kif18a, suppresses kinetochore movements to control mitotic chromosome alignment. *Dev. Cell*, 14:252–262, 2008.

[234] M. Sullivan and D.O. Morgan. Finishing mitosis, one step at a time. *Nat. Rev. Mol. Cell Biol.*, 8:894–903, 2007.

[235] Y. Sun, Y. Zhang, Z. Lang, J. Huang, and Z. Zou. Prognostic and clinicopathological significance of kinesin family member c1 in various cancers: a meta-analysis. *Medicine (Baltimore)*, 98:e17346, 2019.

[236] S. Sutradhar, S. Basu, and R. Paul. Intercentrosomal angular separation during mitosis plays a crucial role for maintaining spindle stability. *Phys. Rev. E*, 92:042714, 2015.

[237] K. Svoboda and S.M. Block. Force and velocity measured for single kinesin molecules. *Cell*, 77:773–784, 1994.

[238] H.L. Sweeney and E.L.F. Holzbaur. Motor proteins. *Cold Spring Harb. Perspect. Biol.*, 10, 2018.

[239] M.A. Tame, J.A. Raaijmakers, P. Afanasyev, and R.H. Medema. Chromosome misalignments induce spindle-positioning defects. *EMBO Rep.*, 17:317–325, 2016.

[240] M.A. Tame, J.A. Raaijmakers, B. van der Broek, A. Lindqvist, K. Jalink, and R.H. Medema. Astral microtubules control redistribution of dynein at the cell cortex to facilitate spindle positioning. *Cell Cycle*, 13:1162–1170, 2014.

[241] R. Tan, P.J. Foster, D.J. Needleman, and R.J. McKenny. Cooperative accumulation of dynein-dynactin at microtubule minus-ends drives microtubule network organization. *Dev. Cell*, 44:233–247, 2018.

[242] M.E. Tanenbaum and R.H. Medema. Mechanisms of centrosome separation and bipolar spindle assembly. *Dev. Cell*, 19:797–806, 2010.

[243] I.M. Tolic. Mitotic spindle: kinetochore fibers hold on tight to interpolar bundles. *Eur. Biophys. J.*, 47:191–203, 2018.

[244] I.M. Tolic and N. Pavin. Mitotic spindle: lessons from theoretical modeling. *Mol. Biol. Cell*, 32:281–222, 2020.

[245] F. Toyoshima and E. Nishida. Integin-mediated adhesion orients the spindle parallel to the substratun in an eb1- and myosin x-dependent manner. *EMBO J.*, 26:1487–1498, 2007.

[246] M. Trokter, N. Mucke, and T. Surrey. Reconstitution of the human cytoplasmic dynein complex. *Proc. Natl. Acad. Sci. U.S.A.*, 109:20895–20900, 2012.

[247] L. Trott, M. Hafezparast, and A. Madzvamuse. A mathematical understanding of how cytoplasmic dynein walks on microtubules. *R. Soc. Open Sci.*, 5:171568, 2018.

[248] K. Tsuchiya, H. Hayashi, M. Nishina, M. Okumura, Y. Sato, M.T. Kanemaki, G. Goshima, and T. Kiyomitsu. Ran-gtp is non-essential to activate numa for mi-

totic spindle-pole focusing but dynamically polarizes hurp near chromosomes. *Curr. Biol.*, 31:115–127, 2021.

[249] N.T. Umbreit, D.R. Gestaut, J.F. Tien, B.S. Vollmar, T. Gonen, C.L. Asbury, and T.N. Davis. The ndc80 kinetochore complex directly modulates microtubule dynamics. *Proc. Natl. Acad. Sci. U.S.A.*, 109:16113–16118, 2012.

[250] L. Urnavicius, C.K. Lau, M.M. Elshenawy, E. Morales-Rios, C. Motz, A. Yildiz, and A.P. Carter. Cryo-em shows how dynactin recruits two dyneins for faster movement. *Nature*, 554:202–206, 2018.

[251] E.A. Vaisberg, M.P. Koonce, and R.J. McIntosh. Cytoplasmic dynein plays a role in mammalian mitotic spindle formation. *J. Cell Biol*, 123:849–858, 1993.

[252] R.G.H.P. van Heesbeen, J.A. Raaijmakers, M.E. Tanenbaum, and R.H. Medema. Nuclear envelope-associated dynein cooperates with eg5 to drive prophase centrosome separation. *Commun. Inter. Biol.*, 6:e23841, 2013.

[253] R.G.H.P. van Heesbeen, M.E. Tanenbaum, and R.H. Medema. Balanced activity of three mitotic motors is required for bipolar spindle assembly and chromosome segregation. *Cell Rep.*, 8:948–956, 2014.

[254] A. Vasquez Limeta and J. Loncarek. Human centrosome organization and function in interphase and mitosis. *Semin. Cell Dev. Biol.*, 117:30–41, 2021.

[255] I. Vernos, J. Raats, T. Hirano, J. Heasman, E. Karsenti, and C. Wylie. Xklp1, a chromosomal xenopus kinesin-like protein essential for spindle organization and chromosome positioning. *Cell*, 81:117–127, 1995.

[256] J.J. Vincente and L. Wordeman. Mitosis, microtubule dynamcs and the evolution of kinesins. *Exp. Cell Res.*, 334:61–69, 2016.

[257] C.E. Walczak, I. Vernos, T.J. Mitchison, E. Karsenti, and R. Heald. A model for the proposed roles of different microtubule-based motor proteins in establishing spindle bipolarity. *Curr. Biol.*, 8:903–913, 1998.

[258] K. Wang, H. Okada, and E. Bi. Comparative analysis of the roles of non-muscle myosin iis in cytokinesis in budding yeast, fission yeast, and mammalian cells. *Front. Cell Dev. Biol.*, 8:593400, 2020.

[259] J.J. Ward, H. Roque, C. Antony, and F. Nedelec. Mechanical design principles of a mitotic spindle. *eLife*, 3:e03398, 2014.

[260] C.M. Waterman-Storer, A. Desai, J.C. Bulinski, and E.D. Salmon. Fluorescent speckle microscopy, a method to visualize the dynamics of protein assemblies in living cells. *Curr. Biol.*, 8:1227–1230, 1998.

[261] K.L. Weber, A.M. Sokac, J.S. Berg, R.E. Cheney, and W.M. Bement. A microtubule-binding myosin required for nuclear anchoring and spindle assembly. *Nat.*, 431:325–329, 2004.

[262] R. Wei, B. Ngo, G. Wu, and W. Lee. Phosphorylation of the ndc80 complex protein, hec1, by nek2 kinase modulates chromosome alignment and signaling of the spindle assembly checkpoint. *Mol. Biol. Cell*, 22:3584–3594, 2011.

[263] R.R. Wei, J. Al-Bassam, and S.C. Harrison. The ndc80/hec1 complex is a contact point for kinetochore-microtubule attachment. *Nat. Struct.*, 14:54–59, 2007.

[264] R.R. Wei, P.K. Sorger, and S.C. Harrison. Molecular organization of the ndc80 complex, and essential kinetochore component. *Proc Natl Acad Sci USA*, 102:5363–5367, 2005.

[265] T. Wittman, M. Wilm, E. Karsenti, and I. Vernos. Tpx2, a novel xenopus map invovled in spindle pole organization. *J. Cell Biol.*, 149:1405–1418, 2000.

[266] E.J. Wojcik, D.M. Glover, and T.S. Hays. The scf ubiquitin ligase protein slimb regulates centrosome duplication in drosophila. *Curr. Biol.*, 10:1131–1134, 2000.

[267] R. Wollman, G. Civelekoglu-Scholey, J.M. Scholey, and A. Mogilner. Reverse engineering of force integration during mitosis in the Drosophila embryo. *Mol. Syst. Biol.*, 4:195, 2008.

[268] R. Wollman, E.N. Cytrynbaum, J.T. Jones, T. Meyer, J.M. Scholey, and A. Mogilner. Efficient chromosome capture requires a bias in the 'search-and-capture' process during mitotic-spindle assembly. *Curr. Biol.*, 15:828–832, 2005.

[269] G.E. Woodard, N. Huang, H. Cho, T. Miki, G.G. Tall, and J.H. Kehrl. Ric-8a and gia recruit lgn, numa, and dynein to the cell cortex to help orient the mitotic spindle. *Mol. Cell. Biol.*, 30:3519–3530, 2010.

[270] S. Woolner, L. O'Brien, C. Wiese, and W.M. Bement. Myosin-10 and actin filaments are essential for mitotic spindle function. *J. Cell Biol.*, 182:77–88, 2008.

[271] L Wordeman. How kinesin motor proteins drive mitotic spindle function: lessons from molecular assays. *Semin Cell Dev. Biol.*, 21:260–268, 2010.

[272] L. Wordeman, M. Wagenbach, and G. von Dassow. Mcak facilitates chromosome movement by promoting kinetochore microtubule turnover. *J. Cell Biol.*, 179:869–879, 2007.

[273] N. Wright, Z. Gong, R. Kittles, R. Natarajan, T. Jovanovic-Talisman, P. Rida, M. LaBarge, and V. Seewaldt. Kinesin family member c1 (kifc1/hset): A potential actionable biomarker of early state breast tumorigenesis and progression of high-risk lesions. *J. Pers. Med.*, 11:1361, 2021.

[274] J. Wu, G. Misra, R.J. Russell, A.J. Ladd, T.P. Lele, and R.B. Dickinson. Effects of dynein on microtubule mechanics and centrosome positioning. *Mol. Biol. Cell*, 22:4834–4841, 2011.

[275] P. Xie. Theoretical analysis of dynamics of kinesin molecular motors. *ACS Omega*, 5:5721–5730, 2020.

[276] P. Xie. A common atp-dependent stepping model for kinesin-5 and kinesin-1: Mechanism of bi-directionality of kinesin-5. *Biophys. Chem.*, 271:106548, 2021.

[277] M. Ykawa, T. Yamauchi, N. Kurisawa, S. Ahmed, K. Kimura, and T. Toda. Fission yeast cells overproducing hset/kifc1 provides a useful tool for identification and evaluation of human kinesin-14 inhibitors. *Fungal Genet. Biol.*, 116:33–41, 2018.

[278] M. Yukawa, Y. Yamada, T. Yamauchi, and T. Toda. Two spatially distinct kinesin-14 proteins, Pkl1 and Klp2, generate collaborative inward forces against kinesin-5 Cut7 in S. pombe. *J. Cell Sci.*, 131:210740, 2018.

[279] Z. Zheng, Q. Wan, J. Liu, H. Zhu, X. Chu, and Q. Du. Evidence for dynein and astral microtubule-mediated cortical release and transport of gαi/lgn/numa complex in mitotic cells. *Mol. Biol. Cell*, 24:901–913, 2013.

[280] J. Zhou, J. Yao, and H.C. Joshi. Attachment and tension in the spindle assembly checkpoint. *J. Cell Sci.*, 115:3547–3555, 2002.